Spring 2019

Improving base metal electrowinning

Charles Ebenezer Abbey

Department: Materials Science and Engineering

IMPROVING BASE METAL ELECTROWINNING

by

CHARLES EBENEZER ABBEY

A DISSERTATION

Presented to the Faculty of the Graduate School of the

MISSOURI UNIVERSITY OF SCIENCE AND TECHNOLOGY

In Partial Fulfillment of the Requirements for the Degree

DOCTOR OF PHILOSOPHY

in

MATERIALS SCIENCE AND ENGINEERING

2019

Approved by:

Michael S. Moats, Advisor
Ronald J. O'Malley
Mark E. Schlesinger
Frank Scott Miller
Kwame Offei-Awuah

PUBLICATION DISSERTATION OPTION

This dissertation consists of the following five articles which have been submitted for publication, or will be submitted for publication as follows:

Paper I, found on pages 31-41, is a conference paper published in the proceedings of 2017 TMS Annual Conference in San Diego, California in February 2017.

Paper II, found on pages 42-61, is a conference paper presented at the 2017 SME Annual Conference in Minneapolis, Minnesota in February 2018 and would be subsequently submitted to the Hydrometallurgy Journal for Publication.

Paper III, found on pages 62-80, is a conference paper published in the proceedings of Extraction 2018 organized by SME, TMS and CIM in Ottawa, Ontario, Canada in August 2018.

Paper IV, found on pages 81-105, is a conference paper published in the proceedings of Extraction 2018 organized by SME, TMS and CIM in Ottawa, Ontario, Canada in August 2018.

Paper V, found on pages 106-131, has been submitted to the Ghana Mining Journal for publication.

ABSTRACT

In zinc electrowinning, Mn oxidizes to form MnO_2 on Pb-Ag anodes, cell walls and pipes. MnO_2 reduces anode corrosion but also leads to short circuits and maintenance issues. MnO_2 is thought to interact with chloride ions and produce oxidized chlorine species. The interactions between Mn and Cl are not well understood. Bench scale experiments were conducted to investigate the effects of the manganese to chloride ratio on anode corrosion rate and electrolyte chemistry using rolled Pb-Ag anodes. Increasing the average Mn/Cl^- ratio from ~7:1 to ~11:1 reduced the anode corrosion rate. Anode scales produced with Mn/Cl^- ratios at or above 11:1 contained some γ–MnO_2 while scales formed with ratios less than 11:1 did not.

In copper electrowinning, the effects of temperature, power outages and concentrations of cobalt and manganese on anode corrosion and current efficiency have not been well investigated. Benchscale tests were used to investigate these effects. Anode corrosion in all experiments was minimal probably due to the presence of at least 150 mg/L Co in each electrolyte. Cathode current efficiency typically ranged between 90 and 95% for the experiments. The range of power outage, temperature and concentrations of Mn and Co tested did not produce a significant effect on current efficiency.

Anode potential estimation equations for industrial tankhouse operations where cobalt is added after solvent extraction and where cobalt concentration is naturally high due to the ores being processed were developed using lab scale tests. These models have been combined with other reported equations to calculate the energy consumption of electrowinning systems for Pb-Ca-Sn anodes in synthetic sulfuric acid electrolytes.

ACKNOWLEDGMENTS

I am grateful to the Almighty God for his abundant grace and providence in my life. Proverbs 4:7: “The beginning of wisdom is this: Get wisdom. Though it cost all you have, get understanding.”

I am also grateful to my advisor Prof. Michael Scott Moats for his guidance, direction, and supervision during my studies. Joining his research group gave me the biggest career boost. Thank you Prof. Moats.

I am grateful to the AMIRA P705 C project for the sponsorship to conduct my PhD research. I am also grateful to Freeport McMoRan for the industrial training and funding.

I am grateful to my PhD committee consisting of Prof. Ronald O’Malley, Prof. Mark Schlesinger, Prof. F. Scott Miller and Prof. Kwame Awuah-Offei.

I also want to thank the staff and faculty of the Materials Science and Engineering Department for their awesome interactions. Notable mentions are Denise, Teneke, Nathan, Jack, Dr.Wisner and Dr. Bohannan. I am also grateful to Janell Kamler, Sharon Matson and Emily Seals.

I enjoyed spending time with some friends (Obinna, Viraj, Maalavan, Julian and Tianju), the Ghanaian and Newman Catholic community in Rolla. Thank you to my research group members: Dr. Wayne Huebner, Margaret, Michael, Kevin, Andrew and John. Thank you my friends,

My strongest pillar of support was my wife Matilda and children’s (Pius, Jonathan and Keziah). Matilda put her career hold to ‘slave’ for the family while I was out most of the time trying to study. Thank you Dad, Mum, Brothers and Sister for your support!

TABLE OF CONTENTS

Page

LIST OF ILLUSTRATIONS

SECTION Page

LIST OF TABLES

PAPER IV

PAPER V

1. INTRODUCTION

1.1. BACKGROUND

This dissertation summarizes research efforts towards a PhD degree. Most of this work was conducted under the auspices of the AMIRA P705C project. AMIRA International is a non-profit entity based in Australia that brings industrial organizations together with research institutions to conduct collaborative research. This arrangement is mutually beneficial to all parties involved and has led to some very important research findings that are vital to the industry. An imperative criterion for developing the various AMIRA projects has been to make sure each sponsor benefits from the research conducted by the projects.

The AMIRA Project P705C started in November 2013 with the objectives of reducing process energy consumption, improving capital utilization, reducing acid mist, and developing better training and technology transfer tools. Project P705C included funds for a doctor of philosophy position to conduct research at the Missouri University of Science and Technology to examine problems encountered by two sponsors. One of the sponsors has a zinc electrowinning cellhouse in Canada and the other has copper electrowinning tankhouses in Laos and the Democratic Republic of Congo (DRC).

This dissertation is, therefore, sectioned into zinc and copper electrowinning (EW) sections to answer pertinent questions in both systems and to study the fundamentals and science of the anode reactions that directly affect key performance indicators (KPI). A bench-scale anode corrosion test system was fabricated to run industrial simulations of EW systems for both copper and zinc. The bench-scale tests were performed first to provide

industrial guidance. Fundamental experiments were designed and performed to better understand anode potential in copper electrowinning.

1.2. PROBLEM STATEMENT

The zinc sponsor reported rapid short-circuiting on their anodes that lead to anode heat damage, anode failure, loss of current efficiency (CE), and other undesirable effects. Operating with electrolytes having manganese concentration to chloride concentration ratios greater than 10 has been observed to avert these problems. Higher Mn/Cl ratios, however, cause excessive MnO_2 formation that can block pipes and form cell sludge. Pipes and cells, therefore, have to be cleaned regularly. Frequent downtimes for cleaning negatively impacts cell availability. It will, therefore, be helpful to inhibit the excessive formation of MnO_2 at higher Mn/Cl ratios or understand the mechanism of short formation at lower Mn/Cl ratios so that they can be prevented.

The copper sponsor's operation in the DRC has more cobalt (about 600 mg/L) in its electrolyte than needed. The high Co concentration is a result of the local high-grade Cu-Co ores. Indeed, most tankhouses maintain approximately 150 mg/L of Co in the electrolyte for anode corrosion reduction and oxygen evolution reaction (OER) depolarization. Cobalt is known to reduce cell energy consumption by catalyzing the oxygen evolution reaction, and it can also reduce anode corrosion by forming a more tenacious and dense anode scale. Another consequent result is the improved cathode quality due to reduced anode corrosion. The DRC subsidiary therefore wanted to understand the consequences of extracting the excess cobalt for sale. Additionally, this industry player was curious to assess the effect of concentrations of cobalt and manganese, temperature,

and power outages on their anode corrosion and current efficiency (CE). Finally, to the impact of Co concentration, Fe concentration, Mn concentration, Cl concentration, acid concentration, temperature, and current density on anode potential and consequently cell voltages were quatified.

This work therefore reports on efforts to study these problems related to zinc and copper electrowinning. While some of this topics have been studied individually, this work represents the examination of complex behaviors and interactions which have not previously been reported.

1.3. RESEARCH OBJECTIVES

The objectives of this research cover two sections. For zinc, the objective was to examine the effect of [Mn]/[Cl] ratio on anode corrosion and electrolyte parameters. For copper, the objectives were to:

- establish the effect of [Mn], [Co], temperature, and power outages on current efficiency (CE) and corrosion rates.
- establish a model for the assessment of the effect of [Co], [Cl], [Fe], [Mn], [H_2SO_4], current density, and temperature on anode potential and energy consumption.

1.4. RESEARCH METHODOLOGY AND SCOPE

The scope of this research covers two sections, zinc and copper, using the Missouri S&T anode corrosion testing facility and fundamental experiments to observe, measure, analyze, and scientifically answer these research questions.

The following methods were used to complete the stated objectives:

- pertinent, comprehensive literature review.
- bench-scale testing.
- laboratory fundamental studies and experiments.
- industrial validation of final empirical anode potential model

2. LITERATURE REVIEW

2.1. COPPER AND ZINC ELECTROWINNING OVERVIEW

Electrochemical cells can be classified into galvanic cells and electrolytic cells [1]. Galvanic cells are spontaneous chemical reactions that produce electron flow, and electrolytic cells use external electrical energy to cause chemical reactions. An important use of electrolytic cells is in the reduction of metal ions called electrowinning. Two electrodes, the cathode (negatively charged) and anode (positively charged) conduct the electrical energy, and at least one electrolyte phase completes the circuit in an electrolytic or electrowinning cell. An example of an electrowinning cell is shown schematically in Figure 2.1 where an external power supply provides electrical current and energy to reduce copper at the cathode and oxidize water at the anode.

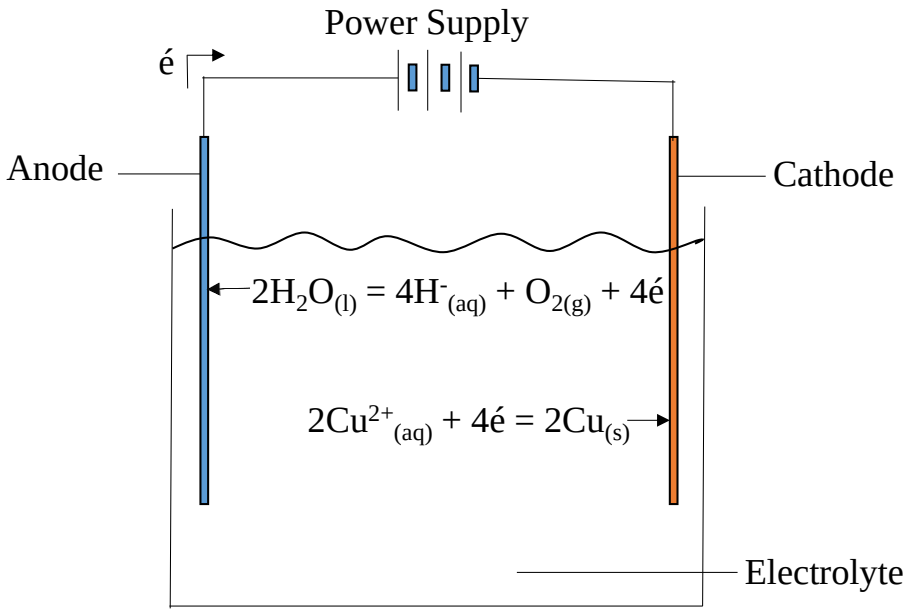

Figure 2.1. A Copper Electrowinning Cell Showing the Electrolyte, Power Supply, Redox Reactions, and Electrodes

Electrowinning (EW) is an important method in the production of commercially pure copper and zinc. EW is the main processing route for the production of Special High Grade Zn. Approximately 20% of the world's refined Cu is produced by electrowinning [2]. EW generally starts with mining the run-of-mine (ROM) ore, as shown in Figure 2.2, followed by mineral processing stages necessary for the particular leaching processes that follow. For example, crushing, screening, and sometimes agglomeration are done before heap leaching.

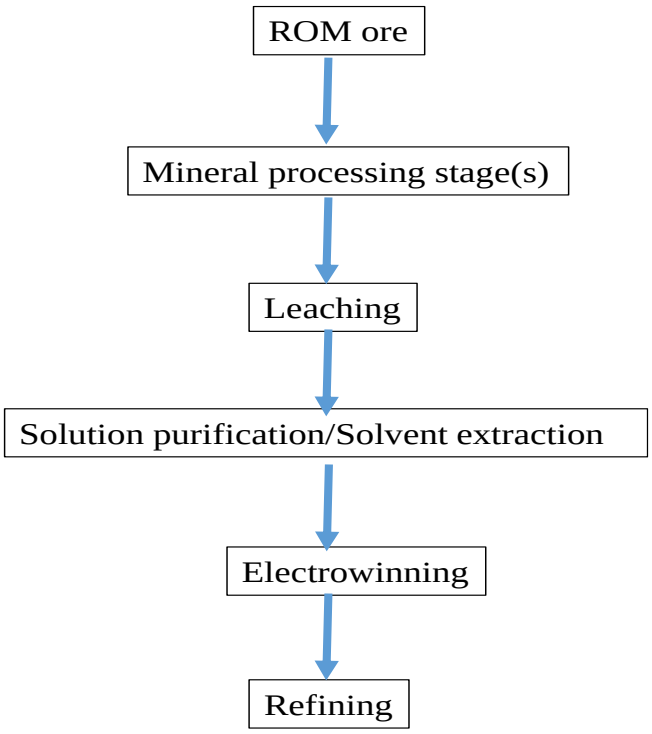

Figure 2.2. Schematic Process Flowsheet of Cu and Zn

Sometimes pressure oxidation, bio-oxidation, roasting, or some other pretreatment methods may also be employed before leaching. Leaching can either be done via agitation leaching or non-agitation leaching depending on the ore grade, economic factors, ore type,

nature, and mineral deportment [3]. Pregnant leach solution (PLS) from leach pads or agitated leach tanks go to solution purification in the case of Zn or solvent extraction (SX) in the case of Cu. Solution purification prior to Zn EW utilizes mostly oversaturation, pH modification, and preferential reduction using metallic zinc to remove impurities. In Cu; SX uses organic reagents mixed with a diluent that selectively extracts the mineral of interest (copper) from the large volumes of low Cu concentration PLS into a reduced volume of organic liquid phase (extraction). The loaded copper is then stripped from the organic solvent into a highly concentrated acid electrolyte for subsequent electrowinning [3]. The reaction for both the extraction and stripping stages are shown by the forward and backward reactions of Equation 2.1, respectively, for Cu SX.

$$2RH_{(org)} + CuSO_{4(aq)} \leftrightarrow R_2Cu_{(org)} + H_2SO_{4(aq)} \quad (2.1)$$

In line with Le Chatelier's principle, we can force the reaction to move backwards and strip Cu off the organic phase by increasing acid concentration or reducing pH, and the reverse is true. Figure 2.3 shows the interconnectivity of the three main vital stages from leaching to electrowinning for copper. In the leaching area, aqueous solutions containing Cu ions exchange into the organic phase to reduce the volume of solution and concentrate the mineral of interest. From the organic phase, it is moved again into a highly acidic aqueous phase to further concentrate the Cu and reduce the solution volume before electrowinning.

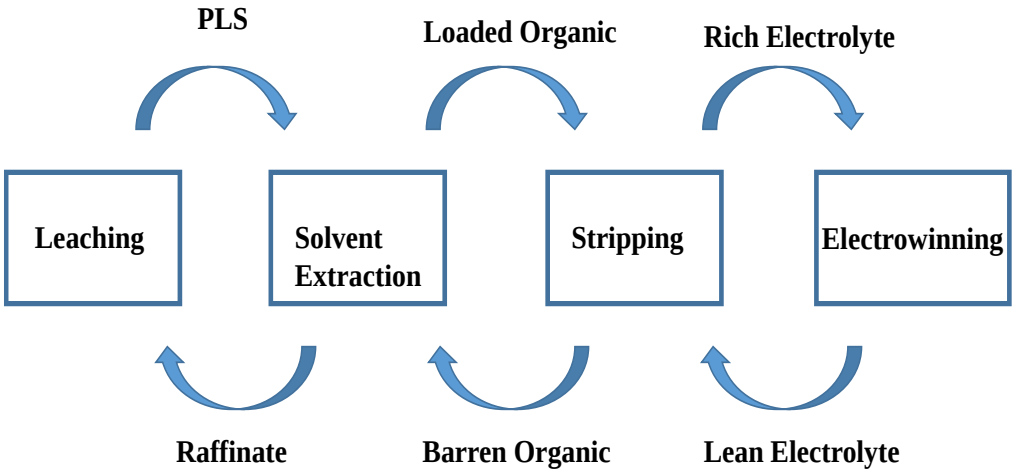

Figure 2.3. Solution Flow Directions in Copper Production

Following solution purification, the electrolyte is cooled before electrowinning. In Cu EW, the rich electrolyte from the SX stripper is mixed with lean electrolyte from the EW tankhouse to produce a constant concentration electrolyte called commercial electrolyte. Commercial electrolytes with constant Cu concentration prevents the need to ramp up or down the current from the rectifier based on the fluctuating Cu concentration. Minimizing the need to ramp the rectifier up or down preserves the life of the rectifier.

The rectifier supplies constant current to cell furniture that is designed to distribute current equally through each cell. Current distribution is critical to the process. Unequal current distribution can lead to short circuits and other pertinent problems.

Co, Mn, and other impurities have to be bled out to prevent their concentrations from exceeding set limits. Since solutions circulate through the EW and cells in Cu production, there is a need for synergistic cooperation and interaction between SX and EW operations.

Electrowinning products are refined further to produce the final purity required for most applications. The positively charged metal ions are reduced from solution at the cathode, and this is accompanied by an anodic reaction to complete the redox pair.

On the industrial scale, multiple anodes and cathodes are inserted into a cell to produce the metal. The industrial anodes are usually made of Pb alloys since Pb is relatively inexpensive and has an acceptable lifetime [2] when the electrolyte is sulfuric acid. In Zn EW, the cathode is typically made of aluminum, in Cu EW, the cathodes can be made with copper starter sheets or stainless steel sheets. In both cases, edge strips are used when re-usable substrates are employed to allow the harvest of plated metal. Generally, Zn industrial electrowinning facilities are referred to as cellhouses, while Cu uses tankhouses.

2.2. ZINC ELECTROWINNING (EW)

Zinc is the third most widely used non-ferrous metal after aluminum and copper with approximately 1.1 million tonnes produced and consumed in June 2018 alone [4]. Zinc is important in anti-corrosion and can be used to galvanize steel and other surfaces. Zn is usually mined from sphalerite ores and recovered as a metal by electrowinning from sulfuric acid electrolytes using Pb-Ag alloys as anodes and aluminum cathodes. Equation 2.2 shows the overall cell reaction for Zn electrowinning which has an E° = -1.992 V.

$$ZnSO_4 + H_2O \rightarrow Zn + {}^{1}/_{2}\, O_2 + H_2SO_4 \qquad (2.2)$$

Zinc can also be hydrometallurgically extracted using various lixiviants from industrial wastes and secondaries [5]. Scheme 1 shows four reactions that happen at both

the anode and cathode with manganese in the electrolyte. Zn is plated on the cathode while hydrogen gas can evolve as a parasitic reaction. On the anode, MnO_2 forms and water is oxidized to evolve oxygen.

Scheme 1

Anode

$$2Zn^{2+}_{(aq)} + 4\acute{e} = 2Zn_{(s)} \qquad E° = -0.763\ V \tag{2.3}$$

$$4H^{+}_{(aq)} + 4\acute{e} = 2H_{2(g)} \qquad E° = 0.000\ V \tag{2.4}$$

Cathode

$$2H_2O_{(l)} = 4H^{+}_{(aq)} + 4\acute{e} + O_{2(g)} \tag{2.5}$$

$$2Mn^{2+}_{(aq)} + 4H_2O_{(l)} = 2MnO_{2(s)} + 8H^{+}_{(aq)} + 4\acute{e} \qquad E° = -1.208\ V \tag{2.6}$$

Overall Main Reactions

$$2Zn^{2+}_{(aq)} + 2H_2O_{(l)} = 2Zn_{(s)} + O_{2(g)} + 4H^{+}_{(aq)} \tag{2.7}$$

Key performance indicators (KPI) for Zn EW are energy utilization or consumption, electrode corrosion rates, current efficiency, and cathode production rate and quality. Although Pb has environmental and health concerns, its performance and cost make it difficult to replace in EW industries [2]. The anode material of choice for Zn EW is Pb-Ag due to its superior performance [6, 7]. Silver in the anode alloy plays a catalytic role for oxygen evolution and corrosion rate reduction [8, 9]. A relatively higher current density yields low unit cost with an optimum around 600 A/m^2 [10]. Zinc is normally electrowon at 38-40 ^oC.

Zn EW is sensitive to impurities [11, 12] such as Co [13] and Ni [14]. The impurities affect the cathodic coulombic efficiency [11]. The electrolyte is purified to minimize these impurities. The order of the impurity effect on Zn Ew is Ge>Sb>Ni>Co>Bi>Cu>As>Sn>Fe [7, 15]. As shown in Figure 2.4, any metal with a higher reduction potential than Zn will be reduced preferentially to Zn, but the main effect of these impurities is the consequent enhancement of H_2 evolution on the cathode reducing the current efficiency. Mn and Cl are also present in the EW electrolytes. Mn is present in sphalerite ores and reports to the electrolyte [8]. Mn is also added to assist iron removal by oxidizing ferrous to ferric during solution purification [5]. Chloride enters the electrolyte from water and the zinc source, especially secondary ones. Mn and Cl interact in the electrolyte during Zn EW, but these interactions have not been fully understood or explained [16-20]. Table 2.1 shows typical Zn Ew operating conditions, parameters, and levels modified after Tjandrawan (2010) to include data from Nicol et al (2017b) and Tjandrawan and Nicol (2013).

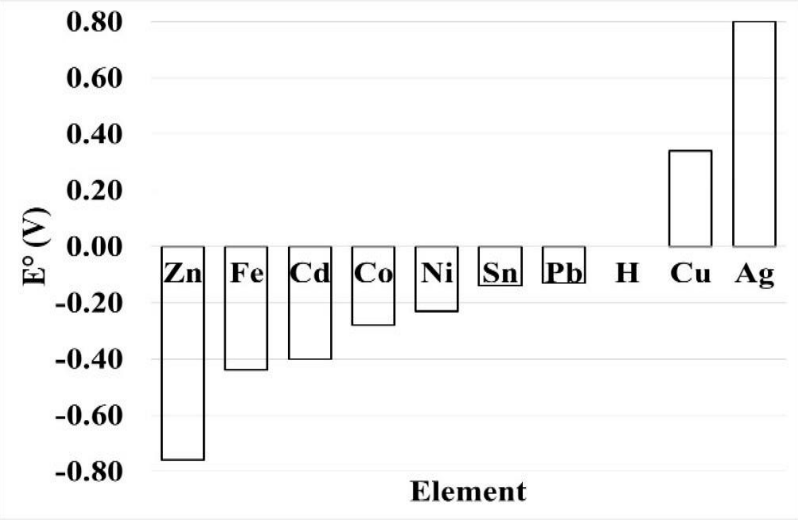

Figure 2.4. Order of Reducibility of Metals before Zinc [10]

Table 2.1. Typical Zn EW Operating Parameters and Conditions [15]

Cathodes	Aluminum alloy sheets
Anodes	Sandblasted Pb-0.75%Ag plates
Anode life (years)	3.5
Current density (A/m^2)	~500
Cell voltage (V)	3.3
Cathode current efficiency (%)	~92
Energy consumption (MW/hr) cathode	~2.95
Temperature (°C)	30-40
Zn (g/L)	50-65
H_2SO_4 (g/L)	150-165
Ca (g/L)	0.43
Mn/Mn^{2+} (g/L)	2.5/2-10
Mg (g/L)	3.2
Na (g/L)	8
Fe/Fe^{2+} (mg/L)	1.5/<1
Cl (mg/L)	1-500
F (mg/L)	21
$SrCO_3$ (g/t)	700
Na_2SiO_3 (g/t)	75
Glue (g/t)	20-25
Licorice (g/t)	60-80

An itinerant problem that accompanies Zn EW is the generation of acid mist due to oxygen bubbles rising in the solution and "bursting" at the electrolyte-air interface, throwing mists of acid into the atmosphere. Additives like licorice can be added into the cells to reduce acid mists, and this allows the current densities to be increased [12]. Ionic liquid salts, namely; 1-Ethyl-3-methylimidazolium chloride [EMIM]Cl, 1-Ehyl-3-methylimidazolium bromide [EMIM]Br, and 1-Ehyl-3-methylimidazolium ethyl sulfate [EMIM]ESO_4 tested on a lab scale decrease the oxygen evolution reaction potential by about 25 mV and decrease the corrosion rate of the Pb-0.7 % Ag anode by as much as 42% [21].

2.2.1. Pb Alloy Anodes. In Zn EW, the main anodes used are lead-based alloys, as the advantages of Pb have been enumerated in previous research [2]. Pb-Ag anodes and sometimes Pb-Ag-Ca are widely used [22]. These anodes have proven to be overall more advantageous than other alloys in terms of energy consumption, corrosion rates, and cathode product quality [22-27]. The electrochemical behavior of Pb-Ag alloys have been extensively studied [25-28]. Pure lead is heavy and soft and has poor mechanical strength, meaning that the amount needed for commercial EW cells will experience bending, warping and creeping, which can cause short circuits, fire and electrocution risks. Therefore pure Pb is alloyed to provide mechanical strength, corrosion resistance, and anode depolarization. Anode alloys have been very well studied; Ag between 0.45-1% is preferred to allow corrosion resistance, conductivity improvements, and oxygen evolution reaction (OER) depolarization [15]. But the Pb-Ag alloy still does not have optimum strength, and hence about 0.05-0.08 % Ca can be added [29]. To maximize the full benefits of Ag, it has to be in the Pb alloy so that it is present in the Pb/PbO_2 layer [15]. Ag forms

an adsorbed species of $AgSO^-_4$ or if there is Mn in the electrolyte, forms an adsorbed species of $AgMnO^-_4$. The two intermediate species ($AgSO^-_4$ and $AgMnO^-_4$) have low conductivities and is not advantageous to the OER but they oxidize to form AgO that catalyzes the OER [30, 31].

Due to the type of anode scales formed peculiar to Zn EW, it is important to allow about three to six months to fully form PbO_2/MnO_2 [32] since the process is slow. Sandblasting, chemical pretreatment and shot peening can be used to prepare the anode surface before Zn EW, but the best and most used method over the long term is sandblasting [33-36]. All these processes seem to aim at making the anode surface rough enough to allow scale adherence. If this is not done, it can cause cathode contamination with Pb and reduce Zn cathode quality. Figure 2.5 shows a cyclic voltammetry scan of a Pb-Ag anode in 1.6 M sulfuric acid at 5 mV/s.

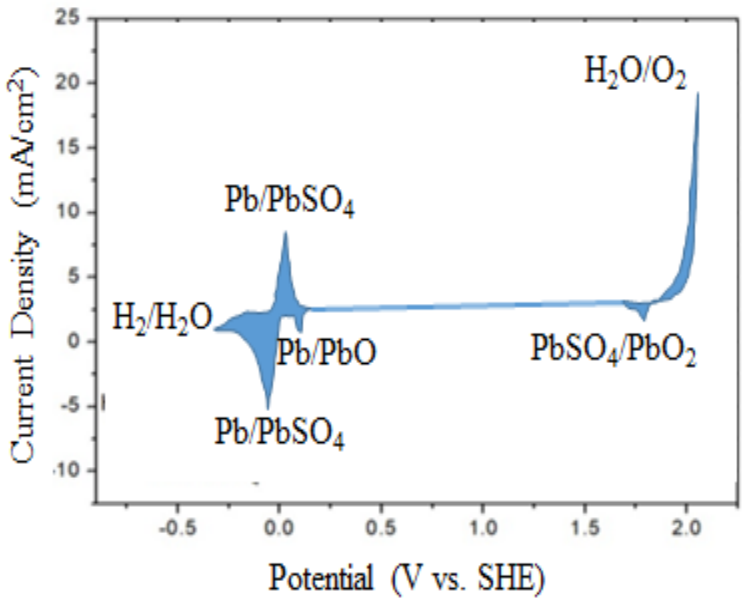

Figure 2.5. Cyclic Voltammetry Scan of a Pb-Ag Anode in 1.6 M Sulfuric Acid at a Scan Rate of 5 mV/s. Modified after [38]

Pb anodes in sulfuric acid under electrical current will go through a series of reactions starting with the Pb forming $PbSO_4$ (non conducting) and the lead sulfate being oxidized to PbO_2 (conducting) [7]. This scan shows the potentials at which various Pb reactions occur. The oxidation evolution reaction (OER) is known to happen only after the potential is high enough to oxidize $PbSO_4$ to PbO_2 [15, 37].

2.2.2. Anode Reactions and Interactions. Lead in contact with sulfuric acid forms $PbSO_4$. Under sufficient voltage, the $PbSO_4$ oxidizes to PbO or PbO_2 and various other phases [38-41]. The various phases affect corrosion resistance and anode potential [6, 7, 38].

Depending on the voltage being applied, a lead oxide scale will form that covers the lead alloy substrate. Various ions in the electrolyte have influences on the system's performance. In the presence of Mn, there may be both a lead oxide scale and manganese oxide scale formed on the anode substrate [8]. It is widely believed that Mn^{2+} in the electrolyte is oxidized to Mn^{4+} (MnO_2), but the mechanism is widely debated. There have been several hypotheses suggesting various intermediates and oxidation states from Mn^{2+} to Mn^{3+}, which in turn disproportionates to Mn^{2+} and Mn^{4+} as shown in Scheme 2 [16, 17, 22, 30, 31, 42-46]. A MnOOH intermediate is said to form [42, 46, 47] as shown in Scheme 2. At lower potential (1.45 V vs. SHE) there is the formation of both MnOOH and MnO_2 as against only MnO_2 formation at higher potentials (>1.55 V vs. SHE) as studied with the electrochemical quartz crystal microbalance (EQCM) with gold and platinum electrodes under conditions similar to Zn EW [48].

Permanganate is believed to be an intermediate species that strongly oxidizes and is able to oxidize other species in the electrolyte to form MnO_2. Permanganate was visually

confirmed within the first few minutes of several lab-scale experiments under conditions similar to ZnEW. Reducing the acidity, increasing temperature, reducing current density, and using new anodes could change the formation of MnO_2 from Mn^{2+} with a permanganate intermediate to directly forming MnO_2 from Mn^{2+} [49]. These hypotheses have not been substantiated due to difficulties in studying the progress of the reaction, characterization, and kinetic measurements. [15] and [17] characterized Mn oxides formed on Pb alloys in sulfuric acids under Zn EW conditions.

Scheme 2

$$Mn^{2+}_{(aq)} = Mn^{3+}_{(aq)} + \acute{e} \tag{2.8}$$

$$Mn^{2+}_{(aq)} = Mn^{3+}_{(aq)} + MnO_{2(s)} \tag{2.9}$$

$$4MnO^{-}_{4(aq)} + 4H^{+}_{(aq)} = 4MnO_{2(s)} + 3O_{2(g)} + 2H_2O_{(l)} \tag{2.10}$$

$$Mn^{3+}_{(aq)} + 2H_2O_{(l)} = MnOOH_{(s)} + 3H^{+}_{(aq)} \tag{2.11}$$

Chlorine is also believed to be oxidized to chlorine gas only at the potential where PbO_2 has been formed, and this oxidation is mass transfer limiting and lowered by the presence of Mn [19]. Kelsall *et al*., (2000) published possible Mn and Cl effects in Zn EW and concluded that MnO_2 on the anode decreases chlorine evolution. The various species of Mn and Cl interact in multiple and sometimes reversible reactions to oxidize and reduce each other [16, 46, 50]. It has been difficult to postulate a concrete reaction mechanism and show proof for the actual Mn-Cl interactions in Zn EW.

2.3. COPPER ELECTROWINNING

Copper is electrowon from copper sulfate - sulfuric acid electrolytes. The KPIs for Cu are energy utilization or consumption, electrode corrosion rates, current efficiency, and cathode product quantity and quality. Future trends will be towards lower energy, increased productivity and improved safety and environmental considerations. Figure 2.6 shows a typical copper EW tankhouse plan view including transformers and rectifiers.

Larger electrodes, longer cells, automation and higher current densities provide better capital effective designs [51]. A common material used for cell construction is polymer concrete to withstand the arduous operating conditions. Cell voltage monitoring with infra-red devices on cranes is being developed to improve short circuit detection. Continuous cathode current measurement that aims at allowing continuous adjustment to produce better cathodes and reduce short circuits has been proposed. These efforts will increase the possibility of fully automating cathode harvesting [52].

Cathodes can be made of stainless steel or copper starter sheets. Edge strips are attached to the sides and bottom of stainless steel blanks to facilitate harvesting. Cathodes have to be cleaned of grease and other organics to reduce the risk of pre-stripping. The cathode may pre-strip and fall off into the cell with serious safety implications. Excess chloride (25-30 ppm) can also corrode (pitting) the stainless steel cathodes leading to ‘stickers’ that make it difficult to harvest the copper off the cathode. Pitted cathode surfaces can be buffed to restore the surface.

Fundamentally, copper in the electrolyte should not be depleted too low as this will cause hydrogen gas formation at the cathode leading to fire and explosion hazards. Chlorine, iron and manganese can build up in the electrolyte and get to deleterious levels

and have to be bled to control their levels. Bleeding can be expensive because of losses of acid and cobalt but several other processes like fixed bed resin ion exchange and precipitation could be employed to recover these compounds [53-57].

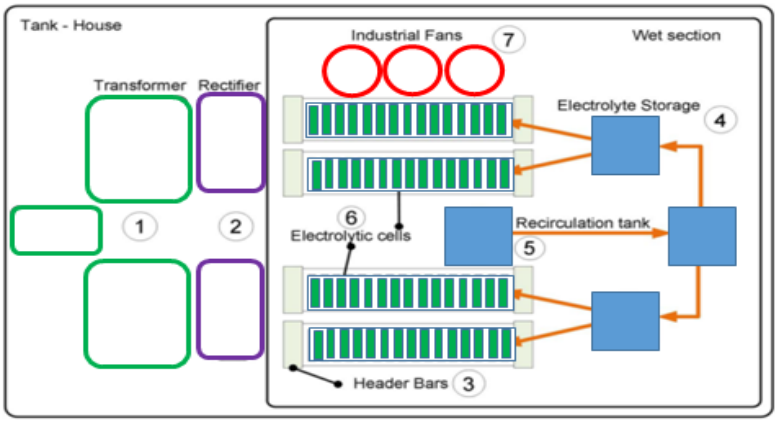

Figure 2.6. Typical Copper Tankhouse Layout Including: 1. Transformers 2. 12 Pulse Rectifiers and Other Entities. Modified after [53]

Acid mist has to be controlled or reduced with mist reduction balls, brushes, hoods, ventilation or surfactants like FC 1100 [58]. Personal protective equipment (PPE) is the last protection resort. Experience with copper tankhouses show that when the acid mist ball layer is thin there is increased localized corrosion that can dissolve the anode at the electrolyte interface and the anode will fall into the cell creating short circuit and fire risks.

The two half cell reactions and the overall reaction are shown in Scheme 3. Copper is reduced at the cathode and water is oxidized at the anode. Harvesting is done every 5-7 days depending on the particular plant, current density and anode to cathode spacing. The anode cathode spacing is critical and hence spacers are placed to maintain the distance. This helps to avoid short circuiting and prevent the anode and cathode from making contact.

Scheme 3

Anode

$$Cu^{2+}_{(aq)} + 2\acute{e} = Cu_{(s)} \qquad E° = 0.337\,V \quad (2.12)$$

Cathode

$$2H^{+}_{(aq)} + 1/2O_{2(g)} + 2\acute{e} = H_2O_{(l)} \quad E° = -1.229\,V \quad (2.13)$$

Overall Main Reaction

$$Cu^{2+}_{(aq)} + H_2O_{(l)} = Cu_{(s)} + 1/2O_{2(g)} + 2H^{+}_{(aq)} \quad E° = -0.892\,V \quad (2.14)$$

Table 2.2 shows typical copper tankhouse operating conditions. EW electrolytes in Africa run at high Co concentrations that come from their natural ores. The anodes and cathodes are placed on several types of cell furniture and contact systems. Furniture helps to align the cells and provide good contacts that reduce stray currents and improve current efficiency and distribution. A few examples of contact systems include dogbone and double double contacts [59]. A trapezoidal hanger with its respective female tooth has been demonstrated to reduce energy consumption by 3 % and avoid open circuits and contact resistance [60].

Organic compounds reduce nodulation, smoothens the copper cathode and prevents short circuiting caused by nodules. The mechanism of preventing nodules on the cathode is that the bulky organic compounds cover high current density points on the cathode surface to allow other points to grow and smoothen. The various ions and impurities in Cu EW electrolytes include Mn, Fe, Cl and Co [61]. Current density is nominally around 300 A/m^2 and temperature is ~50^{o}C. Iron and manganese ions enter the electrolyte through solvent extraction from the leach solution.

Table 2.2. Typical Operating Conditions of Copper Electrowinning [15]

Cathodes	Stainless steel sheets
Copper cathode impurities (mg/L)	Pb (<3), S
Anodes	Rolled Pb-0.08%Ce1.5%Sn plates
Anode life (years)	5
Current Density (A/m^2)	~300
Cell voltage (V)	1.9-2.0
Cathode current efficiency (%)	~92
Energy consumption (MW/hr) cathode	~1.8-1.9
Temperature (°C)	40-50
Cu (g/L)	40-50
H_2SO_4 (g/L)	180
Mn^{2+} (mg/L)	<100
Co (mg/L)	150 (North Americas) 600 (Africa)
Fe^{2+} (g/L)	0.2
Fe^{3+} (g/L)	1.2
Cl (mg/L)	18
Guar gum (g/t)	200

2.3.1. Copper Electrowinning Anodes and Scales. Pb-Ca-Sn alloys are the preferred anode material in Cu EW. Older tankhouses most likely use Pb-Sb anodes due to their advantages [62] whiles newer ones use Pb-Ca-Sn [63]. A critical literature review shows several elements that are added as impurities in the electrolyte or alloying elements

and their effects on anode corrosion, OER potential and other KPIs. Calcium (0.0075 %) provides some strength to the anode alloy since Pb is soft and could fail or creep under its own weight [9]. Ca above 0.08 % increases the likelihood of forming Pb_3Ca that corrodes easily [29]. Tin is added to increase conductivity, reduce corrosion, reduce passivation and prevent PbO formation [9]. Pb-Ca-Sn anodes may contain some minute weights (below 0.1 %) of Co (corrosion resistance and anode potential reduction), Al (anti-drossing to prevent Ca oxidation) and Ag (anode potential depolarization and corrosion rate reduction) to improve the anode properties [64]. Anode lifetime is typically 6 years depending on the current density since increasing the current density translates into decreasing anode lifetime and more frequent cell cleaning which is a consequence of increased anode corrosion.

Pb-Ca-Sn anodes rolled at high temperatures (above 150 °C) produce grain structures having less porosity and increased localized corrosion prevention [29, 65]. The higher the rolling temperature and rolling extent the better the corrosion performance [66] and better reduction in anode potential for the OER [67]. Grain size is inversely proportional to anode corrosion resistance [68]. Rolling affects the microstructure and the anodic electrochemical behavior of Pb-Ca-Sn, Pb-CoO_4 and Pb-W-C anodes [69]. In comparing the characterization scales formed on Pb-Sb, Pb-Ca-Sn and Pb-Co_3O_4 after polarization, they all had similar phases of $PbSO_4$, α-PbO_2 and β-PbO_2 with Pb-Co_3O_4 showing fine grains and a dense structure, Pb-Ca-Sn showing a fibrous structure and Pb-Sb showing loose, spread out coral-like structure [62].

Another study also shows that larger cations ($H^+<Li^+<Na^+<K^+$) increase the ratio of α-PbO_2 to total α-PbO_2 + β-PbO_2 formed while increased electrode thickness and decreased cation size produced decreased ratio of $PbSO_4$ to total α-PbO_2 + β-PbO_2 [70].

The same study mentioned that α-PbO_2 is more compact compared to the more porous β-PbO_2. Corrosion layers with different phases at different potentials built after 24 hours in approximately 400 g/L H_2SO_4 shows the possible phases that can be formed from -0.36 V to 2.14 V vs. SHE (0.64 V vs Hg/H_2SO_4) as seen in Figure 2.7. Contrasting Figure 2.7 to Figure 2.8 which is an Eh-pH diagram of the Pb-H_2O-SO_4 stability system shows consistency. Assuming that the pH of 400 g/L sulfuric acid is below 0, extrapolating the regions for the various phases in Figure 2.8 agrees with that shown in Figure 2.7. Similar consistencies can be observed for both α-PbO_2 and β-PbO_2.

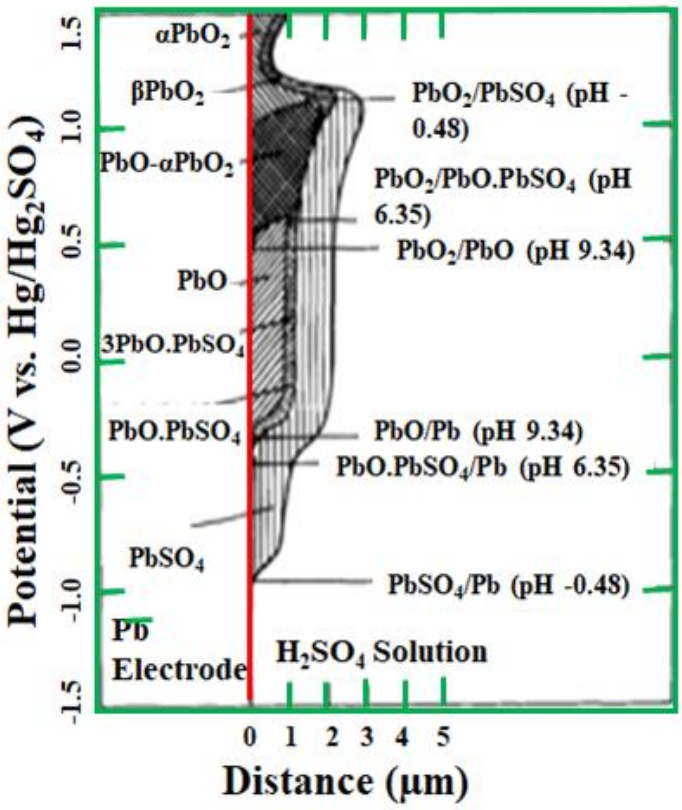

Figure 2.7. Schematic Diagram of Corrosion Layer Created after 24 Hours of Constant Potential Polarization at Approximately 400 g/L Sulfuric Acid Showing Different Phases Formed at Different Potentials. Modified after [37, 40]

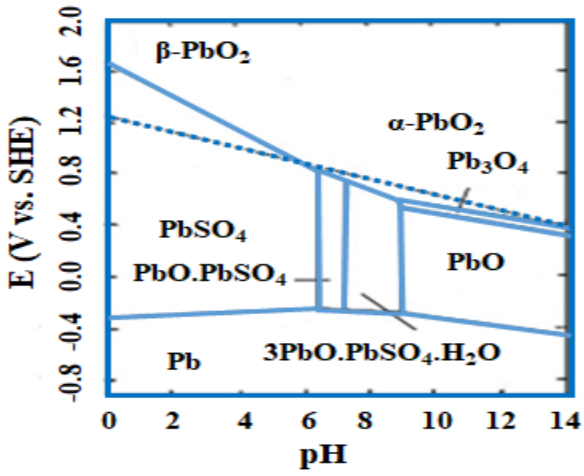

Figure 2.8. Eh-pH Diagram of the Pb-H_2O-SO_4 System. Modified after [15]

2.3.2. Anodic Reactions in Sulfuric Acid. Solutions with 1-10 g/L sulfuric acid and 1-6 g/L Cu after leaching may contain impurities like Mn and Fe. Final electrolytes with between 40-50 g/L Cu and ~180 g/L sulfuric acid is heated and sent to the tankhouse [15]. Mn in copper electrolytes is undesirable without Fe and/or Co. Excessive Mn combined with low electrolyte temperatures causes colloidal MnO_2 particles that impact the cathode quality negatively by being entrapped on the cathode surfaces [53, 55, 56]. Fe reduces the current efficiency by utilizing some of the electrical energy meant for copper platting in the ferric to ferrous reaction. Conversely, ferrous to ferric reactions provides the advantage of reducing the amount of higher oxidation state Mn (like permanganate) in the electrolyte. The minimization or prevention of higher oxidation state Mn means minimal oxidation of the organics in the solvent extraction stages. Oxidized organics have reduced kinetics and forms crud. Ferrous can be oxidized by MnO_4^- in the electrolyte. Ferrous also increases the rate of $PbSO_4$ formation during power outages [37] making the anodes more susceptible to corrosion.

Co reduces both corrosion rates and the overpotential required for oxygen evolution [51, 53-55, 61, 71-74]. The main mechanism behind the advantages Co provides is not well proven. No Co has been characterized on the oxides, scales or cell sludge and hence it is mainly believed to play a catalytic role [75] in the electrolyte. It has been proposed that Co^{2+} is oxidized to Co^{3+} which in turn is reduced by water to form H^{+}, Co^{2+} and O_2 or H_2O_2, Co^{2+} and H^{+} [6, 76]. Two mechanisms, as shown in Schemes 4, and 5, have also been reported in literature. Scheme 4 proposes that Co provides an alternative pathway at a reduced energy requirement [77]. Scheme 5 shows a cyclic catalytic process that produces an unstable Co^{3+} ion that oxidizes water [78] at a lower anode potential. Whichever the mechanism is, it only happens on the PbO_2 scale. The scale is thinner and more tenacious with Co present as shown in Figure 2.9 from initial stages of current application to steady state.

Scheme 4

$$Co^{2+}_{(aq)} = Co^{3+}_{(aq)} + \text{é} \qquad (2.15)$$

$$Co^{3+}_{(aq)} + OH^{-}_{(aq)} = CoOH^{2+}_{(aq)} \qquad (2.16)$$

$$2CoOH^{2+}_{(aq)} = 2Co^{2+}_{(aq)} + H_2O_{(l)} + O \qquad (2.17)$$

$$O + O = O_{2(g)} \qquad (2.18)$$

Scheme 5

$$Co^{2+}_{(aq)} = Co^{3+}_{(ads)} + \text{é} \qquad (2.19)$$

$$4Co^{3+}_{(ads)} + 2H_2O_{(l)} = 4Co^{2+}_{(ads)} + 4H^{+}_{(aq)} + O_{2(g)} \qquad (2.20)$$

Electrochemical response is dependent on anode surface phases, structures formed [46, 79] and electrolyte composition. These parameters determine the corrosion rates, polarization and depolarization, cathode product quality and morphology. Cobalt favors MnO_2 formation at Mn concentration near 2 g/L [46] and also depolarizes the OER and reduces corrosion rates on Pb-Ca-Sn anodes [80, 81]. Due to these advantages, Co concentrations are maintained between 150 and 200 mg/L by addition to electrolytes.

Adding sulfurous acid can also reduce cell voltage and energy consumption [82, 83]. Ferric ions reduce cathode current efficiency but can also reduce the anode potential. Fe (1-2 g/L) lowers solution potential, smooths cathode surface [15], prevents or minimizes the formation of higher oxidation states of Mn [53-55, 80, 81] as mentioned earlier. Industrial tankhouses try to maintain a 10:1 Fe to Mn ratio so that ferrous can reduce permanganate as shown in Scheme 6 [15, 16, 46, 53]. Manganous can reduce permanganate and ferrous can also reduce manganese dioxide as shown in Scheme 6. Generally, the bad effects of Mn can be managed with strategies [53-56, 84] or a wash stage can be incorporated in the SX section to minimize or keep Mn concentration within allowable levels.

Scheme 6

$$3Mn^{2+}_{(aq)} + 2Mn^{7+}_{(aq)} = 5Mn^{4+}_{(s)} \quad \textit{(2.21)}$$

$$Mn^{7+}_{(aq)} + 5Fe^{2+}_{(aq)} = 5Fe^{3+}_{(aq)} + Mn^{2+}_{(aq)} \quad \textit{(2.22)}$$

$$Mn^{4+}_{(s)} + 2Fe^{2+}_{(aq)} = 2Fe^{3+}_{(aq)} + Mn^{2+}_{(aq)} \quad (2.23)$$

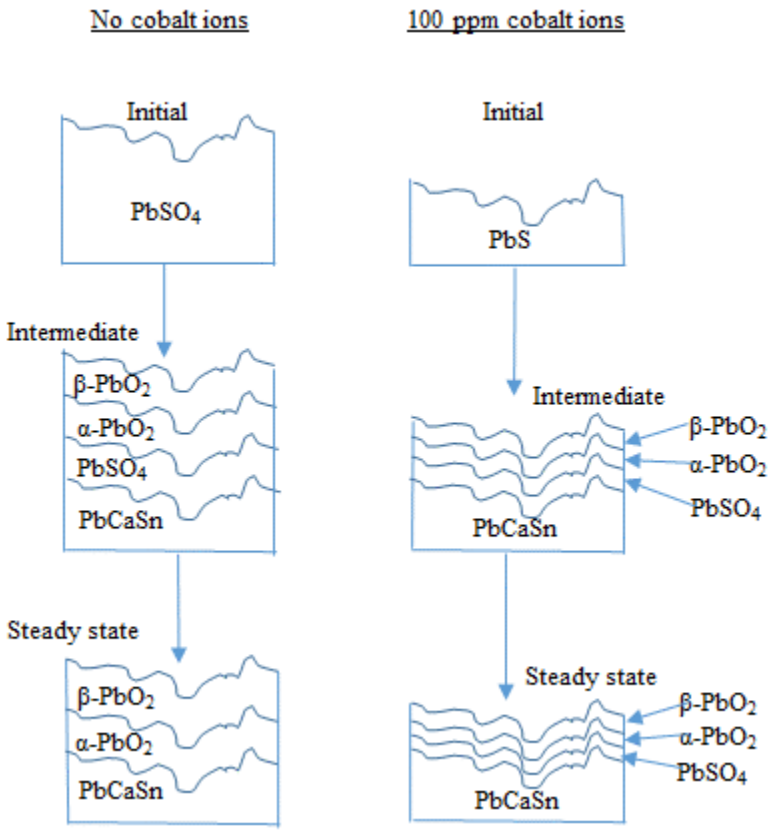

Figure 2.9. Scales Formed With and Without Cobalt from Start to Steady State Showing the Various Phases. Modified after [75]

2.3.3. Electrolyte Conductivity, Current Distribution and Current Efficiency.

Solution conductivity is critical to energy consumption and is proportional to the electrolyte temperature, sulfuric acid concentration and Cu concentration [85, 86]. Lower Cu concentration, higher acid concentration, and higher temperature will increase the solution conductivity.

Current distribution is also critical [52, 60] because when the current is not well distributed there is the likelihood of short circuits since some parts of the cathodes will grow more relative to other parts and this can cause short circuits. Sulfate salts can form

on the hanger bars and other contacts. Stray currents and short circuits should be quickly corrected since they are good indications of bad current distribution.

Current efficiency is calculated from the ratio of the actual weight of electroplated copper to the theoretical weight of copper that could have been plated on the cathode at the same conditions expressed as a percentage [87]. Some of the causes of current inefficiency are auxiliary reactions, short circuits, and stray currents. Temperature, electrolyte flow and ferric ion concentration can also affect current efficiency [87-91]. All these problems lead to bad cathode quality and high short circuit frequency. A current efficiency model estimates the expected current efficiency based on the ferric ion concentration, copper ion concentration and applied current density [89] was developed in 2010 but has limited use outside the tested ranges and under-predicts at current densities below 300 A/m^2. Industrial current efficiencies usually range between 90-95 % due to ferric reduction and dissolved oxygen reduction and shorts circuits [15].

2.3.4. Energy and Power Consumption and Optimization Efforts. Energy consumption and power consumption are both proportional to the cell voltage [92]. Cell voltage in turn consist of anode potential, cathode plating potentials, solution contact voltage and contact voltage. Since EW is an energy intensive process, it is imperative to optimize energy and power consumption to improve the viability of EW operations. Process assessment and optimization is critical in achieving an overall synergistic result. The caveat though, is that energy consumption optimizations may sometimes have side effects and implications on corrosion rates, cathode quality, and productivity.

Optimization efforts include using rolled anodes [67], alternative anode materials [93-97], alternative cathode reactions, alternative anode reaction technology (AART) [82,

92, 98]. Alternative anodes like titanium coated with various precious metal oxides can save about 15 % energy and do not require cleaning and all the problems associated with Pb. The disadvantage about these anodes are that they are expensive and not “self-healing” like Pb. Energy optimization also explores alternative reactions that expend less energy for example plating cupric ions instead of cuprous or oxidizing ferrous ions at the anode instead of water. Ferrous oxidation can reduce energy draw by about 46 % since ferrous is oxidized at approximately half the potential needed for the OER [15]. Anodic ferrous oxidation also does not involve acid mist problems since there is no oxygen evolution. Stainless steel can be used as the anode doing away with the problems associated with Pb including the health and safety of Pb handling. These technologies are yet to be commercialized or have drawbacks that make them inapplicable on the commercial scale.

2.3.5. Cathode Production and Factors Affecting Quality. The preferred growth orientation of copper is (111) followed by (200) and other orientations which changes to (220), (111) *etc.* with the presence of 5 mg/L of Cl [99]. Rene Winand developed a diagram (Figure 2.10) that shows that the morphology and other characteristics of the copper cathode can be controlled by a ratio of the limiting current density to the Cu concentration and the level of inhibition offered to plating [99-101]. In most operations the Cu concentration is mostly constant especially for operations that make commercial electrolyte prior to EW. Therefore, the control parameters for good quality cathodes are the limiting current and inhibition intensity.

This concept and diagram is important in controlling cathode quality and also for trouble shooting cathode quality. Reducing plating inhibition can lead to undesired copper powder production. Additionally, additives like starch, guar, chloride, solvent extraction

(SX) organic, FC-1100 and iron sulfate can also affect the cathode quality [15, 99, 100, 102]. The most pronounced effect seen on the protective PbO_2 layer was found to be from guar and ferric ions [103-105].

Chloride in addition to polyethylene glycol (PEG) is used to suppress deposition or increase the inhibition intensity to produce quality cathodes. Organics are oxidized at the anode and therefore need constant dosing or replenishment. Care must however be taken since organics and/or chlorides can lead to solution line corrosion.

Cathode substrate also plays a role in the cathode quality. Stainless steel is preferred to copper starter sheets because they provide more inhibition and hence higher purity in addition to its ease of maintenance and fewer shorts [106]. The effect of various organics have been reviewed in variation to how Cu crystals are formed with time between Hydrostar, Cyquest N-900 at 2.5 mg/L [99]. There may not be much difference in organics performance but other factors like availability and cost may help the choice of one over the other. DXG-F7 however has the advantage of better/easier dissolution in water [102].

The subsequent sections of this dissertation contains conference papers presented at various conferences and published as conference proceedings and two papers; one submitted to Ghana Mining Journal and a second to be submitted to Hydrometallurgy for publication. It is chronologically ordered and contains one paper on benchscale Mn-Cl interactions in Zn EW and the rest on Cu EW consisting of one paper on the effects of temperature, power outages, Mn and Co concentrations on corrosion and current efficiency, the second paper is on anode potential, energy modelling and optimization in Cu EW.

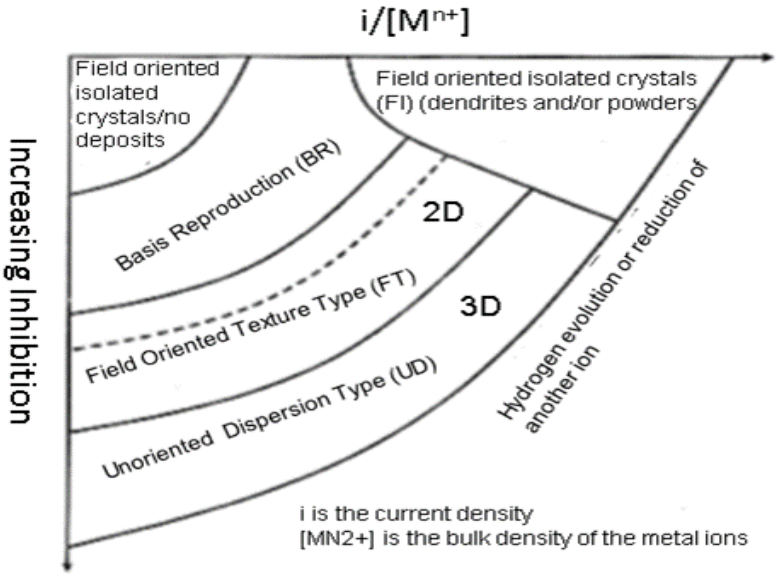

Figure 2.10. Modified Diagram of the Types of Metal Deposits as a Function of Inhibition Intensity and Ratio of Charge Density to Metal Ion Concentration [100, 101]

PAPER

I. EFFECT OF COBALT AND IRON CONCENTRATION ON THE POTENTIAL FOR OXYGEN EVOLUTION FROM PB-CA-SN ANODES IN SYNTHETIC COPPER ELECTROWINNING ELECTROLYTES

C. E. Abbey, and M. S. Moats

Missouri University of Science & Technology

Rolla, MO 65409

Tel:573-308-9236

Email: ceag28@mst.edu

ABSTRACT

It is well known that the addition of cobalt to copper sulfate - sulfuric acid electrolytes decreases the overpotential for oxygen evolution and decreases the rate of corrosion of Pb-Ca-Sn anodes. This effect, however, has not been adequately quantified in the presence of iron and manganese in this type of electrolyte. This work provides quantifiable data on the effect of cobalt concentration in the range of 0 to 0.6 g/L in synthetic electrowinning electrolytes with and without the presence of iron. The effect of cobalt on anode potential was determined using 2 hour and 24 hour chronopotentiometry experiments. As expected, Pb-Ca-Sn potentials increased with decreasing cobalt concentration over the range of 0-0.6 g/L Co with and without the presence of Fe. Two regression models were developed to allow plant operations the ability to predict anode potentials as a function of cobalt concentration with or without iron in the electrolyte.

Keywords: anode potential, copper electrowinning, cobalt, iron, manganese, energy consumption, oxygen evolution.

1. INTRODUCTION

Electrowinning is an imperative determinant of the quality of copper produced [1]. Approximately 30% of the energy consumed during electrowinning is used for anodic reactions, especially oxygen gas evolution [1]. A decrease in the oxygen overpotential and anode oxidation would improve the profitability of copper electrowinning operations. In line with efforts at increasing profitability, cell house design modifications [2] to include more automation, lead alloy variations [3] and cobalt addition [4] have been the foci of electrowinning optimisation research in recent years. These options have been proposed to improve the future of copper electrowinning [5]. Reducing anode potential, energy consumption, and anode corrosion is vital to profitability.

Several reviews have compared different lead alloy [3], coated titanium alloy, and mesh on lead [6-9] anodes. Other non-lead alloys containing titanium have also been compared with lead alloy anodes [10]. Non-lead anodes provide reduced anode potentials but are expensive; hence multi-directionally rolled Pb-Ca-Sn anodes [11] remain the most widely used electrode for many industrial operations.

According to the review by Clancy, Bettles [4], the Pb in the anode reacts with sulfates in the electrolyte to form $PbSO_4$, which has low conductivity, leading to increasing potential under constant current operation. Oxygen evolution occurs after the $PbSO_4$ reacts with H_2O to form either α-PbO_2 [12] or β-PbO_2 [13] depending on the conditions. The

overpotential needed to drive the oxygen evolution reaction is high on lead anodes partly due to the potential needed to form and sustain PbO_2.

Cobalt is known to reduce oxygen overpotential and power consumption, promote higher quality copper and protect lead anodes resulting in longer lifespans. This is true whether it appears in the electrolyte [4, 14-16] or as an alloy in the anode [3]. X-ray Diffraction (XRD) and X-ray Photoelectron Spectroscopy (XPS) characterization of anode surfaces show no Co compounds and indicate that the presence of Co ions do not form a Co film that protects the anode surface from oxidization [14]. This suggests that Co plays a catalytic role in reducing the porosity of the PbO_2 (whether rhombic or tetragonal) layer. This less porous layer is responsible for hindering the oxidation of $PbSO_4$ to PbO_2 [14].

The effect of the Co in the presence of Fe or Mn in the electrolyte has not been sufficiently quantified. The advantages of having about 0.5 g/L Co in the electrolyte have been reported [15] and some have even attempted to explain the mechanism of anode corrosion reduction [15, 17]. Central African ores can produce electrolytes with high [Co] and significant concentrations of manganese and iron. This paper reports quantifiable data on the effects of 0.1 g/L increases in [Co] from 0-0.6 g/L Co on the anode potentials in the presence or absence of Fe in the electrolyte. These conditions are similar to an industrial operation in central Africa.

2. EXPERIMENTAL

All experiments were conducted in an electrolyte (250 mL) with a starting concentration of 170 g/L H_2SO_4, 0.6 g/L Mn, 20 mg/L Cl^- at a temperature of 50°C ± 1°C.

A second batch of tests was performed with the addition of 0.6 g/L Fe (III). In both conditions, cobalt concentrations examined were 0.0, 0.1, 0.2, 0.3, 0.4, 0.5 and 0.6 g/L. Mn and Cl^- concentrations were not controlled during the experiment.

A three electrode cell was used with a Pb-Ca-Sn working electrode with a surface area of ~1 cm^2 placed 3.8 cm from a platinum mesh counter electrode. A mercury-mercury sulfate reference electrode (0.64 V vs. standard hydrogen electrode (SHE), at room temperature, 0.63 V vs. SHE at 50°C) was inserted directly into the cell equidistant from the working and counter electrodes. Electrode potentials are reported versus SHE.

Chronopotentiometry was performed for 2 hours or 24 hours to measure the anode potential of the Pb-Ca-Sn anode as a function of cobalt concentration and to grow anode scale (presumably PbO_2 and MnO_2). A 300 A/m^2 current density was applied based on the measured surface area of each working electrode. Anode potential data was collected every 3 seconds. All experiments were repeated and all measurements presented are averages of at least two runs. There was less than 1% variation between replicates.

3. RESULTS AND DISCUSSION

Pb-Ca-Sn electrodes were operated at 300 A/m^2 in 170 g/L H_2SO_4, 0.6 g/L Mn, and 20 mg/L Cl^- at 50°C ± 1°C. Figure 1 shows a plot of the 24 hour chronopotentiograms with 0.6 g/L Fe. The 2 hour and 24 hour tests and with (MnFeCo) and without Fe (MnCo) reveal that anode potential increases with decreasing cobalt concentration as observed in [15] for different [Co]. The mathematical equations for predicting anode potential at 50°C in 170

g/L H_2SO_4 with and without Fe are given in Eqs. 2 and 3. The correlation coefficient, R^2, for Equations 2 and 3 were 0.915 and 0.715 respectively.

$$y = a + b\,[Co]^n \quad (1)$$

$$MnFeCo \qquad \text{Anode Potential (V vs. SHE)} = 1.928 - 0.135[Co]^{0.32} \quad (2)$$

$$MnCo \qquad \text{Anode Potential (V vs. SHE)} = 1.951 - 0.096[Co]^{0.42} \quad (3)$$

The models can be used to predict anode potential for [Co] over the ranges of 0 to 0.6 g/L Co with or without 0.6 g/L Fe. The data also indicates that Co and Fe individually and jointly reduce the anode potential with the combination giving the highest anode potential decrease. This indicates the possibility of a synergistic interaction between iron and cobalt. While iron appears to reduce the anode potential in these tests, increasing iron concentration also reduces cathodic current efficiency [19]. Overall, the addition of iron to copper electrowinning electrolyte increases energy consumption [21]. Even so, copper electrowinning electrolytes often are maintained with a 8:1 to 10:1 Fe to Mn ratio to avoid the production of high oxidation state manganese species [20].

Reducing the [Co] in the electrolyte increases the anode potential and increases the Mn oxidation rate (cyclic voltammetry data not shown here due to space constraint). Tables 1 and 2 illustrate the effect of reducing [Co] from a baseline concentration (600 mg/L) on power requirements and costs based on the assumptions of a tankhouse with 44,000 A, 156 cells, $0.15/kWh, and a 95 % online factor.

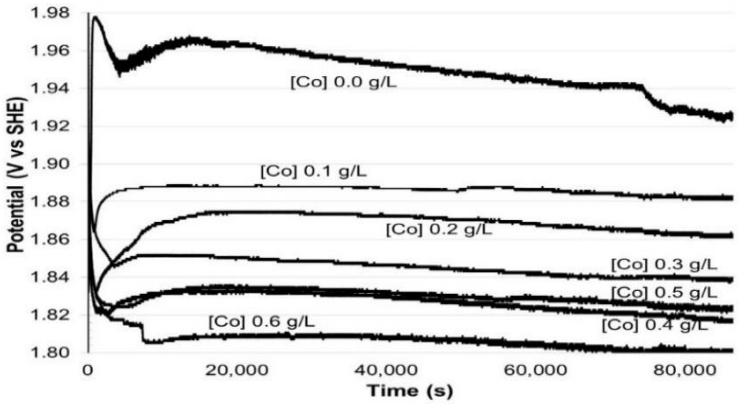

Figure 1. Chronopotentiometry Data for Pb-Ca-Sn Electrode Operated at 300 A/m^2 in 170 g/L H_2SO_4, 0.6 g/L Mn, 0.6 g/L Fe, 20 mg/L Cl^- at 50°C at Various Cobalt Concentrations for 24 hours

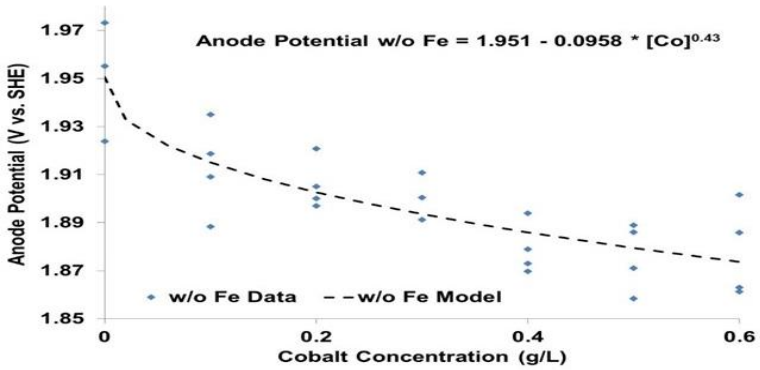

Figure 2. Average Anode Potential for Pb-Ca-Sn over the last 10 Minutes of a 24 hour Experiment and Mathematical Model for Electrolyte versus Cobalt Concentration at 300 A/m^2 in 170 g/L H_2SO_4, 0.6 g/L Mn, 20 mg/L Cl^- at 50°C without Fe

The empirical formulae are valid over the range of 0.0 to 0.6 g/L cobalt concentrations. Hence, the anode potential can be estimated to evaluate electrical costs as a function of cobalt concentration to make informed decisions about operating a tankhouse.

These values are vital for an operation considering lowering their cobalt concentration. The cost involved can be compared with profit from extra cobalt recovered sales to make a decision.

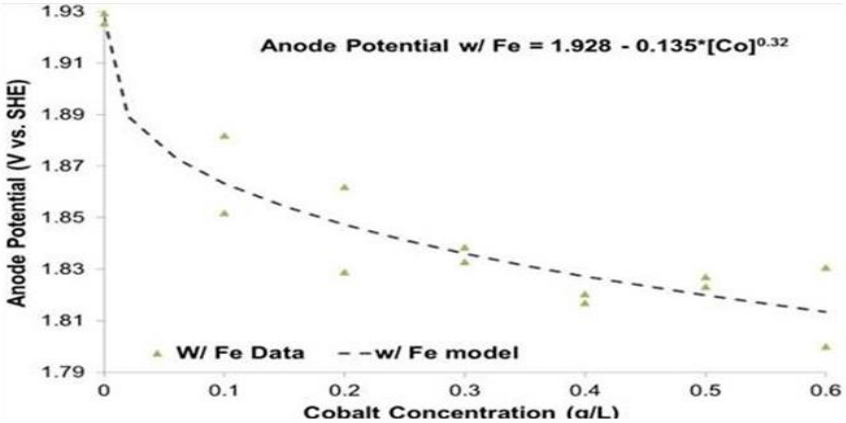

Figure 3. Average Anode Potential for Pb-Ca-Sn over the last 10 Minutes of a 24 hour Experiment and Mathematical Model for Electrolyte versus Cobalt Concentration at 300 A/m^2 in 170 g/L H_2SO_4, 0.6 g/L Mn, 20 mg/L Cl- at 50°C with 0.6 g/L Fe

Table 1. Added Electrical Power Requirement and Power Costs Projected to be caused by Lowering the Cobalt Concentration in Electrolyte from 600 mg/L with 0.6 g/L Fe

Cobalt Concentration (mg/L)	Added Power Requirement (kW)	Added Power Cost ($/year)
600	0 (base case)	0 (base case)
500	44	56,000
400	96	119,000
300	156	195,000
200	233	290,000
150	281	351,000
100	343	428,000

Table 2. Added Electrical Power Requirement and Power Costs Projected to be caused by Lowering the Cobalt Concentration in Electrolyte from 600 mg/L without 0.6 g/L Fe

Cobalt Concentration (mg/L)	Added Power Requirement (kW)	Added Power Cost ($/year)
600	0 (base case)	0 (base case)
500	40	50,000
400	85	105,000
300	136	170,000
200	198	248,000
150	237	296,000
100	283	354,000

4. CONCLUSIONS

Results of experiments examining the effect of cobalt concentration on Pb-Ca-Sn anode potential under typical copper electrowinning conditions have been provided. The results show that the anode potential increases with decreasing cobalt concentration with or without the presence of 0.6 g/L Fe for the [Co] tested. Empirical equations were developed to allow the prediction of anode potentials as a function of [Co] between 0-0.6 g/L when there is Fe in the electrolyte or not. The results indicate that Co, Fe and Mn are likely interacting at or near the anode surface. This interaction should be studied further.

ACKNOWLEDGEMENT

The financial support and permission to publish these results given by the AMIRA Project P705C is highly appreciated. We also immensely appreciate the help of Margaret Scott and Kevin Foster for their experimental assistance.

REFERENCES

1. Tjandrawan, V., *The Role of Manganese in the Electrowinning of Copper and Zinc*, in *School of Chemical and Mathematical Science*. 2010, Murdoch University. p. 153.

2. Robinson, T., et al. *Developments in base metal electrowinning cellhouse design*. in *TMS Annual Meeting*. 2012.

3. Hrussanova, A., L. Mirkova, and T. Dobrev, *Electrochemical properties of Pb–Sb, Pb–Ca–Sn and Pb–Co3O4 anodes in copper electrowinning.* Journal of applied electrochemistry, 2002. 32(5): p. 505-512.

4. Clancy, M., et al., *The influence of alloying elements on the electrochemistry of lead anodes for electrowinning of metals: a review.* Hydrometallurgy, 2013. 131: p. 144-157.

5. Moats, M. and M. Free, *A bright future for copper electrowinning.* JOM, 2007. 59(10): p. 34-36.

6. Kawaguchi, K., G.M. Haarberg, and M. Morimitsu, *Nano-Architecture on the Mud-Cracked Surface of IrO2-Ta2O5 Binary System.* ECS Transactions, 2010. 25(33): p. 67-73.

7. Kawaguchi, K. and M. Morimitsu, *Effects of Oxide Composition on Structure, Surface Morphology, and Oxygen Evolution Behaviors of IrO 2-Ta 2 O 5/Ti Anodes Prepared at a High Temperature.* Electrochemistry, 2015. 83(4): p. 256-261.

8. Morimitsu, M., *Performance and Commercialization of the Smart Anode, MSA™, for Environmentally Friendly Electrometallurgical Process.* Electrometallurgy 2012, 2012: p. 49-54.

9. Zhang, T. and M. Morimitsu, *A Novel Oxygen Evolution Anode for Electrowinning of Non-ferrous Metals.* Electrometallurgy 2012, 2012: p. 29-34.

10. Cifuentes, L., A. Montes, and G. Crisóstomo, *Corrosion behaviour and catalytic effectiveness of Pb–Ca–Sn, RuO2–IrO2/Ti and IrO2–Ta2O5/Ti anodes for copper electrowinning.* Corrosion Engineering, Science and Technology, 2011. 46(6): p. 737-744.

11. Yang, J., et al., *Effect of rolling technologies on the properties of Pb-0.06 wt% Ca-1.2 wt% Sn alloy anodes during copper electrowinning.* International Journal of Minerals, Metallurgy, and Materials, 2015. 22(11): p. 1205-1211.

12. Ivanov, I., et al., *Insoluble anodes used in hydrometallurgy: Part I. Corrosion resistance of lead and lead alloy anodes.* Hydrometallurgy, 2000. 57(2): p. 109-124.

13. Zhang, W. and G. Houlachi, *Electrochemical studies of the performance of different Pb–Ag anodes during and after zinc electrowinning.* Hydrometallurgy, 2010. 104(2): p. 129-135.

14. Nguyen, T. and A. Atrens, *Influence of lead dioxide surface films on anodic oxidation of a lead alloy under conditions typical of copper electrowinning.* Journal of Applied Electrochemistry, 2008. 38(4): p. 569-577.

15. Nguyen, T., et al., *Influence of cobalt ions on the anodic oxidation of a lead alloy under conditions typical of copper electrowinning.* Journal of Applied Electrochemistry, 2008. 38(2): p. 215-224.

16. Yu, P. and T.J. O'Keefe, *Evaluation of lead anode reactions in acid sulfate electrolytes II. Manganese reactions.* Journal of the Electrochemical Society, 2002. 149(5): p. A558-A569.

17. Gendron, A., V. Enel, and S. Abe, *Effect of cobalt added to electrolyte on corrosion rate of Pb-Sb anodes in copper electrowinning.* Canadian Metallurgical Quarterly, 2013.

18. Miller, G., *Methods of managing manganese effects on copper solvent extraction plant operations.* Solvent Extraction and Ion Exchange, 2011. 29(5-6): p. 837-853.

19. Khouraibchia, Y. and M.S. Moats, *Evaluation of the effect of copper electrowinning parameters on current efficiency and energy consumption using surface response methodology.* ECS Transactions, 2010. 28(6): p. 295-306.

20. Miller, G., *The Problem of Manganese and Its Effects on Copper SX-EW Operations, Paper from Copper 95, Volume III, Electrorefining and Hydrometallurgy of Copper, International Conference held in Santiago, Chile, November 26-29, 1995.* Papers, 1995: p. 649-663.

II. MANGANESE CHLORIDE INTERACTIONS ON PB-AG ANODE BEHAVIOR IN SYNTHETIC SULFURIC ACID ELECTROLYTES

C. E. Abbey, W. Jin and M. S. Moats

Missouri University of Science & Technology

Rolla, MO 65409

Tel:573-308-9236

Email: ceag28@mst.edu

ABSTRACT

Manganese in electrolyte has both beneficial and detrimental effects in Zn electrowinning. Mn oxidizes to form MnO_2 on Pb-Ag anodes, cell walls and pipes. MnO_2 reduces anode corrosion but also leads to short circuiting and maintenance issues. MnO_2 is thought to interact with chloride ions and produce oxidized chlorine species. The interactions between Mn and Cl are not well understood. Therefore, two sets of 45+ day bench scale experiments were conducted to investigate the effects of the manganese to chloride ratio on anode corrosion rate and electrolyte chemistry using rolled Pb-Ag anodes. Daily manganese and chloride losses from the electrolyte appeared to be correlated. Increasing the average Mn/Cl^- ratio from ~7:1 to ~11:1 reduced the anode corrosion rate. Increasing the ratio above 11 did not reduce the corrosion rate further. Anode scales produced with Mn/Cl- ratios at and above 11:1 contained some γ–MnO_2 while scales formed with ratios less than 11:1 did not.

Keywords: manganese, chloride, zinc, electrowinning, anode corrosion, anode scales, electrolyte composition.

1. INTRODUCTION

The electrolytic recovery of zinc (Zn) is a well-known process and is estimated to have produced approximately 13.7 million tons of Zn in 2017 [1]. The main anode reaction in Zn electrowinning is the evolution of oxygen. In addition to the main reaction, Mn^{2+} ions in the electrolyte are oxidized at the anode to form insoluble MnO_2 or MnOOH and/or soluble Mn^{3+} and MnO^{4-}. Chloride ions also can oxidize to form chlorine gas and other oxidized chlorine species.

The range of Mn concentrations in industrial zinc electrowinning electrolytes has been reported to be 2-10 g/L [2]. Apart from being an impurity in the feed source, Mn is also added to Zn electrolytes to serve as an oxidizing agent during solution purification. The presence of Mn^{2+} ions during zinc electrolysis has been shown to reduce the oxygen evolution overpotential and rate of anode corrosion of commonly used lead-silver alloy anodes [3-5]. The presence of Mn^{2+} in the Zn electrolyte has also been shown to promote the formation of MnO_2 on the anode surface [6], which reduces the rate of lead alloy corrosion and the contamination of the zinc cathode. However, excessive amounts of MnO_2 on the anode surface have a tendency to break away into the electrolyte bulk. Therefore, the anodes must be periodically cleaned to remove the anode scale. Otherwise, the anode scale could result in increased ohmic resistance and short-circuiting between anode and cathode. Finally the disproportionation of Mn^{3+} leads to the formation of MnO_2 and Mn^{2+}

which promotes the formation of cell mud and formation of scales on cell walls and into cellhouse piping [7, 8].

Chloride (Cl^-) anions (1-500 mg/L) can also affect anode corrosion [9]. However, Cl^- ions have been reported to have little effect on corrosion without the presence of Mn^{2+} ions [9]. Zn deposition is depolarized in the presence of Cl^- ions and this can affect the preferred orientation of Zn deposited [10].

The interaction between Mn and Cl- during zinc electrolysis is not fully understood. This paper therefore examined various concentrations of Mn and Cl ions in industrially applicable ranges using bench scale electrolysis tests to assess their interactions on anode scale formation and corrosion rates of Pb-Ag anodes.

2. EXPERIMENTAL

A bench scale anode corrosion system consisting of four or five 12 L cells was utilized. Each cell had two rolled Pb-0.45% Ag anodes connected to copper header bars using brass screws. The anodes were sandblasted with 70 grit Al_2O_3 prior to operation. Anodes were sheared by a sponsor and had slightly different sizes, which caused variation in current density. Each cell used three Al cathodes with Al header bars and Al screws. The aluminum cathode materials were water jetted from fresh commercial blanks and had ~450 cm^2 of submerged area per electrode.

Cells were connected electrically in series and electrodes of the same polarity were in parallel within a cell. 25 amps of dc current were supplied to the system using a BK Precision Model 1694 DC power supply. The average anodic current density was 470 A/m^2

(+/-15%). Cathode and anode currents were measured daily using a clamp-on ammeter to monitor current distribution.

Each cell had its own electrolyte and electrolyte reservoir. The cells contained 12 L of electrolyte and the reservoirs had 4 L making the total volume of electrolyte 16 L. The electrolyte was sulfuric acid based with various chloride and manganese concentrations to examine different manganese to chloride (Mn/Cl) ratios. Mn/Cl ratios are calculated and presented on a gram per liter basis unless otherwise noted. Analytical grade sulfuric acid, sodium chloride and manganese sulfate pentahydrate were used in electrolyte preparation. Electrolyte flow rate to each cell was ~150 mL/min per cell using a multichannel peristaltic pump. Electrolyte overflowed from a cell was returned to a reservoir. Make up water was added to the reservoir using a secondary pump to replace losses for evaporation and water decomposition. The cells were operated in a water bath with immersion heaters and a circulation pump. Temperature control of 38 °C +/- 4 °C was achieved with most data between +/- 2 °C.

Two long term corrosion tests were performed. The first test (Module One) used electrolyte with similar chloride concentrations and various manganese concentrations to generate different Mn/Cl ratios. The second test (Module Two) used similar Mn concentrations and various chloride concentrations to generate Mn/Cl ratios similar to those tested in Module One. In Module One, five cells were used. In Module Two, four cells were used.

The solution volume was maintained by adding distilled deionized water, and solution analyses for H_2SO_4, Cl^-, total Mn, Mn^{2+} and Mn^{3+} were performed daily. A Metrohm Auto-Titrator was used to analyze Mn^{2+}, Mn^{3+}, H_2SO_4 and Cl^- concentrations.

Total [Mn] was measured using a Thermo-Fisher ICE 3000 series Atomic Adsorption Spectrometer (AAS). Prior to analysis, all solution samples were filtered using a 0.45 micron syringe filter. Analytical details can be provided upon request.

For both Modules One and Two, all cells were operated at the same Mn/Cl to "pickle" the anodes before adjusting the electrolyte to the intended Mn/Cl ratios. At the start of each test, the electrolyte was 160 g/L H_2SO_4 with a Mn/Cl ratio of 11 ([Mn] = 3.3 g/L and [Cl^-] = 300 mg/L). Anode pickling occurred for at least 9 days of stable operation at an anodic current density of ~470 A/m^2. Electrolyte compositions were monitored daily. Chemicals were added to the electrolyte to return the solution to its original concentrations on a daily basis.

2.1. MODULE ONE

Following pickling, the cells were re-started and the electrolyte allowed to change by either adding Mn or not replacing Mn while returning the chloride concentration to 300 mg/L after each day of operation. The daily starting manganese concentration targets were 1.5 g/L, 2.1 g/L, 2.7 g/L, 3.3 g/L and 3.9 g/L to obtain Mn/Cl ratios of 5, 7, 9, 11 and 13, respectively. At the end of each experiment, dried anode weights were measured. Anode scales were also characterized using x-ray diffractometry (XRD).

2.2. MODULE TWO

After pickling, the cells were re-started and the electrolyte concentrations changed to target Mn/Cl ratios of 13, 11, 9 and 7. Mn concentration was targeted at 3.3 g/L in all four cells while [Cl^-] was aimed to be 0.254 g/L, 0.300 g/L, 0.367 g/L and 0.471 g/L,

respectively. Electrolyte samples were taken, filtered, analyzed and used to control the system on a daily basis. The anodes and cathodes were weighed before the start of the system and reweighed after each stage to determine corrosion rates.

3. RESULTS AND DISCUSSION

The bench scale tests to examine manganese to chloride ratios in sulfuric acid electrolytes on anode corrosion and scale formation were challenging to operate and control. The electrolyte composition changed daily requiring significant chemical additions. Even so, interesting findings were produced and are presented to assist future researchers in the field. The results are discussed based on Module. In Module 1, chloride was maintained as consistently as possible among the cells. In Module 2, manganese concentrations were similar among cells.

3.1. MODULE ONE

The initial loss of chloride during the first two hours of operation was monitored and found to be quite high. This was not unexpected based on industrial observations where new anodes promote chlorine evolution for a short period of time. Average chloride loss from new sandblasted Pb-0.45% Ag anodes in the first two hours of operation was calculated at 252 g/day/m^2 of anode or 21 g/kAhr. Once the anodes were covered with manganese oxide and the system was under control, chloride loss was 27.2 g/day/m^2 of anode or 2.3 g/kAhr in Module One pickling.

The losses of Mn and Cl^- from the electrolytes were not equal. The data indicated the Mn/Cl ratio generally increased during the course of each day of operation. The average Mn/Cl ratio at the end of each operating day was 13.2 over the last six days of pickling. As the Mn/Cl ratio was returned to 11 after each day, the Mn/Cl ratio varied between 10.6 and 15.2 during the last six days of pickling with an average (calculated by assuming a linear behavior of Mn and Cl^- loss versus time) ratio of 12.1. There was no statistical difference in electrolyte composition among the five cells during pickling in Module 1.

Another way to examine Mn/Cl loss is to determine if one ion is preferentially removed. The starting Mn/Cl ratio on a mole basis of the electrolyte is 7.1 (0.060 M Mn/0.0085 M Cl^-). The molar ratio of Mn loss/Cl loss during the last six days of pickling was 3.6 (range 2.5 to 4.8). Even though more Mn is lost than Cl^- during electrolysis, given the initial ratio of Mn and Cl^- in the electrolyte (recall the electrolyte is returned to Mn/Cl = 11 on a g/L basis every day), Cl^- appeared to be preferably lost during pickling on a molar basis.

The loss of Mn from the electrolyte occurred by the formation of anode and cell mud. MnO_2 formed on all internal surfaces of the system (anodes, walls, tubes, etc.). This required that the tubes be cleaned twice a week to insure adequate electrolyte flow. The tubing was cleaned using a sulfuric acid/hydrogen peroxide mixture. The cleaning solution was not returned to the testing system. Chloride loss was presumed to have occurred by the formation of chlorine gas or perchlorate ion, but this was not validated during the study. Given the size and complexity of the testing system, a complete mass balance was not achievable for either manganese or chloride.

Anodes from cells 1, 2, 4 and 5 exhibited large-flaky scales that were loosely adherent. The anode from cell 3 had a more adherent scale. Samples of scale were collected from one anode in cells 3, 4 and 5 after pickling. The scale samples were examined by XRD. XRD patterns are not shown but are available upon request.

MnO_2 was detected and phase determination was attempted but was challenging. Alpha (α)-MnO_2 (JSDS 030-0820) and epsilon (ε)-MnO_2 (JSDS 044-0141) have many of the same peaks. ε-MnO_2 has a peak at 29°, which α-MnO_2 does not exhibit. Thus, in most samples which are characterized as ε-MnO_2, it is possible that α-MnO_2 is also present. In this document, most MnO_2 appears to be ε-MnO_2 because of the peaks at 29° and 37°. However, the presence of α-MnO_2 cannot be ruled out. Most electrolytic manganese dioxide (EMD) literature discusses the presence of ε-MnO_2 and α-MnO_2. Determination of these phases is based on characteristic peaks at 29° for ε-MnO_2 and 37° for α-MnO_2. A broad peak at 22° in several samples indicates the presence of γ-MnO_2.

Using this methodology, the scale samples from pickling were analyzed. Each sample reveals the peaks for ε-MnO_2. One sample from cell 3 also showed peaks for Mn_2O_3. The samples from cells 4 and 5 reveal the broad peak at 22° indicating the presence of γ-MnO_2. As these anodes experienced similar Mn/Cl ratios (Cell 3 average = 12.1, Cell 4 average = 11.7, Cell 5 average = 11.5), the scales are expected to be similar. The predominant phase appears to be ε-MnO_2 with minor amounts of γ-MnO_2 or Mn_2O_3. Mud samples from the bottom of cells 3 and 5 were also analyzed by XRD. The patterns match those of pyrolusite, which is β-MnO_2.

Following pickling, the electrolyte composition was altered to target different Mn/Cl ratios. The average values were calculated assuming linear depletion (e.g. [average

analysis + target ratio]/2). Based on this analysis, the average Mn/Cl ratio experienced by the anodes were 5.8, 8.7, 11.6, 14.3, and 17.7. More detailed data regarding the ranges in Mn, Cl and Mn/Cl experienced can be estimated using data in Tables 1 and 2.

Mn^{2+} and Mn^{3+} concentrations and the calculated Mn losses are summarized in Table 1. The data indicates that Mn^{3+} increased with increasing total Mn concentration. The percentage of the total Mn in solution that was Mn^{3+} was fairly consistent at 4-8% with an average of 5.4% during steady state operation of the cells. It is believed that the Mn^{3+} concentration is controlled by the kinetics of oxidation of manganese at the anodes and the disproportionation reaction to form Mn^{2+} and the MnO_2 on the cell walls, anode and tubing [7]. The percent Mn^{3+} was found to be similar to an industrial cellhouse of one of our sponsors. There was no obvious correlation between [Mn] and Mn loss in the electrolytes in the system. Cell 3 routinely had the highest Mn loss, but no physical reason could be assigned for the cause of this observation. Statistically, Mn loss from the electrolyte did not correlate to [Mn]. This observation does not match industrial observations that scale formation increases with increasing Mn concentration.

The measured chloride concentrations were intended to be similar among the five cells and this was achieved as shown in Table 2. From the chloride measurements, the daily chloride loss was calculated and is also presented in Table 2. The chloride loss during corrosion testing was 2-3X higher than during pickling. This result was unexpected and is not understood. Interestingly, Mn loss during corrosion testing was similar to that observed during pickling. The data from the corrosion system indicates that chloride loss was not dependent on the Mn/Cl ratio used during testing. A correlation was found between the chloride loss and manganese loss from each electrolyte during corrosion testing in Module

1 as shown in Figure 1. The Mn loss was on average three times greater than the chloride loss on a weight basis (1.9 on a molar basis). Given that the weight ratio of Mn to Cl was 5.8 to 17.7, it still appears that Cl loss is preferred over Mn loss as indicated in the pickling portion of the testing.

Anode corrosion was examined quantitatively by weight loss and qualitatively by visual examination of the surface after the corrosion test (15 days of pickling, 45 days of operation at different Mn/Cl ratios). The anode plates were weighed before and after corrosion testing. Scales were removed from the anode using a peer reviewed procedure [11]. The corrosion data (see Fig. 2) reveals that when the average Mn/Cl ratio was 11 or above the corrosion rate was nearly half the rate when the average Mn/Cl ratio was 9 or less. The data appear to indicate that increasing the Mn/Cl ratio above 11 does not provide significant corrosion reduction. Large indentations are observed on all anodes, indicating pitting was probably occurring to some degree on all anodes.

Samples of anode scale and cell mud were collected and examined by XRD. XRD patterns are not shown but are available upon request. The anode scales sampled after 40 days of operation and examined using XRD shows that samples from cells 1 and 2 (average Mn/Cl ratios of 5.8 and 8.7, respectively) show signs of $PbSO_4$ and ε-MnO_2. Samples from cells 3, 4, and 5 (average Mn/Cl were 11.6, 14.7 and 17.7, respectively) also show signs of $PbSO_4$ and ε-MnO_2 along with trace amounts of γ-MnO_2. The lack of PbO_2 and the strong presence of $PbSO_4$ may indicate a problem with scale sampling. Based on the XRD of scale samples, it appears that average Mn/Cl ratios greater than 11 produced ε-MnO_2 with some γ-MnO_2 while those that operated at average Mn/Cl ratios less than 9 produced only ε-MnO_2.

Table 1. Summary of Mn (II) and Mn (III) as a Function of Target Mn/Cl

Cell	Target Mn (g/L)	Mn (II) Concentration (g/L)			Mn (III) Concentration (g/L)			Mn Loss g/day/m^2 (g/kAhr)		
		Min	Ave	Max	Min	Ave	Max	Min	Ave	Max
1	1.5	0.6	1.0	1.2	0.05	0.08	0.22	64.5 (5.9)	138.7 (12.6)	172.2 (15.7)
2	2.1	1.3	1.6	1.8	0.06	0.10	0.23	54.0 (5.4)	120.6 (12.0)	188.3 (18.8)
3	2.7	1.7	1.9	2.1	0.08	0.12	0.25	132.0 (12.8)	186.0 (18.0)	236.4 (22.9)
4	3.3	2.3	2.7	3.0	0.13	0.17	0.24	42.1 (3.7)	114.4 (10.1)	225.5 (20.0)
5	3.9	2.7	3.1	3.7	0.16	0.19	0.25	7.0 (0.7)	147.3 (14.1)	267.8 (25.6)

Table 2. Measured Cl Concentrations and Calculated Chloride Loss

Cell	Average Mn/Cl	Cl^- (mg/L)			Cl^- Loss (g/day/m^2)		
		Min	Ave	Max	Min	Ave	Max
1	5.8	89	170	231	34	49	65
2	8.7	95	164	220	14	44	60
3	11.6	100	145	180	12	52	70
4	14.3	105	172	213	14	45	61
5	17.7	95	159	222	14	48	67

Thus a Mn/Cl ratio above a certain value appeared to produce a different MnO_2 scale. Visual inspections of anodes after 40 days of corrosion testing shows that the anodes

from cells 1-3 exhibited a black scale. The scale on anodes from cells 4 and 5 were more gray or brownish in color. Thus, it appears that the Mn/Cl ratio affected the color of the scales formed in the corrosion tests.

Scales were removed from the anodes by brushing after day 26 and day 45. The scale weight and Mn/Cl ratio or Mn concentration did not correlate. This was unexpected and not fully understood. During scale collection, the following observations were made:

1) Scales on anodes in cells 1 and 3 were easily removed with a soft plastic brush.

2) The rinse water from cells 1 and 3 anodes exhibited a vivid violet hue indicating the likely presence of permanganate.

3) The scales on anodes from cells 2, 4, and 5 were adherent. The rinse water was brownish and not violet.

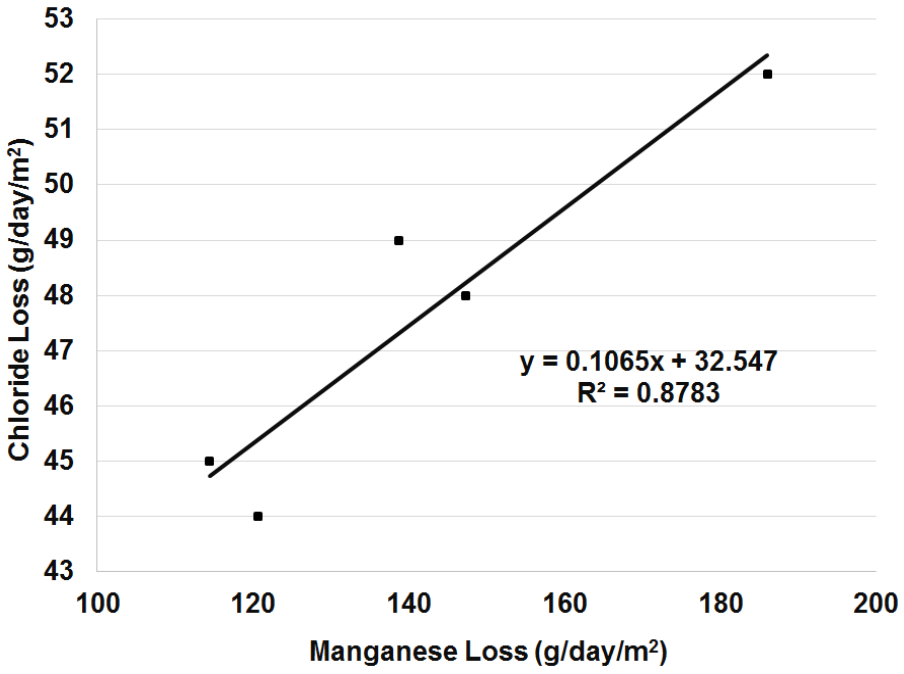

Figure 1. Graph of Cl^- Loss Versus Mn Loss from Electrolyte During Module 1

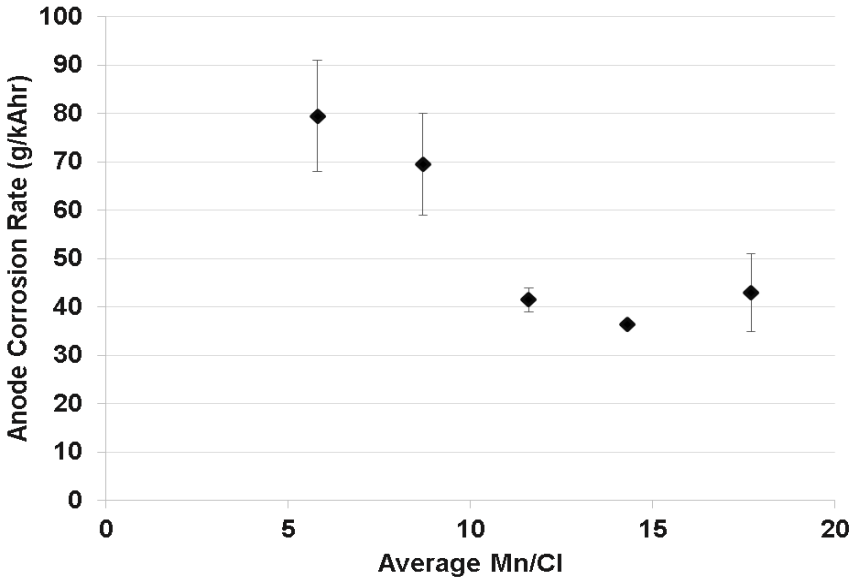

Figure 2. Plot of Anode Corrosion vs. Average Mn/Cl Ratios

3.2. MODULE TWO

Anodes were pickled for 21 days to pre-condition them for later testing. The initially clear electrolyte turned pink within minutes of applying current. This is an indication that Mn^{3+} again formed very quickly. Daily Mn^{3+} measurements were around 5 % of the total Mn as with Module 1. The targeted Mn/Cl set point for all four cells during pickling was 11:1. The Mn/Cl ratios varied from 7 to 15, with average Mn/Cl ratios during pickling between 9.2 and 11.4 as summarized in Table 3.

After pickling, the chemical concentrations were adjusted to target different Mn/Cl ratios in each cell. Cells 1, 2, 3 and 4 were adjusted to target ratios of 13, 11, 9 and 7, respectively. Table 3 shows the minimum, maximum and average ratios of each cell that was achieved. Mn^{3+} concentrations were between 20 and 160 mg/L and were 2-4% of the total Mn measured, which was slightly below previously measured values, but similar.

After trial one, the cells were turned off and the anodes pulled out immediately into a container. A bright purple solution dripped from the anodes in Cell 2. The solution is believed to contain permanganate ions.

Table 3. Minimum, Maximum and Average Mn/Cl Ratios for the Individual Cells During the Module Two – Pickling, Trail One and Trail Two

Cell	Mn/Cl Ratio – Module Two									Corrosion Rates, anode (g/kAhr)
	Pickling			Trail One			Trail Two			
	Min	Max	Ave.	Min	Max	Ave.	Min	Max	Ave.	
1	8.4	14.8	10.7	8.6	20.4	12.2	9.0	27.0	13.0	5.9, 7.8
2	6.6	13.1	9.2	8.0	14.6	10.9	8.7	20.6	11.1	4.4, 9.1
3	8.4	15.0	11.4	6.3	12.4	9.1	2.1	13.1	8.9	5.9, 9.0
4	7.7	14.7	11.0	5.1	12.4	7.2	5.9	12.9	7.7	6.6, 10.2

After trial one, the anodes were rinsed and sampled for scale characterization according to Chen and Dutrizac's published procedure [11]. The anodes were rinsed with excess DI water to remove as much entrained electrolyte as possible. The anodes in cells 1 and 2 had a bright silver gloss at the surface of the anodes. Cells 3 and 4 had a less shiny gloss to the anodes. The scales looked very different than the scales produced by Module One cells. Anode scales were characterized using XRD after sampling at the top, middle and bottom into a composite sample for each face of the anode. The scale samples were dried in an oven at 105 °C for 12 hours. XRD patterns for the anode scales show 3 phases - $PbSO_4$, PbO_2 and a Mn bearing phase - for each cell. The manganese bearing phase fits

the XRD pattern of MnO_2 and coronadite ($Pb_{1.4}Mn_8O_{16}$). Based on the glossy/shiny appearance of the scale, it is possible that a non-common scale phase could have been formed in the test. Further analysis is needed to confirm the presence or absence of coronadite. As such, no comment can be made on the scale phase based on Mn/Cl ratio from this module.

Cell bottom sludge samples were also sampled. Sludge samples were observed to contain only anglesite ($PbSO_4$) in all four cells. MnO_2 was not detected in the cell sludge. The amount of cell mud generated in this experiment was significantly less than that found in Module One.

After anode scale samples were collected following trial one, the anodes were re-inserted into the cells and trial two was conducted. The anodes were operated for a total of 21 days in trial two. Table 4 shows the minimum, maximum and average Mn/Cl ratios for the cells. Mn^{3+} concentrations showed values between 30 and 100 mg/L. This translates to about 4 % of total [Mn]. Total [Mn] was generally between 2.5-3.5 g/L.

Trial two produced even more distinct and clear evidence about the shiny nature of the scale and how it varied with respect to the cells. Cell 1 was the shiniest and Cell 4 was the least shiny. Visual observations of the scales showed that the higher Mn/Cl ratio scales (Cells 1 and 2) had some silver color, were thicker and easier to physically remove than with the lower ratios. The anode appearances in Module 2 were dramatically different from those in Module 1.

Immediately after the power was turned off to the cells at the end of the second trial, one liter of DI water was used to rinse the anodes into a pitcher to wash out residual electrolyte. It was observed that the solutions were of different colors. Cell 1 with an

average Mn/Cl ratio of 13.0 showed a very distinct purple color that was indicative of permanganate. It was difficult to tell between cells 2 (Mn/Cl ratio 11.1) and 3 (Mn/Cl ratio 8.9) which one had a more purple color, but they both looked browner with some purple tint. Cell 4 (Mn/Cl ratio 7.7) looked very brown and it was clear that cell 4 was browner than the other cells. The solutions were left for 48 hours and cell 1 was still purple while cells 2, 3 and 4 had become clear and debris had dissolved or settled to the bottom.

Table 3 shows corrosion data after trial two. Anodes were thoroughly rinsed with distilled water, cleaned with mannitol solution to remove all scales, and dried. The anodes were then weighed to determine the corrosion rates and calculate the average corrosion rates per cell. The results indicate that cells with higher Mn/Cl ratios had the least corrosion rates. Cells with lower Mn/Cl ratios were more corroded. The corrosion rate in Module Two was less than Module One. The cause for this difference is unknown, but it is believed to be related to the difference in scale appearance between the Modules.

Scales collected from various locations on the anodes were characterized using XRD. The samples were washed with water and dried in an oven at 105 °C for 12 hours. All samples contained anglesite ($PbSO_4$), plattnerite (PbO_2) and Pyrolusite (MnO_2). There was no clear trend of Mn/Cl ratio to the percentages of the three phases.

3.3. MODULE ONE AND TWO COMPARISONS

The major observations from Module One and Module Two are summarized in Table 4. While the experiments were difficult to operate and control, the two Modules produced similar trends in terms of corrosion rate versus Mn/Cl ratio, the percentage of Mn in the electrolyte that is Mn^{3+}, and that easily removed scales also had a violet solution

drain from the anode when it was removed. Unfortunately, the Modules produced contradictory or incomplete information regarding scale appearance, correlation between scale tenacity and Mn/Cl ratio and the phases present in the anode scale.

Table 4. Module One and Two Comparisons

Observation	**Module One – various Mn**	**Module Two – various Cl-**
Mn^{3+}	4-8% of total Mn; not related to Mn/Cl ratio	2-5% of total Mn; not related to Mn/Cl ratio
Mn and Cl Loss from Electrolyte	Higher than commercially experienced in commercial cellhouse	Much lower than Module One
Mn scale in tubes	Large amounts	Much less scale
Anode Corrosion Rate	Rate increases from Mn/Cl 5.8 to 11.6 and then plateaus up to 17.7 Corrosion rates were ~6X Module 2	Rate increases from Mn/Cl ratio 7.9 to 11.0 and then plateaus up to 13.0 Corrosion rates were ~6X less than Module 1
Scale Appearance	Black, matte, flakes	Gray, shiny, compact More shiny with increasing Mn/Cl

Table 4. Module One and Two Comparisons (cont.)

Observation	**Module One – various Mn**	**Module Two – various Cl-**
Scale Tenacity	Easy to remove at Mn/Cl of 5.8 and 11.6; hard to remove at 8.7, 14.3 and 17.7	Easy to remove at Mn/Cl of 11.0 and 13.0; hard to remove at 7.9 and 8.9
Scale Phases	Mn/Cl > 11 produced ε-MnO_2 with some γ-MnO_2; Mn/Cl < 9 produced only ε-MnO_2.	No correlation found between scale phases and Mn/Cl ratio
Scale Weight	Amount of scale did not correlate with changes in Mn/Cl ratio	Amount of scale did not correlate with changes in Mn/Cl ratio
Anode/Scale Layer Solution	Violet at Mn/Cl of 5.8 and 11.6; Brown at 8.7, 14.3 and 17.7	Violet at Mn/Cl at 13.0, all others brown, browner with decreasing Mn/Cl ratio.

4. CONCLUSIONS

The highly dynamic nature of anode oxidation of water, manganese and chloride made these experiments difficult to control. From the results, it was concluded that [Mn^{3+}] is approximately 4-5% of the total [Mn] in zinc electrowinning electrolyte. Mn/Cl ratio

affects anode corrosion rate. The anode corrosion rate decreases with increasing Mn/Cl ratio to about 10 and then plateaus. Mn and Cl^- losses from the electrolyte were correlated but not correlated to the Mn/Cl ratio. Chloride loss was found to be higher than manganese loss in the electrolyte.

The anode scale appearance, phases, and tenacity were not correlated to the Mn/Cl ratio. Scale tenacity did correlate to presence of permanganate ion in the electrolyte that drained from the anode scale layer. Scales that were less tenacious had a purple solution drain from the anode layer when the electrodes were removed from the cell. These experiments indicate that scale appearance and structure were affected by an uncontrolled variable, but it is not clear what that variable was.

ACKNOWLEDGEMENT

The financial support of the AMIRA P705 C Project sponsors and specific guidance from Teck Metals is appreciated. The authors would like to thank Margaret Scott and Kevin L. Foster of Missouri S&T for their dedication and hard work without which the completion of this work would not have been possible.

REFERENCES

1. Group, I.L.a.Z.S. *Lead and Zinc Statistics*. 2018 [cited 2018 2/26/2018]; Available from: http://www.ilzsg.org/static/statistics.aspx?from=1.

2. Tjandrawan, V. and M.J. Nicol, *Electrochemical oxidation of iron (II) ions on lead alloy anodes.* Hydrometallurgy, 2013. 131: p. 81-88.

3. Cachet, C., C. Le Pape-Rérolle, and R. Wiart, *Influence of Co2+ and Mn2+ ions on the kinetics of lead anodes for zinc electrowinning.* Journal of Applied Electrochemistry, 1999. 29(7): p. 811-818.

4. Clancy, M., et al., *The influence of alloying elements on the electrochemistry of lead anodes for electrowinning of metals: a review*. Hydrometallurgy, 2013. 131: p. 144-157.

5. Yu, P. and T.J. O'Keefe, *Evaluation of lead anode reactions in acid sulfate electrolytes II. Manganese reactions.* Journal of the Electrochemical Society, 2002. 149(5): p. A558-A569.

6. Cachet, C., C. Rerolle, and R. Wiart, *Kinetics of Pb and Pb-Ag anodes for zinc electrowinning—II. Oxygen evolution at high polarization.* Electrochimica Acta, 1996. 41(1): p. 83-90.

7. Kelsall, G., et al. *Effects of manganese (II) and chloride ions in zinc electrowinning reactors*. in *Proceedings—Electrochemical Society*. 2000.

8. Mahon, M. and A. Alfantazi, *Manganese consumption during zinc electrowinning using a dynamic process simulation.* Hydrometallurgy, 2014. 150: p. 184-191.

9. Nicol, M., et al., *The effects of halides in the electrowinning of zinc. I. Oxidation of chloride on lead-silver anodes.* Hydrometallurgy, 2017. 173: p. 125-133.

10. Kashida, K., S. Oue, and H. Nakano, *Effect of Chloride Ions in Electrowinning Solutions on Zinc Deposition Behavior and Crystal Texture.* Materials transactions, 2017. 58(10): p. 1418-1426.

11. Chen, T. and J. Dutrizac. *Characterization of the Manganese Oxide Scales Formed on a Grooved Cast Pb-Ag Anode from a Zinc Electrowinning Operation*. in *EPD Congress 2011*. 2011. Wiley Online Library.

III. PB-CA-SN ANODE POTENTIAL AS A FUNCTION OF COBALT, IRON AND MANGANESE IN SYNTHETIC SULFURIC ACID ELECTROLYTES

C. E. Abbey, and M. S. Moats

Missouri University of Science & Technology

Rolla, MO 65409

Tel:573-308-9236

Email: ceag28@mst.edu

ABSTRACT

Cobalt, iron and manganese play various roles in copper electrowinning using lead-calcium-tin alloyed anodes. Cobalt catalyzes electrochemical water decomposition resulting in lower anode potential and reduced corrosion rates. Iron reduces cathodic current efficiency, but is used to reduce higher oxidation states of manganese that oxidize organics in solvent extraction. Manganese also produces anode scale and is generally considered a problematic impurity. The effect of the combined interaction of these three metal ions on the anode potential has not been quantified yet. The current work used a three factor, two level, three replicate central composite design of experiments to analyze the effects and potential interactions among cobalt, iron and manganese. The experiments consisted of chronopotentiometric analysis to assess anode potential after 24 hours of operation. Higher [Co], lower [Mn] and either high or low [Fe] yielded lower anode potentials. Two regression models were developed to predict anode potential as a function

of [Co], [Fe] and [Mn]. A method to estimate electrical energy consumption for copper electrowinning is also presented.

Keywords: anode potential, copper electrowinning, cobalt, iron, manganese, energy consumption model.

1. INTRODUCTION

Electrical energy utilization in copper electrowinning is a vital profitability determinant [1]. For a hypothetical tankhouse (156 cells, 44000 A, 0.95 online factor, and 6.7 cents per kWh (Arizona)), the calculated energy savings of reducing anode potential by 10 mV would be approximately 30 kW and 38000 USD per year. Thus, efforts at reducing electrical energy consumption can be rewarding. Energy efficiency with all its parameters in copper electrowinning has been recently reviewed [2]. Energy consumption (EC) and power consumption (PC) can be estimated using average cell voltage (CV) as shown in equations 1 and 2 respectively. These calculated values do not include energy consumption related to rectification and transmission of energy from the rectifiers to the electrowinning circuit.

$$EC\ (kWhr/tonne) = [84350 \times CV\ (V)] / Current\ Efficiency\ (\%) \quad (1)$$

$$PC\ (kW) = Current\ (A) \times CV\ (V) \times number\ of\ cells \quad (2)$$

Cell voltage is determined by the sum of the voltages associated with thermodynamics (~0.9 V), solution resistance (~0.25-0.3 V), contact resistance (~0.3 V),

cathode overpotential (~0.05-1 V) and the anode overpotential (~0.5 V for a lead alloy anode). The cell voltage for copper electrowinning using a lead-alloy anode with cobalt in the electrolyte is approximately 2 V [3]. The biggest contributors to the cell voltage are the thermodynamics and the anode overpotential. Without changing the anode oxidation reaction, the anode overpotential presents the largest opportunity to reduce the cell voltage [4, 5]. Anode potential for a lead based anode can be affected by the anode composition, the electrolyte composition or the electrolysis conditions [6]. Co is known to reduce the anode potential [7]. The advantages of Co can occur by its presence in the electrolyte [8], anode or anode coating [9, 10]. Co has low solubility in Pb and makes it difficult to make effective Pb-Co anode alloys [11]. Many industrial tankhouses maintain a cobalt concentration between 150 and 200 mg/L in their electrolytes [12]. Co can reduce cell voltage and consequently the power consumption by about 15 kWh per ton of copper produced using Pb-Ca-Sn anodes under specific conditions. Mixed metal oxide coated titanium anodes promise a Co free process with lower EC [13], [14], [15].

Fe and Mn can also be found in various concentrations in electrolytes due to geogenic sources. These ions in solution may have a concomitant effect on the energy draw of the electrowinning system. Abbey and Moats [16] indicated possible interactions among Co, Fe and Mn when studying the effect of Co on the anode potential in the presence of Mn with and without Fe. Fe (0.6 g/L) reduces cathode current efficiency but may also lower the anode potential by about 50-60 mV over the range of 100-600 mg/L Co. Periodic current reversal may partially compensate for current efficiency losses in high Fe electrolytes [17] but this is not industrially practiced. Mn, however, is undesirable in Cu electrowinning unless it is in addition with Co and/or Fe [10, 18]. The effect of Mn in the

electrolyte negatively affects conductivity, density and viscosity but has not been shown to have any effect on anode potential [19] though anodes coated with MnO_2 have lower anode potentials [6].

2. EXPERIMENTAL

2.1. DESIGN AND ANALYSIS OF EXPERIMENTS

A full factorial central composite design (CCD) of experiments using 2 levels and a centroid for three continuous factors [20] was employed to design the experimental conditions. An alpha (α) of 1.5 was used so that the test values are more representative of industrial conditions. The parameters and levels examined are shown in Table 1.

To achieve a 95 % confidence level with 95 % accuracy, each run was performed in triplicate. A random number generator was used to randomize the order of the run to eliminate any systematic errors. MiniTab Statistical software was used to generate and analyze the experiments and its results respectively by response surface methodology.

2.2. MATERIALS AND SETUP

250 mL of synthetic electrolytes with 170 g/L sulfuric acid, 20 mg/L Cl- ions and the various concentrations of the ions were used. All chemicals used were research grade analytical reagents. Deionized distilled water was used and the electrolyte composition was not controlled during the experiment. The solution was placed in the beaker and heated to 50 °C +/- 2 °C with stirring.

Rolled Pb-Ca-Sn anode samples were provided by a commercial supplier. 1 cm x 1 cm specimens were cut from the samples. A copper wire was soldered to one face of a specimen. The specimen was mounted in epoxy resin to control contact with the electrolyte. One surface of the mounted specimen was then ground in succession with 36-grit, 100-grit, and 200-grit silicon carbide sandpaper until it was fully exposed and level.

All electrochemical experiments were conducted using a three electrode cell. The rolled Pb-Ca-Sn anode working electrode was placed a distance of 3.8 cm from a platinum mesh counter electrode. A mercury-mercury sulfate electrode (0.64 V vs. standard hydrogen electrode, SHE at room temperature, 0.6174 V vs. SHE at 50 °C) inserted directly into the cell was used as the reference electrode. Measured potentials were converted to SHE. The reference electrode was positioned equidistant between the anode and cathode.

A Gamry Reference 3000 Galvanostat Potentiostat was used to apply a constant current and record the anode potential versus a mercury-mercury sulfate electrode every 3 seconds. Constant current electrolysis or chronopotentiometry was performed to measure the anode potential of the Pb-Ca-Sn anode as a function of the various CCD conditions for 24 hours. The applied current density was 300 A/m^2 based on the measured surface area of the working electrode.

3. RESULTS AND DISCUSSION

Table 1 shows the AP data for each condition and replicate. The anode potential (AP) was stable in the last ten minutes of operation for each experiment.

Table 1. Average Anode Potentials of the Last Ten Minutes of Chronopotentiometry Operations for all the Runs and the Average of the Runs in the Individual Run Replicates

Run #	**[Fe] g/L**	**[Mn] g/L**	**[Co] g/L**	**AP 1 (V)**	**AP 2 (V)**	**AP 3 (V)**
1	0.5	0.067	0.05	1.937	1.929	1.909
2	0.5	0.067	0.25	1.915	1.922	1.908
3	0.5	0.333	0.05	1.943	1.941	1.935
4	0.5	0.333	0.25	2.019	1.918	1.913
5	2.5	0.067	0.05	1.956	1.953	1.927
6	2.5	0.067	0.25	1.908	1.903	1.914
7	2.5	0.333	0.05	1.948	1.942	1.934
8	2.5	0.333	0.25	1.919	1.936	2.113
9	1.5	0.200	0.15	1.935	1.926	1.937
10	1.5	0.200	0.15	1.966	1.936	1.938
11	1.5	0.200	0.15	1.943	1.947	1.948
12	1.5	0.200	0.15	1.931	1.939	1.922
13	1.5	0.200	0.15	2.199	1.947	1.933
14	1.5	0.200	0.15	1.935	1.943	1.941
15	3.0	0.200	0.15	1.923	1.923	1.919
16	0.0	0.200	0.15	1.921	1.911	1.929
17	1.5	0.400	0.15	1.983	2.090	1.940
18	1.5	0.000	0.15	1.924	1.915	1.922
19	1.5	0.200	0.30	1.919	1.909	1.922
20	1.5	0.200	0.00	2.000	1.989	2.101

The last ten minutes of the recorded anode potentials were averaged for each run and used for statistical analysis. The variances calculated for all the runs were deemed reasonable.

All data points were evaluated and no points were removed based on outlier statistical analysis. The AP data was analyzed using 1) standard response surface methodology (RSM) and 2) using an equation with the form: anode potential = $a + b\,[Co]^x$ based on Miller's analysis [7]. Inherent to RSM, linearity of the output variable with respect to changes in an experimental factor was assumed.

3.1. RESPONSE SURFACE METHOD ANALYSIS

RSM analysis was performed with the AP data. Individual linear and square interactions, and two way interactions for the factors of [Fe], [Mn] and [Co] were investigated. Table 2 shows the analysis of variance (ANOVA) results obtained with MiniTab. To achieve a 95 % confidence interval the cut-off P-value was 0.05. AP was found to be statistically significant versus [Mn] and [Co] as shown in the ANOVA analysis in Table 2. Increasing [Co] reduced AP and confirms previous studies [6, 8, 9, 11, 16]. [Fe] was found to have a relatively high P-value for the linear response, but it was not rejected because it had a statistically significant squared response (as shown in Table 2) and rejecting the linear Fe term would make it impossible to include the square term in the hierarchical analysis. Fe shows a quadratic interaction that peaks at 1.5 g/L. The squared Mn*Mn and Co*Co interactions were rejected as statistically insignificant. Two-way interactions investigated also showed relatively high P-values indicating interactions were

unlikely over the concentrations examined. Figure 1 shows the response of anode potential versus the three individual parameters as confirmed by the ANOVA analysis in Table 2.

Table 2. Analysis of variance details run with MiniTab for RSM Showing the P-Values, F- Values, Linear, Square and Two Way Interactions

Source	**DF**	**Adj. SS**	**F-Value**	**P-Value**
Model	9	0.0124	7.44	0.000
Linear	3	0.0087	15.7	0.000
Fe	1	0.0002	1.04	0.313
Mn	1	0.0012	6.65	0.013
Co	1	0.0068	36.8	0.000
Square	1	0.0038	6.87	0.001
Fe*Fe	1	0.0034	18.2	0.000
Mn*Mn	1	0.0003	1.57	0.217
Co*Co	1	0.0002	1.08	0.305
2-Way Interaction	3	0.0004	0.65	0.589
Fe*Mn	1	0.0000	0.01	0.943
Fe*Co	1	0.0003	1.46	0.234
Mn*Co	1	0.0001	0.45	0.506

The analysis of variance (ANOVA) was performed again using only the statistically significant values listed previously (Mn, Co, Fe and Fe*Fe). From this analysis an empirical formula was derived (Equation 3). Concentrations in Equation 3 are in grams per liter. Residual plots comparing calculated values to the raw data, standardized residuals,

fitted value and observation order were done (not shown). The residual plots show that all values were within 3 standard deviations from the mean. The histogram shows an almost normal distribution. The order of the observation did not result in systematic error.

The analysis of variance (ANOVA) was performed again using only the statistically significant values listed previously (Mn, Co, Fe and Fe*Fe). From this analysis an empirical formula was derived (Equation 3). Concentrations in Equation 3 are in grams per liter. Residual plots comparing calculated values to the raw data, standardized residuals, fitted value and observation order were done (not shown). The residual plots show that all values were within 3 standard deviations from the mean. The histogram shows an almost normal distribution. The order of the observation did not result in systematic error.

$$AP\ (V\ vs.\ SHE) = 1.924 - 0.143\ [Co] + 0.0481\ [Mn] + 0.0348\ [Fe] - 0.0108\ [Fe]^2 \quad (3)$$

Figure 2 shows contour plots of anode potential versus composition in two dimensions. The non-plotted parameter values for the plots are 1.5 g/L Fe, 0.2 g/L Mn and 0.15 g/L Co as these are common values in solvent extraction (SX) electrowinning (EW) electrolytes. These plots help to visualize the effects of the statistically significant parameters, [Co], [Mn] and $[Fe]^2$. Lower AP is achieved by operating in an electrolyte of low [Mn], low or high [Fe] and high [Co]. High [Fe] leads to a decrease in cathodic current efficiency due to ferric reduction. Thus low [Mn], high [Co] and low [Fe] should minimize energy consumption for a copper electrowinning cell.

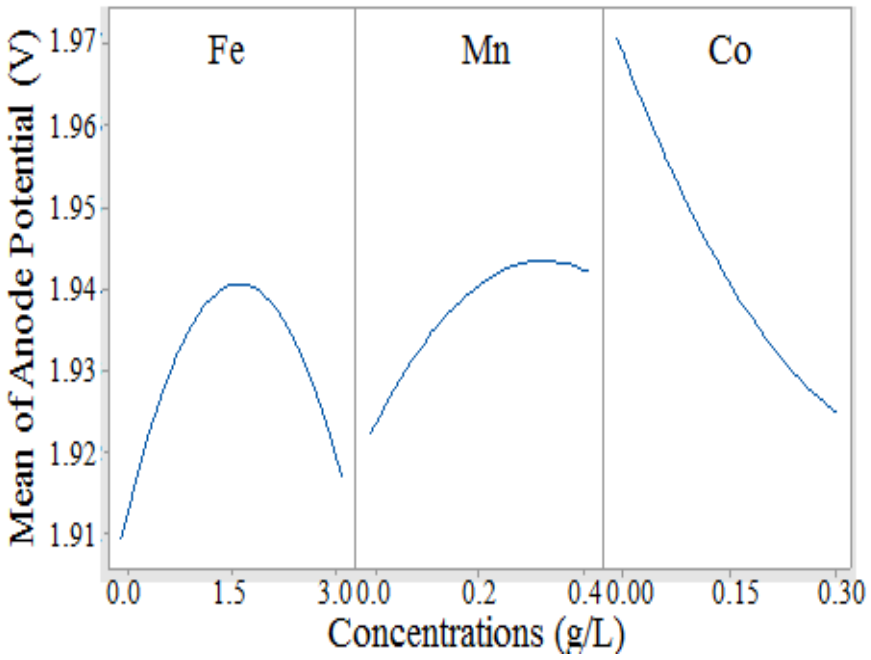

Figure 1. Main Interaction Effects of the Anode Potentials Caused by the Three Factors; [Co], [Fe] and [Mn]

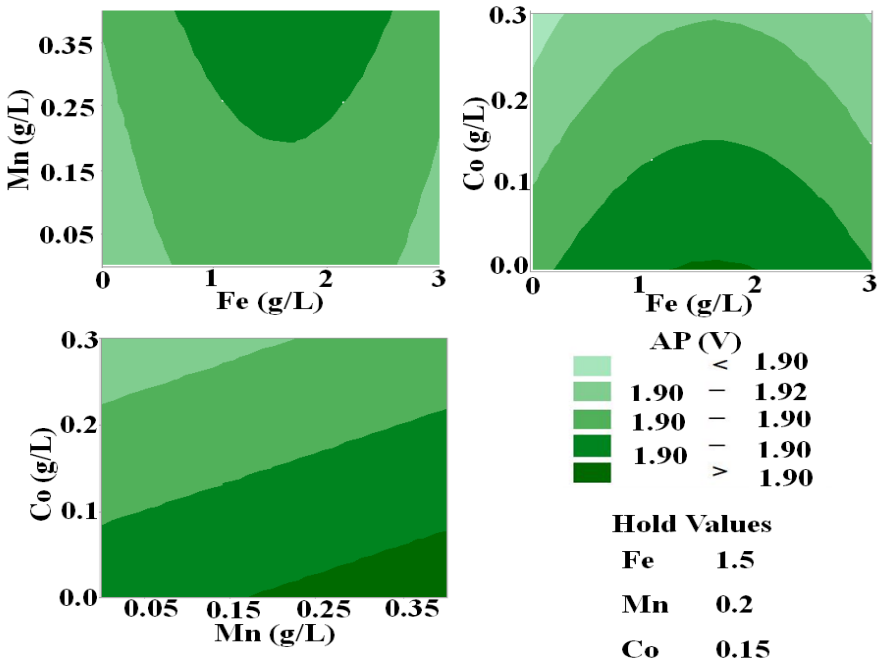

Figure 2. Contour Plots for Anode Potentials of Mn*Fe, Co*Mn and Co*Fe. All Concentrations are in g/L. The First Variable Listed is on the y-axis and the Second Variable is on the x-axis

3.2. AP ANALYSIS AS A FUNCTION OF COBALT CONCENTRATION

Analysis of the raw anode potential data reveals a trend of anode potential decreasing with increasing cobalt concentration as shown in Figure 3. Previous work [7, 16] indicated that an equation of the form $AP = a + b\,[Co]^x$ produced a reasonable empirical fit. The data were examined using a formula of a similar form and it was found that when [Co] is raised to the 0.32 power, a solid fit to the data is generated. This power term is the same as previously calculated with 0.6 g/L Fe, 0.6 g/L Mn containing electrolyte [16].

To this basic formula, addition components were manually added using a combination of minimized sum of squares and regression analysis to produce a formula with the best empirical fit with a minimal number of parameters. The best empirical fit equation produced is given in equation 4.

$$AP\ (V\ vs.\ SHE) = 1.961 - 0.0962\,[Co]^{0.32} + 0.0524\,[Mn] + 0.0114\,[Fe]^{0.25} \quad (4)$$

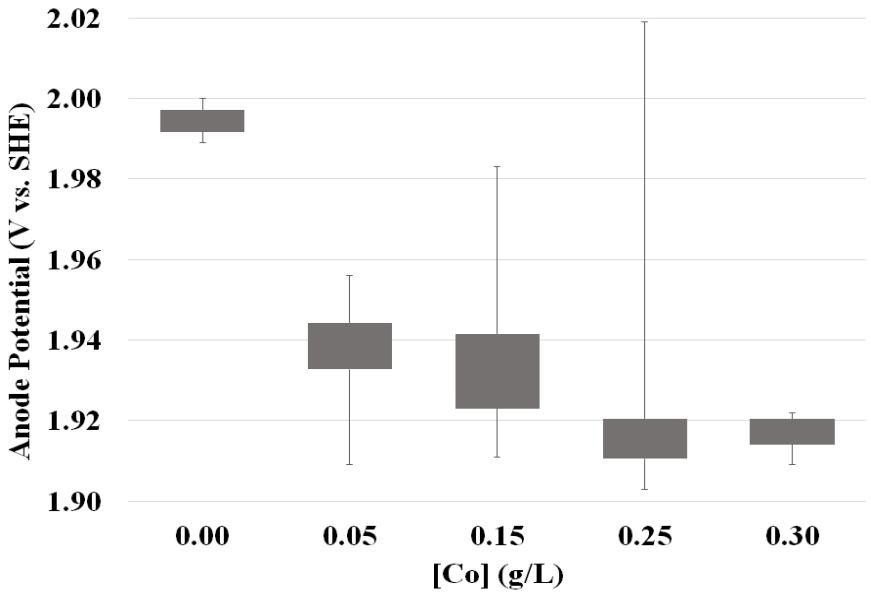

Figure 3. Measured Anode Potential versus Cobalt Concentrations in Electrolyte for Non-outlier Experiments

3.3. COMPARISON OF THE TWO EMPIRICAL MODELS

Both empirical formulas (Eq. 3 and 4) produce similar correlation coefficients with the real data (see Figure 4) and total sum of square values from residual values. Either equation might be useful to evaluate the effects of [Co], [Mn] and [Fe] on anode potential trends in a common copper electrowinning electrolyte. Equation 4 is better at predicting AP at cobalt concentration less than 50 mg/L.

3.4. EXAMINING ELECTROLYTE EFFECTS ON ENERGY CONSUMPTION

From Equation 1, energy consumption is proportional to the ratio of the cell voltage and the current efficiency. Cell voltage can be calculated using Equation 5 [1].

$$Cell\ Voltage\ (V) = (E_a + \eta_a) - (E_c - \eta_c) + IR_{solution} + IR_{contacts} \qquad (5)$$

where Ec is the thermodynamic potential of the cathode, ηc is the cathodic overpotential to electrodeposit copper, Ea is the thermodynamic potential of the anode, ηa is the anodic overpotential to breakdown water and evolve oxygen. IRsolution and IRcontacts are the voltage contribution of the solution and contacts respectively.

Ea + ηa is equal to the AP as calculated by Equation 3 or 4, using Equation 4 at industrially relevant Co and Mn concentrations of 0.15 g/L, and 0.2 g/L, respectively. For Fe however, the Fe concentration used was 2 g/L because the CE in Equation 6 is valid only above 1.27 g/L [21]. The AP is therefore calculated to be 1.931 V.

Ec - ηc is the cathode potential. Ec (0.275 V) was obtained from data published from cyclic voltammograms produced using 40 °C electrolyte with 40 g/L Cu, 180 g/L

H_2SO_4, 20 mg/L Cl^- with various concentrations of HydroStar (a commercial smoothening agent) [22]. Cathode overpotential of plating copper on stainless steel was obtained by the voltage difference between the backward sweep and the standard potential at 300 A/m2 in the cyclic voltammogram from the same publication [22]. The various concentrations of the organic additive did not affect polarization significantly. ηc was measured at 0.1 V.

The voltage drop caused by solution resistance can be calculated using current density and electrolyte conductivity. A suitable empirical equation for electrolyte conductivity was presented by Price and Davenport [23]. The conductivity of a 40 g/L Cu, 170 g/L sulfuric acid, 50°C electrolyte was calculated at 62.79 S/m. Using 300 A/m^2, electrode areas of 1m^2 (typical industrial electrode area) and a face-to-face anode to cathode separation of 0.0465 m (105 mm cathode-to-cathode centerline distance with 9 mm thick anodes and 3 mm cathodes) [8], IRsolution was calculated to be 0.222 V.

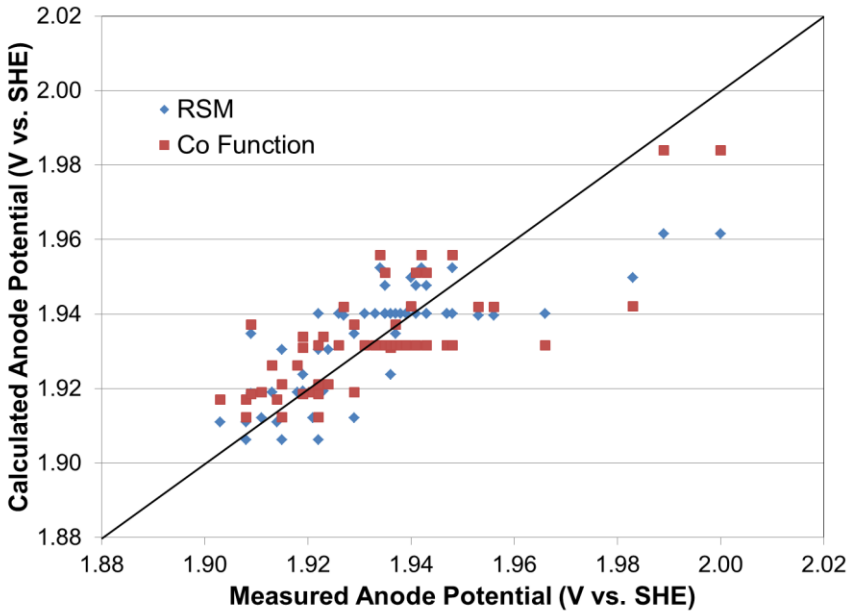

Figure 4. Comparison of Calculated Anode Potential versus Measured Anode Potential for both Response Surface Method and the Co Function Equation

The voltage component related to the contact resistance between electrode header bars and the cell busbars was also calculated. A contact resistance of 50 μΩ was calculated at triangular and dogbone contacts [24] which are commonly used [8]. Combining this with a 300 A/m^2 current density (2 m^2 per electrode) at two contact points per cell (one anode and one cathode) produces a potential drop of 0.060 V.

Combining all the individual voltage components as shown in Table 3 produces a cell voltage of about 2.040 V. This cell voltage value is similar to commonly reported values [3].

A predictive formula for current efficiency controlled by ferric reduction is presented in Equation 6 [21], where Fe(III)(g/l) is the ferric concentration in (g/l), Cu(II) is the copper concentration in (g/l) and C.D.(A/m^2) is the current density in (A/m^2). For consistency, values of 40 g/L Cu, 2 g/L ferric and 300 A/m^2 were used to calculate a current efficiency of 93.4 %.

Table 3. Values of Voltage Contributors for Cell Voltage Including Anode Potential, Cathode Potential, Solution Voltage and Contact Voltage Calculated from Various Sources

Cell Voltage Component	**Value (V)**
Anode Potential ($E_a + \eta_a$)	1.931
Cathode Potential ($E_c - \eta_c$)	0.175
$IR_{Solution}$	0.222
$IR_{Contacts}$	0.060
Total Cell Voltage	2.040

$$CE\ (\%) = 88.19 - 4.91 \times Fe(III)(g/l) + 0.52 \times Cu(II)(g/l) + 1.81 \times 10^{-3} \times CD(A/m^2) - 6.83 \times 10^{-3} \times Cu(II)^2(g/l) + 0.028 \times Fe(III)(g/l) \times Cu(II)(g/l) + 4.015 \times 10^{-3} \times Fe(III)(g/l) \times CD(A/m^2) \quad (6)$$

To minimize electrical energy consumption, an operation should attempt to minimize cell voltage and maximize current efficiency. For this example, electrical energy consumption was calculated by combining the calculated cell voltage and current efficiency to be 1840 kWh/tonne. This value is lower than the average energy 2000 - 2160 kWh/tonne [1, 3] reported to produce eletrowon Cu. The present calculation assumes no short circuiting and does not include electrical consumption due to rectification and resistances in the electrical bus system.

3.5. SENSITIVITY ANALYSIS

Sensitivity analysis for EC using ± 10, 30 and 50 % of [Co] and [Mn] and ± 10, 25 and 35 % of [Fe] was conducted as shown in Figure 5. Fe is plotted on the secondary horizontal axis at the top while Co and Mn are plotted on the primary horizontal axis at the bottom. Figure 5 shows that Fe and Mn have positive slopes indicating their adverse effect on the anode potential while Co shows a negative trend that is desired for minimizing the anode potential.

The slope gradient also indicates the magnitude of the parameter on optimizing the anode potential. Mn increases the anode potential but not as drastically as Fe does. The centroid represents the concentrations tested ([Co] = 0.15 g/L, [Fe] = 2 g/L and [Mn] = 0.2 g/L). These sensitivity analyses, predictive models and energy consumption calculations

are valid only for the ranges tested as described in previous sections. This makes it restrictive and leaves room for expansion of the model. For example, in estimating the cathode overpotential the conditions used were 40 g/L [Cu], and 40 °C. A model can be built to factor in varied temperatures and [Cu] among other variables within the typical ranges of Cu EW. In addition, the temperature and acid concentration dependence of the anode potential was not exploited in this model as shown in Equations 3 and 4. This is an area for future work.

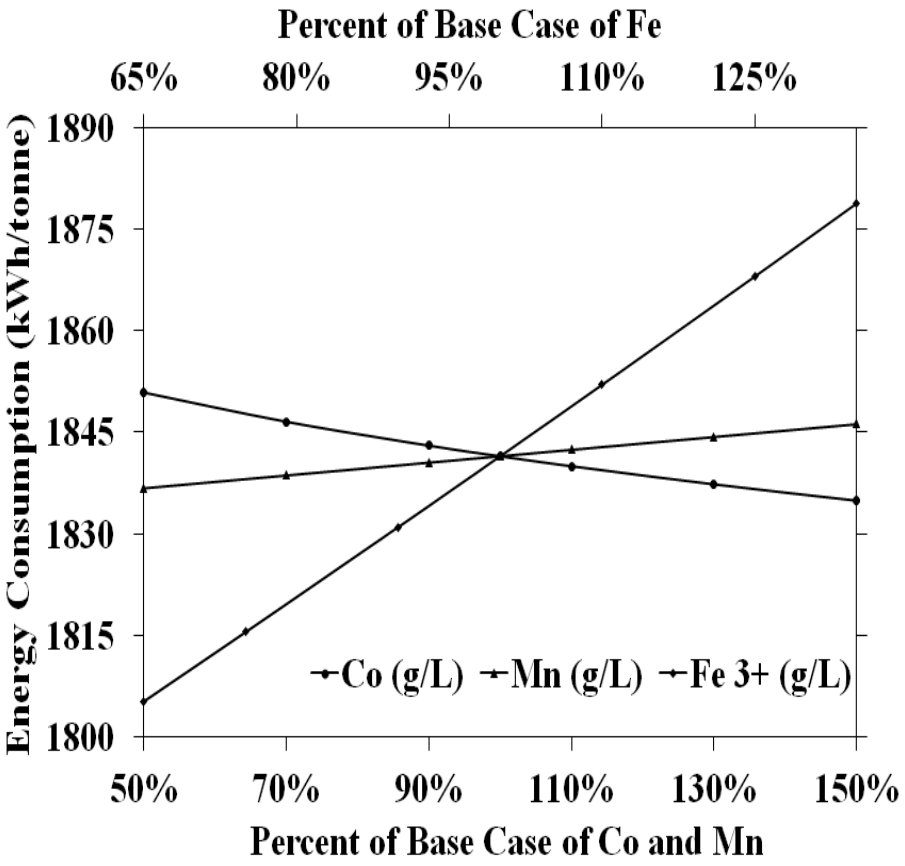

Figure 5. Sensitivity Analysis of Energy Consumption vs. Variation in [Co], [Fe] and [Mn]. Base Case: [Co] = 0.15 g/L, [Fe] = 2.0 g/L and [Mn] = 0.2 g/L

4. CONCLUSIONS

A CCD experimental design was used to evaluate the response of anode potential of rolled Pb-Ca-Sn samples versus [Fe], [Mn] and [Co] in synthetic electrolytes. ANOVA analyses show that there is no significant interaction among Co, Fe and Mn within the ranges tested and the significant effects were caused by Co, Mn and Fe*Fe. AP was found to be lowest at high [Co], low [Mn] and either low or high [Fe]. Response surface methodology was used to analyze the data and an empirical equation was developed to estimate the anode potential (AP) at various concentrations of Co, Fe and Mn. The data was again used to obtain a second model for estimating the anode potential by using a Co function constraint. The two models are comparable with the Co function model being more accurate at higher anode potentials. Combining one of the anode potential equations with other equations and estimations in literature yielded a method to estimate cell voltage, current efficiency and energy consumption within industrially relevant concentration ranges for Co, Mn and Fe. Process engineers may find the ability to estimate energy consumption useful while optimizing their copper electrowinning operation.

ACKNOWLEDGEMENT

The S&T research team would like to thank the AMIRA P705C sponsors for their financial assistance. The experimental assistance of Kevin Lee Foster is greatly appreciated.

REFERENCES

1. Free, M., et al., *Electrometallurgy-Now and in the Future.* Electrometallurgy 2012, 2012: p. 3-28.

2. Moats, M.S., *Energy efficiency of electrowinning*, in *Energy Efficiency in the Minerals Industry*. 2018, Springer. p. 213-232.

3. Schlesinger, M.E., et al., *Extractive metallurgy of copper*. 2011: Elsevier.

4. Cooper, W.C., *Advances and future prospects in copper electrowinning.* Journal of applied Electrochemistry, 1985. 15(6): p. 789-805.

5. Moats, M. and M. Free, *A bright future for copper electrowinning.* JOM Journal of the Minerals, Metals and Materials Society, 2007. 59(10): p. 34-36.

6. Clancy, M., et al., *The influence of alloying elements on the electrochemistry of lead anodes for electrowinning of metals: a review.* Hydrometallurgy, 2013. 131: p. 144-157.

7. Miller, G., *Methods of managing manganese effects on copper solvent extraction plant operations.* Solvent Extraction and Ion Exchange, 2011. 29(5-6): p. 837-853.

8. Huang, H., J.-Y. Zhou, and Z.-C. Guo, *Effect of added cobalt ion on copper electrowinning from sulfate bath using doped polyaniline and Pb-Ag anodes.* Transactions of Nonferrous Metals Society of China, 2010. 20: p. s55-s59.

9. Barmi, M.J. and A.N. Nikoloski, *Electrodeposition of lead–cobalt composite coatings electrocatalytic for oxygen evolution and the properties of composite coated anodes for copper electrowinning.* Hydrometallurgy, 2012. 129: p. 59-66.

10. Nikoloski, A. and M. Nicol, *Effect of cobalt ions on the performance of lead anodes used for the electrowinning of copper—A literature review.* Mineral Processing and Extractive Metallurgy Review, 2007. 29(2): p. 143-172.

11. Nikoloski, A. and M. Nicol, *Addition of cobalt to lead anodes used for oxygen evolution—a literature review.* Mineral Processing and Extractive Metallurgy Review, 2009. 31(1): p. 30-57.

12. Robinson, T.G., et al., *Copper Electrowinning: 2013 World Tankhouse Operating Data.* Copper 2013 Proceedings, 2013. V, Santiago, Chile, IIMCh.

13. Moats, M., K. Hardee, and C. Brown Jr, *Mesh-on-lead anodes for copper electrowinning.* JOM, 2003. 55(7): p. 46.

14. Morimitsu, M., et al. *Energy-efficient Electrowinning Process with smart anode comprising nanooxide catalyst*. in *Proceedings of European Metallurgical Conference*. 2011.

15. Cifuentes, L., A. Montes, and G. Crisóstomo, *Corrosion behaviour and catalytic effectiveness of Pb–Ca–Sn, RuO2–IrO2/Ti and IrO2–Ta2O5/Ti anodes for copper electrowinning.* Corrosion Engineering, Science and Technology, 2011. 46(6): p. 737-744.

16. Abbey, C. and M. Moats, *Effect of Cobalt and Iron Concentration on the Potential for Oxygen Evolution from Pb–Ca–Sn Anodes in Synthetic Copper Electrowinning Electrolytes*, in *Applications of Process Engineering Principles in Materials Processing, Energy and Environmental Technologies*. 2017, Springer. p. 89-95.

17. Bautista, R. and R. Wesely, *Energy reduction techniques in metal electrochemical processes*. 1985, The Metallurgical Society, Inc., Warrendale, PA.

18. Nijjer, S., J. Thonstad, and G. Haarberg, *Oxidation of manganese (II) and reduction of manganese dioxide in sulphuric acid.* Electrochimica acta, 2000. 46(2): p. 395-399.

19. Tjandrawan, V., *The role of manganese in the electrowinning of copper and zinc*. 2010, Murdoch University.

20. Montgomery, D.C., *Design and analysis of experiments*. 2017: John Wiley & Sons.

21. Khouraibchia, Y. and M.S. Moats, *Evaluation of the effect of copper electrowinning parameters on current efficiency and energy consumption using surface response methodology.* ECS Transactions, 2010. 28(6): p. 295-306.

22. Cui, W., *Effect and interactions of commercial additives and chloride ion in copper electrowinning*. 2014: Missouri University of Science and Technology.

23. Price, D.C. and W.G. Davenport, *Densities, electrical conductivities and viscosities of CuSO4/H2SO4 solutions in the range of modern electrorefining and electrowinning electrolytes.* Metallurgical Transactions B, 1980. 11(1): p. 159-163.

24. Boon, C., et al., *Comparison of intercell contact bars for electrowinning plants*, in *Ni-Co 2013*. 2013, Springer. p. 177-189.

IV. EFFECTS OF TEMPERATURE. POWER OUTAGES, COBALT AND MANGANESE CONCENTRATIONS ON CORROSION AND CURRENT EFFICIENCIES IN COPPER ELECTROWINNING.

C. E. Abbey, and M. S. Moats

Missouri University of Science & Technology

Rolla, MO 65409

Tel:573-308-9236

Email: ceag28@mst.edu

ABSTRACT

A benchscale testing facility was used to measure the effect of temperature, power outages, Co and Mn concentrations on current efficiency and anode corrosion during 28 day experiments. Copper electrowinning was performed using two Pb-Ca-Sn anodes and three copper starter sheet cathodes per cell with an anodic current density of 380 A/m^2. The effects of Co concentration (150 and 600 mg/L), Mn concentration (50 and 600 mg/L Mn), temperature (35 and 45 °C) and power outages (6 hours per outage, three outages per week) were investigated. Anode corrosion in all experiments was minimal probably due to the presence of at least 150 mg/L Co in each electrolyte. Cathode current efficiency typically ranged between 90 and 95% for the experiments. The range of power outage, [Mn], [Co] and temperature tested did not produce a significant effect on current efficiency. Some variation in cell mud formation was noted when operating at 35 °C and 600 mg/L Mn.

Keywords: temperature, power outages, cobalt, manganese, current efficiency, copper electrowinning.

1. INTRODUCTION

Copper electrowinning can be monitored by several key performance indicators (KPI) including current efficiency cathode product quality, and anode corrosion rate [1-3]. Various measures can be put in place to control or optimize these KPIs including adding organics like DXG-F7 to prevent nodule formation and improve the smoothness of the cathode [4]. This single move has a two prong effect by increasing current efficiency and improving cathode quality. The KPIs are interactive and produce ripple effects. Several variables can therefore be optimized to improve KPIs namely, electrolyte composition, agitation, current density [5] and temperature [2, 6-12]. Recent copper electrowinning research has focused on corrosion control [5, 13-15] and energy reduction strategies with most of them on the anode reactions and the effect of Co [16-19], Mn [8], anode alloying materials [20-22] and additives on energy consumption. It has been estimated by [23] that approximately 2160 kWh of electrical energy is expended for every tonne of Cu produced. Alfantazi and Valic in 2002 assessed the effect of current density, copper ion concentration and temperature for short time experiments on an electrolyte without Fe, Mn and Co.

Intermittent power outages are inevitable in industrial base metal electrowinning establishments. This has deleterious effects on the protective layers of the anode material [5] and with Fe^{2+} in the electrolyte will cause sulfation [24]. The effect of Fe^{2+} observed in [24] was made without Co ions in the electrolyte. Temperature affects corrosion rates and

depolarizes oxygen evolution at 45°C [22]. Mn can be problematic due to its high oxidation states especially in low temperature electrolytes and so an industrial ‘rule of thumb’ to maintain an [Fe] to [Mn] ratio of 10:1 has been established and shown to work [7]. CE is dependent on [Fe^{3+}], [Cu^{2+}] and current density and their interactions [25]. This work therefore investigated the effect of temperature, [Mn], [Co], temperature and power outages on corrosion rates and cathode current efficiency using 28 day benchscale tests with Fe in solution.

2. EXPERIMENTAL

2.1. TESTING SYSTEM

Four runs were conducted with the experimental design summarized in Table 1. The Missouri S&T bench scale anode corrosion testing facility (shown in Figure 1) consisted of four cells (12 L) in two water baths to maintain a set temperature with water circulation pumps. Each cell was connected via tubes to a reservoir that held electrolyte. Electrolyte was pumped with peristaltic pumps at 150 ml/min to the individual cells from each reservoir. A flow rate of 150 mL/min provides an average residence time of ~45 minutes for the electrolyte in the cell. A network of overflow tubes and hoses ensured that the cells, water baths and water tank did not overflow. The tubes were periodically cleaned with a solution made of sulfuric acid and hydrogen peroxide to remove MnO_2 that formed during testing. Distilled deionized (DDI) water was pumped into the electrolyte reservoirs to counter the effect of evaporation and water decomposition.

Every chemical containing part of the system was placed in secondary containment to abide by University Environmental Health and Safety (EHS) regulations.

Table 1. Design Matrix of Parameters for Testing in Cu EW System

Run #	Cell #	Temp. (^{0}C)	Mn (mg/L)	Co (mg/L)	Open Circuit?
1	1	35	600	150	No
	2	35	600	150	Yes
	3	35	600	600	No
	4	35	600	150	No
2	1	45	50	150	No
	2	45	50	150	Yes
	3	45	50	600	No
	4	45	50	150	No
3	1	45	600	150	No
	2	45	600	150	Yes
	3	45	600	600	No
	4	45	600	150	No
4	1	35	50	150	No
	2	35	50	150	Yes
	3	35	50	600	No
	4	35	50	150	No

Each cell contained three cathodes and two anodes. The anodes were commercial rolled Pb-Ca-Sn (sheared and provided by an anode supplier) connected to copper header

bars with brass screws. The anode samples were not pre-treated prior to use as is the standard practice in copper electrowinning (EW). The cathodes were industrial copper starter sheets (supplied by a copper mining company) and were connected to copper header bars with brass screws.

Figure 1. Missouri S and T's Anode Testing System

The cells were connected electrically via copper wires in series. Each set of electrodes were connected in parallel within a cell. A direct current of 11.4 A was supplied by a BK Precision Model 1694 DC power supply to the cells to provide an anodic current density of ~380 A/m^2 (current density was calculated based on the submerged anode area). The contacts and connections were made using corrosion resistant zinc coated alligator

clips. Cathode and anode currents were measured daily using a DC clamp-on ammeter to monitor current distribution. Power outages were achieved by electrically isolating the particular cell three times a week for six hours at each instance.

Cells were operated for 28 days per run. Plating copper was deemed necessary to ensure that the cells replicated the redox conditions in a commercial cell. The electrolyte was recirculated through the cell and a reservoir throughout the experiment. The temperature of each cell was manually recorded once per day. Heater control used a thermocouple feedback control loop and was performed on a continuous basis.

2.2. ELECTROLYTE

The base electrolyte at the start of each run was 180 g/L sulfuric acid, 20 mg/L chloride, 1.2 g/L iron, 40 g/L copper and the target concentrations of Mn and Co listed in Table 1. All chemicals used in this test work were analytical grade.

Solution volume was maintained by adding distilled deionized water daily. A Metrohm 862 Compact Auto-Titrator was used to analyze H_2SO_4 and Cl^- concentrations daily. A Thermo-Fisher ICE 3000 series Atomic Adsorption Spectrometer (AAS) was used to analyze Mn, Fe, Co and Cu concentrations daily. Prior to analysis, all solution samples were filtered using a 0.45 micron syringe filter.

Chemical additions were made daily to return the electrolyte to the target concentrations on an as needed basis. Copper was replenished by the addition of copper oxide which also served to consume acid generated during electrolysis. Twice per day, additions of 0.3 g DXGF-7 were made to each electrolyte system to prevent nodule formation and consequently short circuiting.

2.3. ELECTRODES

Cathodes and anodes were weighed before being placed into the cells. Cathodes were harvested weekly, washed, dried and weighed. Cathode current efficiency was calculated for each week using the total electrical current run time for the week. Hence cathode CE for the cells that experience power outages were calculated using the actual time that those cathodes were supplied with current. After 28 days, when the system was shut down final cathode and anode pictures were taken. Anode scales and oxides were then dissolved in a prepared mannitol and NaOH solution similar to the procedure in [26]. Anodes were then air dried and weighed to determine their corrosion rates.

3. RESULTS AND DISCUSSION

3.1. RUNS ONE, TWO, THREE AND FOUR

System monitoring and control were reasonably good given the daily adjustments to electrolyte chemistry. The subsequent sections present measurement results and calculated variables that were used to control and maintain the system. A detailed discussion is presented for Run One to illustrate the variation in operating parameters. Variation in parameters for Runs Two, Three and Four are not provided for brevity and they do not affect the results of the study. Additional information about Runs Two, Three and Four are available upon request.

A summary of the average values for each parameter measured and used to control the system are shown in Tables 2, 3 and 4 for Run 1. During Run One, [Mn] measured for cells 1 and 4 which were being run under identical conditions (control experiments)

however showed high and consistently increasing values. The system was turned off and the electrolytes in those cells were changed but the Mn concentrations still kept increasing. Therefore in cells 1 and 4, [Mn] averaged 808 mg/L and 788 mg/L respectively as against the 600 mg/L target.

Acid concentrations were reasonably constant. The overall averages were slightly higher than the targets as they ranged between about 182 g/L and 188 g/L. Daily acid concentration determination showed increased values higher than the set point of 180 g/L as the measurement is taken prior to the addition of copper oxide which neutralized the acid generated at the anodes.

Table 2. Average Measurement Parameters against Targets (B) for Run One

Cell #	T (°C)	Mn (mg/L)	Cl (mg/L)	Acid (g/L)	Fe (g/L)	Co (mg/L)	Cu (g/L)
B	35.0	600	20.0	180	1.20	150/600	40.0
1	35.2	809	19.4	189	1.23	158	21.1
2	35.7	603	20.9	185	1.28	161	23.0
3	35.6	434	12.0	184	1.23	595	21.8
4	35.4	788	22.4	183	1.21	151	21.0

Fe concentrations were within reasonable variation (1.10-1.45 g/L) of the 1.2 g/L target. Co also showed similar and acceptable variation from the set point of 600 mg/L in cell 3 and 150 mg/L in the other cells. Cell 2 was within 140 mg/L and 200 mg/L while cells 1 and 4 were between 140 and 170 mg/L. Cell 3 ranged between 550 mg/L and 680

mg/L. Copper was replenished daily by the addition of CuO. Daily Cu analysis ranged between 15 and 28 g/L. As seen in Table 2 the average electrolyte [Cu] reduced by about 19 g/L from 40 g/L daily. This means that with 16 L of electrolyte, an average of about 304 g of Cu was plated on the cathodes daily. This is consistent with the weights of CuO additions daily after compensating for the weight of oxygen in the CuO powder (Table 4).

Table 3. Average Solution Levels, Cathode (C1, C2 and C3) and Anode (A1 and A2) Currents Measured (A), System Voltage (SV) and Applied Current for Run One

Cell #	Solution Level (cm)	C1 (A)	C2 (A)	C3 (A)	A1 (A)	A2 (A)	SV (V)
1	6.62	3.39	5.07	3.05	5.66	5.91	8.53
2	6.38	3.80	4.43	3.30	5.72	5.85	
3	6.63	4.02	3.89	3.59	5.63	5.89	
4	6.41	3.85	4.31	3.40	5.81	5.74	

Table 4. Calculated Average Daily Water and Chemical Additions for Run One

Cell #	Water Added (ml)	$MnSO_4$* H_2O (g)	NaCl (g)	Acid (ml)	$Fe_2(SO_4)_3$ *$5H_2O$ (g)	$CoSO_4$*7 H_2O (g)	CuO (g)
1	265	2.93	0.07	35.6	1.52	0.18	386
2	370	0.80	0.03	19.2	0.07	0.07	346
3	277	8.34	0.21	51.3	1.75	1.44	373
4	413	2.83	0.08	46.0	2.08	0.29	388

Solution levels were measured daily to know the amount of water that had evaporated. A water addition pump added about 600 mL per day of distilled DI water continuously to each reservoir. This was however inadequate and so various calculated volumes of distilled DI water was added after daily measurements. Average solution level values and water addition volumes for Run One are shown in Tables 3 and 4 respectively.

Daily cathode current measurements ranged between 2.5 A and 5 A. Anode currents were between about 5 A and 6.6 A and the two anodes in a cell were about the same as each other. Sometimes when the current deviated from these trends it was an indication of salt formation and build up or faulty electrical connections. These were investigated and corrected immediately by screw tightening or water washing to clean off salts.

Tables 5, 6 and 7 show the average values calculated over all the 28 days for Run Two. Solution levels were measured daily to know the amount of solution that had evaporated. Since the operating temperature was higher in this run the addition water pump was increased. Average solution level values and water addition volumes for Run Two are shown in Tables 6 and 7 respectively.

Table 5. Average Daily Measured Parameters and the Targets (B) for Run Two

Cell #	T (^{0}C)	Mn (mg/L)	Cl (mg/L)	Acid (g/L)	Fe (g/L)	Co (mg/L)	Cu (g/L)
B	45.0	50.0	20.0	180	1.20	150/600	40.0
1	44.0	53.2	21.7	200	1.22	156	23.9
2	44.3	49.0	21.8	183	1.17	147	22.4
3	45.1	54.7	22.1	206	1.23	618	21.9
4	44.2	56.1	21.4	202	1.23	161	21.3

Cathode and anode currents measurements were within expected ranges. Occasional spikes measured were indications of salt build up and they were resolved immediately. Average values of all parameters measured are shown in Tables 5, 6 and 7.

Run Two was generally better controlled than Run One. As can be seen in Table 5, the average cell temperatures attained for all four cells approximately ranged between 43 °C and 45 °C. All other parameters were within reasonable deviations except for acid concentration which increased to averages of about 205 g/L versus the targets of 180 g/L. Cell 2 alone averaged about 183 g/L. This was the lowest and expected. Cells 1, 3 and 4 had constant currents and so produced acid with the plating of Cu. Cell 2 had lower acid concentrations because of the power outages. Cell 2 also had lower average Fe, Co and Mn concentrations.

Table 6. Average Solution Levels, Cathode (C1, C2 and C3) and Anode (A1 and A2) Currents Measured (A), System Voltage (SV) and Applied Current for Run Two

Cell #	Solution Level (cm)	C1 (A)	C2 (A)	C3 (A)	A1 (A)	A2 (A)	SV (V)
1	6.38	2.40	5.42	2.26	5.06	5.11	8.45
2	5.59	3.05	4.61	2.60	5.01	5.21	
3	6.37	3.49	4.06	2.48	5.06	4.94	
4	6.12	3.22	4.33	2.81	5.35	4.89	

Monitoring and control for Run Three was good especially for Cl as can be seen in the average values shown in Tables 8, 9 and 10. Again, cell temperatures averaged approximately between 43 °C and 45 °C. Monitoring and control data for Run 4 was also

good especially for temperature, Cl, Mn and acid as shown in Tables 11, 12 and 13. The authors were satisfied with the level of control across the four runs bearing in mind the dynamic nature of the systems and difficulty in maintaining control of such a dynamic system.

Table 7. Calculated Water and Chemical Additions for Run Two

Cell #	Water Added (ml)	$MnSO_4$* H_2O (g)	NaCl (g)	Acid (ml)	$Fe_2(SO_4)_3$ *$5H_2O$ (g)	$CoSO_4$*7 H_2O (g)	CuO (g)
1	356	0.02	0.02	5.64	3.36	0.23	330
2	847	0.07	0.02	53.3	3.28	0.58	360
3	401	0.03	0.01	10.3	1.17	1.01	370
4	550	0.03	0.01	3.68	1.21	0.23	382

Table 8. Measured Parameters and the Targets (B) for Run Three

Cell #	T (^{0}C)	Mn (mg/L)	Cl (mg/L)	Acid (g/L)	Fe (g/L)	Co (mg/L)	Cu (g/L)
B	45.0	600	20.0	180	1.20	150/600	40.0
1	44.6	640	22.4	196	1.33	168	21.1
2	44.3	598	22.4	174	1.19	151	22.5
3	44.0	637	23.3	187	1.30	649	21.1
4	43.0	613	22.2	180	1.23	165	20.3

Table 9. Average Solution Levels, Cathode (C1, C2 and C3) and Anode (A1 and A2) Currents Measured (A), System Voltage (SV) and Applied Current for Run Three

Cell #	Solution Level (cm)	C1 (A)	C2 (A)	C3 (A)	A1 (A)	A2 (A)	SV (V)
1	6.73	2.77	5.14	2.83	5.46	5.35	
2	5.88	3.54	4.11	3.06	5.42	5.35	8.18

Table 9. Average Solution Levels, Cathode (C1, C2 and C3) and Anode (A1 and A2) Currents Measured (A), System Voltage (SV) and Applied Current for Run Three (cont.)

Cell #	Solution Level (cm)	C1 (A)	C2 (A)	C3 (A)	A1 (A)	A2 (A)	SV (V)
3	6.83	3.33	4.12	3.23	5.23	5.56	8.18
4	5.89	3.10	4.23	3.60	5.24	5.71	

Table 10. Calculated Average Daily Water and Chemical Additions for Run Three

Cell #	Water Added (ml)	$MnSO_4$* H_2O (g)	NaCl (g)	Acid (ml)	$Fe_2(SO_4)_3$* $5H_2O$ (g)	$CoSO_4$*7 H_2O (g)	CuO (g)
1	238	0.93	0.00	20.9	0.30	0.18	386
2	639	1.24	0.01	75.5	2.64	0.54	358
3	208	0.31	0.00	24.5	0.49	0.90	386
4	649	0.85	0.01	46.9	1.29	0.36	403

Table 11. Measured Parameters and their Targets (B) for Run Four

Cell #	T (^{0}C)	Mn (mg/L)	Cl (mg/L)	Acid (g/L)	Fe (g/L)	Co (mg/L)	Cu (g/L)
B	35.0	50.0	20.0	180	1.20	150/600	40.0
1	35.2	53.5	21.4	186	1.28	174	21.1
2	35.3	53.8	21.0	190	1.32	179	23.3
3	34.5	52.9	19.6	189	1.28	613	21.1
4	34.1	52.0	20.7	182	1.28	156	20.9

Table 12. Average Solution Levels, Cathode (C1, C2 and C3) and Anode (A1 and A2) Currents Measured (A), System Voltage (SV) and Applied Current for Run Four

Cell #	Solution Level (cm)	C1 (A)	C2 (A)	C3 (A)	A1 (A)	A2 (A)	SV (V)
1	6.96	2.92	5.75	2.87	5.79	5.74	8.54

Table 12. Average Solution Levels, Cathode (C1, C2 and C3) and Anode (A1 and A2) Currents Measured (A), System Voltage (SV) and Applied Current for Run Four (cont.)

Cell #	Solution Level (cm)	C1 (A)	C2 (A)	C3 (A)	A1 (A)	A2 (A)	SV (V)
2	7.11	3.92	3.75	3.95	5.65	5.85	8.54
3	7.20	3.73	4.11	3.66	5.65	5.85	
4	6.54	3.71	4.37	3.45	5.66	5.82	

Table 13. Calculated Average Daily Water and Chemical Additions for Run Four

Cell #	Water Added (ml)	$MnSO_4$* H_2O (g)	NaCl (g)	Acid (ml)	$Fe_2(SO_4)_3$ *$5H_2O$ (g)	$CoSO_4$*7 H_2O (g)	CuO (g)
1	250	0.02	0.01	19.8	0.38	0.16	387
2	248	0.01	0.02	22.5	0.47	0.22	342
3	250	0.01	0.04	24.4	0.64	0.72	386
4	383	0.01	0.02	26.0	0.73	0.15	390

3.2. OUTPUT SUMMARY

In each run, cells 1 and 4 were set up as the control experiments. They both had the same parameters. Cell 2 had power outages for 6 hours a day, three times a week. Cell 3 had a higher [Co]. This made it possible to compare the effect of Co and power outages in each run at the two temperatures and [Mn]. Temperature and [Mn] were varied across runs to know their respective effects. Therefore, each parameter level was tested at least twice.

Anode corrosion rates and current efficiency data collected and calculated for each cell and each run. The averages for these output variables are shown in Tables 14 and 15. In each run, Cells 1 and 4 were replicates and both indications of experimental error. The variation analysis show minimal variation in the individual runs between cells 1 and 4.

Table 14. Anode Corrosion and Current Efficiency Averages for the Four Cells and the Runs One and Two

Cell #	Run 1		Run 2	
	Anode Corrosion (g/day)	CE (%)	Anode Corrosion (g/day)	CE (%)
1	$7x10^{-3}$	92.7	$-8x10^{-2}$	90.3
2	$3x10^{-2}$	92.5	$-1x10^{-1}$	90.0
3	$1x10^{-2}$	89.7	$-1x10^{-1}$	92.8
4	$2x10^{-2}$	90.1	0	90.2

Table 15. Anode Corrosion and Current Efficiency Averages for the Four Cells and the Runs Three and Four

Cell #	Run 3		Run 4	
	Anode Corrosion (g/day)	CE (%)	Anode Corrosion (g/day)	CE (%)
1	$-1x10^{-2}$	94.4	$1x10^{-2}$	95.8
2	$1x10^{-2}$	93.7	$-1x10^{-2}$	92.6
3	$-1x10^{-2}$	94.4	$-1x10^{-2}$	94.2
4	$-1x10^{-2}$	95.0	$1x10^{-2}$	95.1

3.3. ANODE CORROSION

Corrosion was determined by weight change of the base lead anode. After each run, scale was both manually and chemically removed. Several anodes experienced a small weight gain (denoted by a negative corrosion rate). This probably indicates that not all scale was removed even though the cleaning procedure was consistent. This could be indicative of scales that are different. Even for anodes that experienced a decrease in weight, the reduction was minimal (0.1-1.0 g for 704-751 g anodes). The changes in weight are so small that it probably reflects mostly measurement error.

Visual inspections of the anodes after each run only showed discoloration of the immersed anode surface area but there were no visible signs of preferential or localized corrosion. A picture of Run Two's anodes after operation is shown in Figure 2.

The low corrosion rates in all of the tests is attributed to the presence of Co in the electrolyte. Co is known to catalyze the water breakdown reaction reducing the power utilization [13, 16, 18, 19]. More importantly it helps to form a more tenacious scale on the lead alloy anode that reduces corrosion [13, 16, 18, 19]. Hence industry operations generally maintain electrolyte concentrations of at least 150 mg/L Co to reduce anode corrosion rates [8]. All the cells had at least 150 mg/L of Co and that could explain the very low corrosion rates which in this case makes it difficult to confidently quantify the anode corrosion rates. From the corrosion data, it is believed that maintaining [Co] greater than 150 mg/L overwhelmed any effect that might have been caused by power outages, temperature and [Mn] as recommended by [8].

Figure 2. Anode Pictures after Corrosion Tests for Run Two

3.4. CATHODE CURRENT EFFICIENCY

Cathode current efficiency was also examined for each of the runs. No short circuits were observed during the runs. Current efficiency values were collated and compared across all the cells and runs. A Q test for bad data was conducted on the outlier points to determine if they should be discarded or not. No data points were discarded. Signal to noise (S/N) ratio calculations also show that none of the levels of parameters investigated have a significant effect on the CE as shown in Table 16.

It is believed that the 10 or less degree difference in temperature was not enough to highlight any temperature effects as seen in the S/N ratios for the two factor levels. The effect of temperature on the ferric diffusion coefficient which is a vital parameter in CE is approximately 1.5 % for every degree celcius variation [2]. This is a 15 % variation effect on the diffusion coefficient which overall may not be enough to be significant given the

electrode configuration used (3 cathodes and 2 anodes – hence the outer cathodes had less current than the inside cathode).

This work is consistent with 16 hour experiments [10, 11] that [Mn], [Co] and [Cl] have no significant effects on CE while [Fe] and power consumption were proportional and indirectly proportional to the CE respectively [10]. The results of this study are inconsistent with [1] with relation to the effects of temperature perhaps because of the absence of Co, Mn and Fe in the electrolyte. There is an indicative parameter interaction between these ions that could overwhelm the effects of temperature. Also [1] establishes that increasing temperature increases CE, this is contrary to [2].

Table 16. Parameter Means and Signal to Noise Ratios Calculated

Parameter	**Level**	**Mean**	**S/N**
Temp	35	92.8	39.3
	50	91.8	39.2
Mn	50	91.8	39.2
	600	92.8	39.3
Co	150	92.2	39.2
	600	92.8	39.3
Power Outage	Yes	92.2	39.3
	No	92.4	39.3

3.5. MANGANESE AND CHLORINE LOSSES FROM ELECTROLYTE

Daily Mn and chloride losses from the electrolyte were calculated by comparing the measured value with the previous value to determine a loss or gain. When the measured value was lower than the target, chemical addition was done. On days that the values were higher than the targets, that chemical was not added. These values are reported in Table 15. A negative loss means that the measured value was higher than the target.

Daily Mn losses correlated well with daily Cl losses as shown in Tables 17 and 18 with an approximate R squared value of 93%. This indicated some parameter interaction that has to be further investigated. A reaction between dissolved Mn and Cl to form MnO_2 and $Cl_2(g)$ has been proposed by [27]. $Cl_2(g)$ evolution was not monitored or measured in this study. MnO_2 formation occurred with the formation of a black powdery film that formed on cell walls, cell bottoms and in the various tubes. The formation of MnO_2 can also occur by the disproportionation reaction of Mn^{3+} [28].

Table 17. Mn and Cl Losses and their Respective Loss Ratios for each Cell for Runs One and Two

Cell #	Run 1			Run 2		
	Mn Loss (mg)	Cl Loss (mg)	Mn/Cl	Mn Loss (mg)	Cl Loss (mg)	Mn/Cl
1	554	40.4	13.7	4.9	10.6	0.46
2	245	16.3	15.0	22.9	10.0	2.28
3	2697	129.0	20.9	4.1	4.5	0.93
4	554	42.0	13.2	5.3	8.2	0.65

High [Mn], lower temperature saw the greatest Mn and Cl losses, higher temperature saw less Cl losses Examining the ratio of Mn loss to Cl loss for Runs 1 and 3 indicates that the least average Mn/Cl ratios was above 11 for high [Mn] at both low and high temperatures. Further statistical data analysis (including student t tests) indicated no significant differences between the means of parameters investigated at the levels chosen on the output signals.

Table 18. Mn and Cl Losses and their Respective Loss Ratios for each Cell for Runs Three and Four

Cell #	Run 3			Run 4		
	Mn Loss (mg)	Cl Loss (mg)	Mn/Cl	Mn Loss (mg)	Cl Loss (mg)	Mn/Cl
1	155	0.99	156	3.86	8.30	0.47
2	275	3.39	81	1.65	12.38	0.13
3	-47	-4.16	11	2.85	22.21	0.13
4	79	2.31	34	3.17	13.28	0.24

3.6. CELL MUD

Generally, the low temperature runs (runs one and four) had formations of blue crystal salts (shown in Figure 3) at the bottom of the solution reservoirs. Low temperature reduces the solubility and cause crystallization of Cu salts.

The low temperature, high [Mn] run (Run One) produced thicker black scale and deposition. Cells 1 and 4 (controls) had more cell mud at the bottom of their reservoirs then

the other two cells (see Figure 3). The mud was sand-like in appearance. Cell 2 which underwent power outages had very little mud comparable to the other cells. The mud was also sand-like. Cell 3 for Run 1 (600 mg/L Co, 600 mg/L Mn, 35°C) did not have any blue crystals at the bottom but a black substance that had stained the inside of the cell reservoir. The cell mud looked glossy and blacker than the other runs as shown in Figure 3.

The cell insides also had cell mud at the bottom as shown in Figure 4. This could likely be as a result of the higher [Co]. Cell 3 had a black substance which is believed to be MnO_2. These results indicate that power outages and [Co] affect the formation of MnO_2 cell mud at 35°C.

While differences in cell mud were observed in Run One, no differences were noted in Runs Two, Three and Four. All of the cells and reservoirs appeared similar to the cell 2 images in Figures 3 and 4.

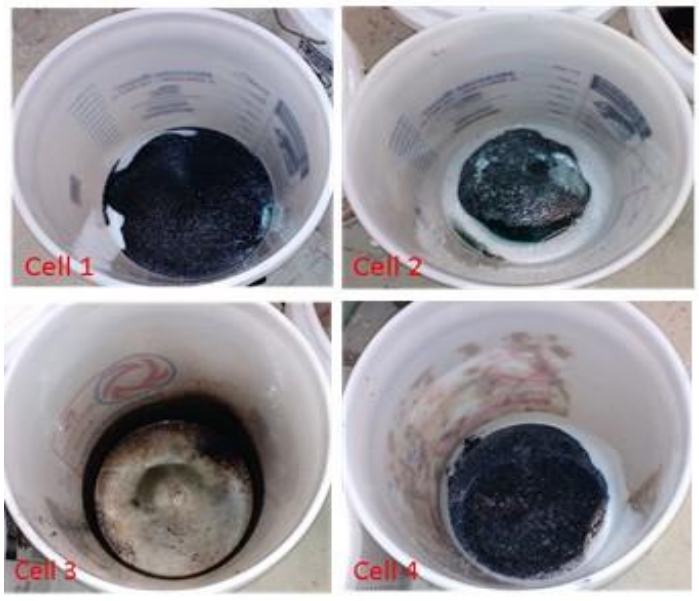

Figure 3. Pictures of Reservoir Bottoms after Run One

Figure 4. Cell Inside and Floors Pictures after Draining Electrolyte Solutions

4. CONCLUSIONS

Four runs of 28 day testing was completed in an anode corrosion testing system to evaluate the effects of power outage, temperature and [Mn] and [Co]. The corrosion rates after 28 days did not show any significant trends. It is believed the presence of at least 150 mg/L Co in all of the experiments minimized corrosion. Maintaining a 150 mg/L minimum [Co] seems to have overwhelmed any effect of power outages, temperature or [Mn] on anode corrosion. Temperature, power outages, [Mn] and [Co] at the levels tested did not significantly affect the current efficiency. The losses of Mn and Cl from the electrolytes were correlated (R^2 = 93 %). Larger losses occurred at the higher [Mn] concentration. The low temperature high Mn run showed the most MnO_2 formation and Cl_2 evolution. The low temperature high Mn run also showed differences in cell mud formation and revealed the power outages and [Co] affected the amount and type of mud formed.

ACKNOWLEDGEMENT

The S&T research team would like to thank the AMIRA P705C sponsors for their assistance and guidance in the design of our testing system and protocols and supplying copper starter sheets and Pb-Ca-Sn anodes. The experimental assistance of Margaret Scott and Kevin Lee Foster is greatly appreciated for the successful completion of this work.

REFERENCES

1. Alfantazi, A. and D. Valic, *A study of copper electrowinning parameters using a statistically designed methodology.* Journal of applied electrochemistry, 2003. 33(2): p. 217-225.

2. Andersen, T., C. Wright, and K. Richards. *Important electrochemical aspects of electrowinning copper from acid leach solutions*. in *International Symposium on Hydrometallurgy. AIME, New York*. 1973.

3. Aqueveque, P.E., et al. *Measurable variables in copper Electrowinning and their relevance to predict process performance*. in *Industry Applications Society Annual Meeting, 2013 IEEE*. 2013. IEEE.

4. Luyima, A., et al., *Examination of copper electrowinning smoothing agents. Part II: Fundamental electrochemical examination of DXG-F7.* Minerals and Metallurgical Processing, 2016. 33(1): p. 14-22.

5. Cifuentes, G., et al. *The corrosion of lead anodes in copper electrowinning*. in *Proceedings of the Copper'99 International Conference*. 1999.

6. Joy, S., et al., *Understanding and improvement of electrowinning current efficiency at Freeport-McMoRan Bagdad.* Copper 2010 proceedings, 2010. 4: p. 1379-1392.

7. Miller, G., *Recent Experience with Manganese and its Effects on Copper SX-EW Operations.* 2011.

8. Miller, G., *Methods of managing manganese effects on copper solvent extraction plant operations.* Solvent Extraction and Ion Exchange, 2011. 29(5-6): p. 837-853.

9. Miller, G., D. Readett, and P. Hutchinson, *Experience in operating the Girilambone copper SX-EW plant in changing chemical environments.* Minerals Engineering, 1997. 10(5): p. 467-481.

10. Moats, M. and Y. Khouraibchia. *Effective diffusivity of ferric ions and current efficiency in stagnant synthetic copper electrowinning solutions*. in *SME Annual Meeting and Exhibit and CMA's 111th National Western Mining Conference 2009*. 2009.

11. Moats, M.S., *How to evaluate current efficiency in copper electrowinning.* Separation Technologies for Minerals, Coal, and Earth Resources, 2012: p. 333.

12. Moats, M.S., *Energy efficiency of electrowinning*, in *Energy Efficiency in the Minerals Industry*. 2018, Springer. p. 213-232.

13. Barmi, M.J. and A.N. Nikoloski, *Electrodeposition of lead–cobalt composite coatings electrocatalytic for oxygen evolution and the properties of composite coated anodes for copper electrowinning.* Hydrometallurgy, 2012. 129: p. 59-66.

14. Cifuentes, L., A. Montes, and G. Crisóstomo, *Corrosion behaviour and catalytic effectiveness of Pb–Ca–Sn, RuO2–IrO2/Ti and IrO2–Ta2O5/Ti anodes for copper electrowinning.* Corrosion Engineering, Science and Technology, 2011. 46(6): p. 737-744.

15. Gendron, A.S., V.A. Enel, and S. Abe, *Effect of cobalt added to electrolyte on corrosion rate of Pb-Sb anodes in copper electrowinning.* Canadian Metallurgical Quarterly, 1975. 14(1): p. 59-61.

16. Abbey, C. and M. Moats, *Effect of Cobalt and Iron Concentration on the Potential for Oxygen Evolution from Pb–Ca–Sn Anodes in Synthetic Copper Electrowinning Electrolytes*, in *Applications of Process Engineering Principles in Materials Processing, Energy and Environmental Technologies*. 2017, Springer. p. 89-95.

17. Nguyen, T. and A. Atrens, *Influence of lead dioxide surface films on anodic oxidation of a lead alloy under conditions typical of copper electrowinning.* Journal of Applied Electrochemistry, 2008. 38(4): p. 569-577.

18. Nguyen, T., et al., *Influence of cobalt ions on the anodic oxidation of a lead alloy under conditions typical of copper electrowinning.* Journal of Applied Electrochemistry, 2008. 38(2): p. 215-224.

19. Nikoloski, A. and M. Nicol, *Effect of cobalt ions on the performance of lead anodes used for the electrowinning of copper—A literature review.* Mineral Processing and Extractive Metallurgy Review, 2007. 29(2): p. 143-172.

20. Clancy, M., et al., *The influence of alloying elements on the electrochemistry of lead anodes for electrowinning of metals: a review.* Hydrometallurgy, 2013. 131: p. 144-157.

21. Hrussanova, A., L. Mirkova, and T. Dobrev, *Electrochemical properties of Pb–Sb, Pb–Ca–Sn and Pb–Co3O4 anodes in copper electrowinning.* Journal of applied electrochemistry, 2002. 32(5): p. 505-512.

22. Hrussanova, A., et al., *Influence of temperature and current density on oxygen overpotential and corrosion rate of Pb–Co 3 O 4, Pb–Ca–Sn, and Pb–Sb anodes for copper electrowinning: Part I.* Hydrometallurgy, 2004. 72(3): p. 205-213.

23. Free, M., et al., *Electrometallurgy-Now and in the Future.* Electrometallurgy 2012, 2012: p. 3-28.

24. Tjandrawan, V. and M.J. Nicol, *Electrochemical oxidation of iron (II) ions on lead alloy anodes.* Hydrometallurgy, 2013. 131: p. 81-88.

25. Khouraibchia, Y. and M.S. Moats, *Evaluation of the effect of copper electrowinning parameters on current efficiency and energy consumption using surface response methodology.* ECS Transactions, 2010. 28(6): p. 295-306.

26. Nicol, M., et al., *Effect of halides in the electrowinning of zinc. II. Corrosion of lead-silver anodes.* Hydrometallurgy, 2017. 173: p. 178-191.

27. Kelsall, G., et al. *Effects of manganese (II) and chloride ions in zinc electrowinning reactors*. in Proceedings—Electrochemical Society. 2000.

28. Yu, P. and T.J. O'Keefe, *Evaluation of lead anode reactions in acid sulfate electrolytes II. Manganese reactions.* Journal of the Electrochemical Society, 2002. 149(5): p. A558-A569.

V. A NEW PB-CA-SN ANODE POTENTIAL (AP) MODEL FOR COPPER ELECTROWINNING IN SYNTHETIC SULFURIC ACID ELECTROLYTES

C. E. Abbey, and M. S. Moats

Missouri University of Science & Technology

Rolla, MO 65409

Tel:573-308-9236

Email: ceag28@mst.edu

ABSTRACT

In copper electrowinning, a high overpotential is associated with oxidation of water to evolve oxygen on lead alloys. This high overpotential provides the biggest avenue for energy reduction when plating copper. Overpotential is affected by various conditions including the chemistry of the electrolyte, electrode alloy, temperature, anode surface finish, anode age and current density. The knowledge of what affects the anode potential and to what extent is an important utility for energy optimization. In this study, a new Pb-Ca-Sn anode potential estimation model has been developed to estimate the effect of industrially relevant parameters on anode potential and consequently, energy consumption. An initial design of experiments was performed to determine significant parameters and a subsequent full quadratic design of experiments focusing on the significant parameters. The test work consisted of chronopotentiometric analysis using Pb-Ca-Sn anodes with a platinum counter electrode and measuring the anode potential against a mercury - mercurous sulfate reference electrode every 3 seconds. Four main effects and one two-way

interaction parameters were significant at a 95 % confidence level with the most influential determined to be temperature, followed closely by current density, acid concentration, and finally, Co concentration. The new model was validated at 4 circuits in 2 industrial copper tankhouses. Validation shows that the model has a maximum variation below 10 % and a maximum standard deviation of 0.13. Linear sweep voltammetry established that the phases of the anode scales are possibly PbO_2, $PbSO_4$ and PbO.

Keywords: anode potential, copper electrowinning, temperature, current density, cobalt, sulfuric acid.

1. INTRODUCTION

Copper electrowinning is an energy intensive process. Electrical energy utilized for electrochemical reactions accounts for about 80 % of the total energy with an estimated average of 2.0 kWh per kilogram of copper produced. Thus, savings on energy can improve project economic viability and profits [1-3]. Energy consumption, cathode production rate and quality are the three most important performance measurement responses in the copper electrowinning industry [4, 5]. In addition to anode corrosion, these four parameters contribute to overall process profitability [6]. Energy optimization strategies practiced and proposed include high Fe electrolytes coupled with periodic reverse current methods [7], electrode alloy composition [8, 9], electrolyte chemistry [10, 11], alternative anode technology [12-14], reduction of cuprous ions instead of cupric and anodic half-cell reaction substitution with the ferric/ferrous redox pair [15, 16] or SO_2 [17].

Both energy consumption and power consumption are directly proportional to cell voltage. Cell voltage constituents include the voltages associated with thermodynamics (~0.9 V), solution resistance (~0.25-0.3 V), contact resistance (~0.1-0.3 V), cathode overpotential (~0.05-1 V) and anode overpotential (~0.5 V for a lead alloy anode) [18]. The cell voltage for copper electrowinning using a lead-alloy anode with cobalt in the electrolyte is approximately 2 V [18].

Depending on the facility, electrolytes may have various concentration of Cl, Mn, Co and Fe. Electrolyte chemistry may have a concomitant effect on the energy draw of the electrowinning system. Cobalt in solution reduces the anode potential and corrosion rates [19-23]. The effect of pertinent Co concentrations in the presence of Mn with and without 0.6 g/L Fe has been quantified [24]. Fe reduces anode potential [24] but is detrimental to cathodic current efficiency when ferric reduces to ferrous. Mn can also be found in various concentrations in electrolytes and an Fe:Mn ratio of 10:1 with a minimum of 1 g/L Fe has been recommended for SX-EW operations [25]. The effect of Mn in the electrolyte negatively affects conductivity, density and viscosity but has not yet been shown to have any effect on anode potential [26] though anodes coated with MnO_2 have lower anode potentials [9]. Other parameters that may affect anode potential include temperature, current density, chloride ions, acid concentration, and anode age and chemistry.

This work therefore utilized a design of experiments approach to find significant factors affecting anode potential, quantify their effects, develop an anode potential estimation model and study anode scale products for possible mechanisms and explanations of the effect of these parameters on the anode potential and hence energy consumption. The model was also validated with industrial tankhouse measurements. The

phases of scales formed on the anode after polarization were also studied using physical and electrochemical characterization techniques.

2. EXPERIMENTAL

2.1. DESIGN AND ANALYSIS OF EXPERIMENT

JMP statistical software was used to design the experimental conditions. The design provided the minimum number of experiments required and sufficient to completely specify a full quadratic effects of the testing parameters. The design consisted of 2 parameter levels and a centroid for seven continuous factors [27]. The seven parameters examined are temperature, current density, and concentrations of Cl, Co, Fe, Mn and sulfuric acid. The design considered only parameter main effects, two-way and squared interactions of significance. The parameter levels including centroids are shown in Table 1.

Table 1. Design of Experiments Parameter Levels

Parameter	**Minimum**	**Centroid**	**Maximum**
Cl (mg/L)	20	40	60
Co (mg/L)	80	130	180
Fe (g/L)	1.50	2.25	3.00
Mn (mg/L)	10	60	110
Acid (g/L)	160	180	200
Temperature (°C)	35.0	42.5	50.0
Current Density (A/m^2)	200	300	400

Parameter levels were chosen so that the test values are representative of North American industrial tankhouse conditions.

To achieve a 95 % confidence level with 95 % accuracy, each run was performed in triplicate. A random number generator was used to randomize the order of the run to eliminate any systematic errors. MiniTab and JMP statistical softwares were used to analyze the experiments and results.

2.2. MATERIALS AND METHODS

Synthetic electrolyte volumes of 300 mL containing various concentrations of sulfuric acid, Cl^- ions from NaCl, Co from $CoSO_4.7H_2O$, Fe from $FeSO_4.5H_2O$ and Mn from $MnSO_4.H_2O$ were prepared according to the experimental design factorial matrix using the levels in Table 1. All chemicals used were research grade analytical reagents. Deionized distilled (DI) water was used and the electrolyte composition was not controlled during the experiment.

Specimens of a rolled Pb-Ca-Sn anode provided by a commercial supplier were cut with dimensions 1 cm x 1 cm for the analysis. A copper wire was soldered to one face of each specimen. The specimen was also acrylic spray painted leaving only one face of the specimen for electrolyte contact. The specimen was mounted in epoxy resin to control contact with the electrolyte. One surface of the mounted specimen was then ground in succession with 36-grit, 100-grit, and 200-grit silicon carbide sandpaper until it was fully exposed and level.

2.3. CHRONOPOTENTIOMETRIC ANALYSIS

All electrochemical experiments were conducted using a three electrode cell in a three neck round bottom flask. The rolled Pb-Ca-Sn working electrode was placed at a controlled distance of 3.8 cm from a platinum mesh counter electrode. A mercury-mercury sulfate reference electrode (0.64 V vs. standard hydrogen electrode, SHE) connected using a luggin capillary tube was inserted into the cell as the reference electrode. Measured potentials were converted to SHE potentials. The distance between the reference electrode and the anode was maintained constant throughout all the experiments. Preliminary tests showed that the distance did not significantly affect the anode potential. The three neck round bottom flask was heated to the desired temperature and maintained at +/- 3 °C of the target temperature using a water bath with a feedback control loop.

A Gamry Reference 3000 Galvanostat Potentiostat was used to apply a constant current and record the anode potential versus a mercury-mercury sulfate reference electrode every 3 seconds. Constant current electrolysis or chronopotentiometry was performed to measure the anode potential of the Pb-Ca-Sn anode as a function of the various conditions for 24 hours. The applied current was calculated based on the measured surface area of the working electrode determined using Image J software.

2.4. ANODE POTENTIAL VALIDATION

Freeport McMoRan provided permission to measure anode potentials in two tankhouses to validate the anode potential model. An anode potential measuring probe was designed and constructed. The schematic diagram and fabricated anode potential probe is shown in Figure 1. During validation, measurements were taken on random anodes from

every 10 cells in an electrical circuit. Two circuits were examined at two tankhouses. At the time of the measurements, electrolyte samples were collected and analyzed for Co and acid concentrations. Electrolyte temperature was collected using a type K thermocouple probe inserted into the cell at the time of the anode potential measurement. Anode current density was calculated by dividing the rectifier current by the number of anodes in the cell and the submerged anode surface area.

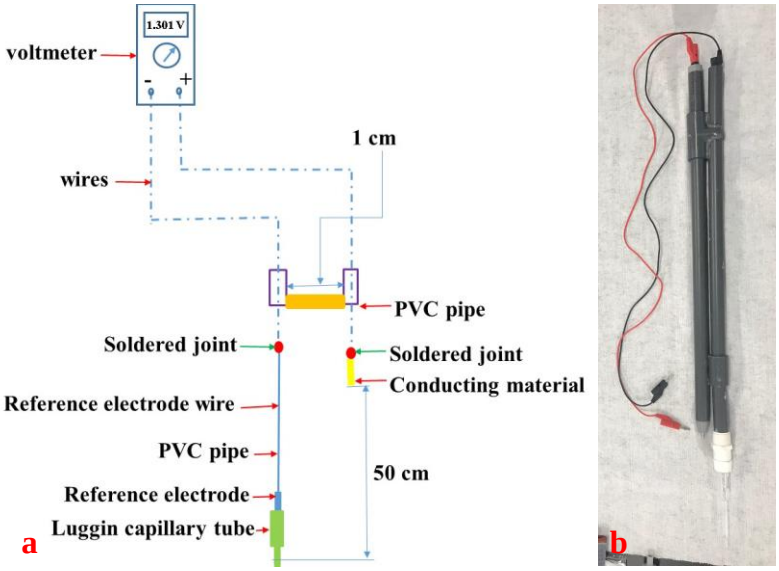

Figure 1. Designed Anode Potential Probe (a) Schematic (b) Fabricated Probe with Wires that Connect to Voltmeter

2.5. ELECTROCHEMICAL ANALYSIS AND CHARACTERIZATION

Linear sweep voltammetry (LSV) was performed to examine the electrochemical behavior of the anode after being conditioned. The potential was swept from 1.976 V to -0.922 V vs. SHE at a rate of 1 mV/s for LSV. The current values were collected and converted into current density using the measured surface area of the individual working

Pb-Ca-Sn electrode. The purpose of the linear sweep voltammetry was to examine the reduction of scales that had formed on the anode during constant current oxidation.

Conditions using the minimum levels of each of the parameters in Table 1 was tested as the base condition. Changing one of the significant parameters (Co, H_2SO_4, temperature and current density) at a time, tests were conducted to compare to the base conditions to ascertain the effect of the particular parameter. Hence, to determine the effect of Co concentration on anode potential a test was conducted with all the base conditions but changing Co concentration to the maximum Co value in Table 1. The results were then compared with the base condition test results.

3. RESULTS AND DISCUSSION

3.1. MAIN EFFECT PARAMETER SCREENING

Seven parameters namely temperature, current density, concentrations of Cl, Co, Fe, Mn and sulfuric acid were initially tested to screen out insignificant parameters. Analysis of variance (ANOVA) and residual analysis were conducted to determine the significance of each parameter. The individual contributions of each parameter to the predicted value and p-values for each parameter for the screening analysis are shown in Table 2. Only main effects were used in the screening analysis. This model therefore assumes linear response relationships with the factors.

The regression coefficient (R^2) was approximately 0.97. As shown in Table 2, Fe, Mn and Cl were deemed as insignificant parameters in the industrially relevant ranges tested because their probability values were more than 0.05. This meant that in developing

the final anode potential model those parameters should be exempted. In a previous work [28] the effect of Fe was found to be quadratic when tested at a 0 g/L to 3 g/L range peaking at 1.5 g/L. This observation is consistent with the current study which only examined the 1.5 g/L to 3 g/L range tested. The results for Mn and Co are also consistent with the same previous work [28] in terms of the proportionality and its effects on the AP but shows that Mn is not significant in the concentration ranges tested since the range was more narrow.

Table 2 also shows parameters significant to anode potential and whether the effect scaled estimates are positive or negative. Negative scaled estimates show that the anode potential decreases with increasing parameter levels, and positive scale estimates show that the anode potential increases with increasing parameter levels.

Table 2. Analysis of Variance Results for Initial Parameter Screening

Source	Contribution	P-Value	Scaled Estimates
Model	96.60%	0.009	
Linear	96.60%	0.009	1.9388
Co (mg/L)	9.83%	0.027	-0.0083
Fe (g/L)	0.36%	0.548	-0.0016
Mn (mg/L)	1.13%	0.313	0.0028
Acid (g/L)	10.19%	0.026	0.0085
Temperature (°C)	44.95%	0.002	-0.0178
Current Density (A/m^2)	28.13%	0.005	0.0141
Cl (mg/L)	2.02%	0.198	0.0038
Error	3.40%		
Total	100.00%		

3.2. NEW ANODE POTENTIAL MODEL

Using the screening results, four parameters (Co, acid, temperature and current density) were used in a new custom full quadratic design of experiments running three replicates each. New chronopotentiometric analysis for 24 hours were conducted and the average of the last ten minutes of each replicate was used as the response in calculating the ANOVA tables and other statistical results. Residuals were examined for quality assurance purposes and were found to be acceptable. Table 3 shows p-value results for full quadratic analysis tested at various levels for the significant parameters.

Table 3. Anode Potentials Analysis of Variance Results

Source	P-Value
Model	0.000
Linear	0.000
Co (mg/L)	0.000
Acid (g/L)	0.001
Temperature (°C)	0.000
Current Density (A/m^2)	0.000
Square	0.550
Co (mg/L)*Co (mg/L)	0.969
Acid (g/L)*Acid (g/L)	0.633
Temperature (°C)*Temperature (°C)	0.607
Current Density (A/m2)*Current Density (A/m^2)	0.172
2-Way Interaction	0.180
Co (mg/L)*Acid (g/L)	0.673
Co (mg/L)*Temperature (°C)	0.037
Co (mg/L)*Current Density (A/m^2)	0.719
Acid (g/L)*Temperature (°C)	0.181
Acid (g/L)*Current Density (A/m^2)	0.698
Temperature (°C)*Current Density (A/m^2)	0.115

The anode potential (AP) was stable in the last ten minutes of operation for each experiment. The variances calculated for all the replicate runs were within 5 mV and

deemed reasonable. All data points were statistically evaluated and no points were removed based on outlier statistical analysis.

Temperature, current density and concentrations of Co and acid were confirmed to be significant but all squared interactions were shown to be insignificant. All 2-way interactions were also insignificant except Co*temperature.

The results of the scaled estimates were consistent with those reported in Table 2. Acid and current density had positive scaled estimates while Co concentration and temperature had negative scaled estimates over the ranges tested. Previous reports [19, 24. 28] show that Co has a sharp almost linear reduction effect on anode potential from 0 mg/L to about 150 mg/L [Co] and hence a linear estimation as provided by the response analysis would be sufficient. No modifications were required to constraint the model towards a quadratic Co effect. Additionally, the contribution of Co to the prediction model was approximately 10 % as shown in Table 2. Current density [29, 30] reponses agree with previous. Sulfuric acid increases the anode potential and it also increases electrolyte conductivity which consequently reduces cell voltage [30]. Temperature and current density effects were also consistent with [29].

Current density (CD), sulfuric acid concentration, and temperature effects on the AP can be explained by both the Tafel equation and Nernst Equations which describe the kinetics and thermodynamics of electrode reactions respectively. The Nernst equation describes the overpotential (η) as a function of the temperature (°K) and the natural logarithm of the ratio of the activities of the products to the reactants raised to their stoichiometric coefficients. In the case of the oxygen evolution reaction (OER), the

activities of water and oxygen are unity and so the overpotential is proportional to the temperature and the pH as shown in Equation 1, T is the temperature in °K.

Equation 2 shows charge transfer resistance (R_{ct}) derived from the Tafel equation of electrode kinetics that indicate that for the same R_{ct}, increasing temperature has to be compensated by a decrease in overpotential which is consistent with the anode potential results scaled estimates. The Tafel equation as shown in Equation 3 describes the kinetics of electrode reactions. This Tafel equation is a simplified version of the Butler Volmer equation that plots the overpotential of an electrode against the logarithm of the specific current density. The slope is b and the intercept is a and the overpotential is η. For a large positive overpotential (>100 mV), η increases with increasing logarithm of the current density (i).

$$\eta = -4.96x10^{-5}T * log(a_{H+})^{-4} \quad (1)$$

$$R_{ct} = {}^{\eta}/_{T} = {}^{-R_i}/_{i_o F} \quad (2)$$

$$\eta = a + b\ log\ i \quad (3)$$

An interesting observation was that separately Co concentration and temperature have a negative effect on the AP, but their 2-way interaction (Co*temperature) had a positive effect on AP. This might provide an opportunity for further investigation.

With the five established significant parameters, a regression model was calculated. The AP model using units commonly employed in operations is shown in Equation 4 with an R^2 of approximately 96%. Residual analysis show a normal distribution with maximum variation below +/- 7.5 mV. Figure 2 shows a plot of 30 predicted values of anode

potentials against their respective measured values of lab-scale experiments performed separately from the experiments that were used to develop the model. The figure shows a good spread of the data points with an R^2 of approximately 96%. This compares well with the R^2 values obtained from the model. From [19, 24, 28], Co has an exponential effect on AP but at the ranges of concentrations tested it has an essentially linear response and hence Equation 4 did not require placing the exponential restraint as done in [24, 28].

$$AP\ (V) = 1.9884 - 0.393\ Co\ (g/L) + 0.000189\ Acid\ (g/L) - 0.002736\ T\ (℃) + 0.000147\ CD\ (A/m^2) + 0.00591\ Co\ (g/L) * T\ (℃) \quad (4)$$

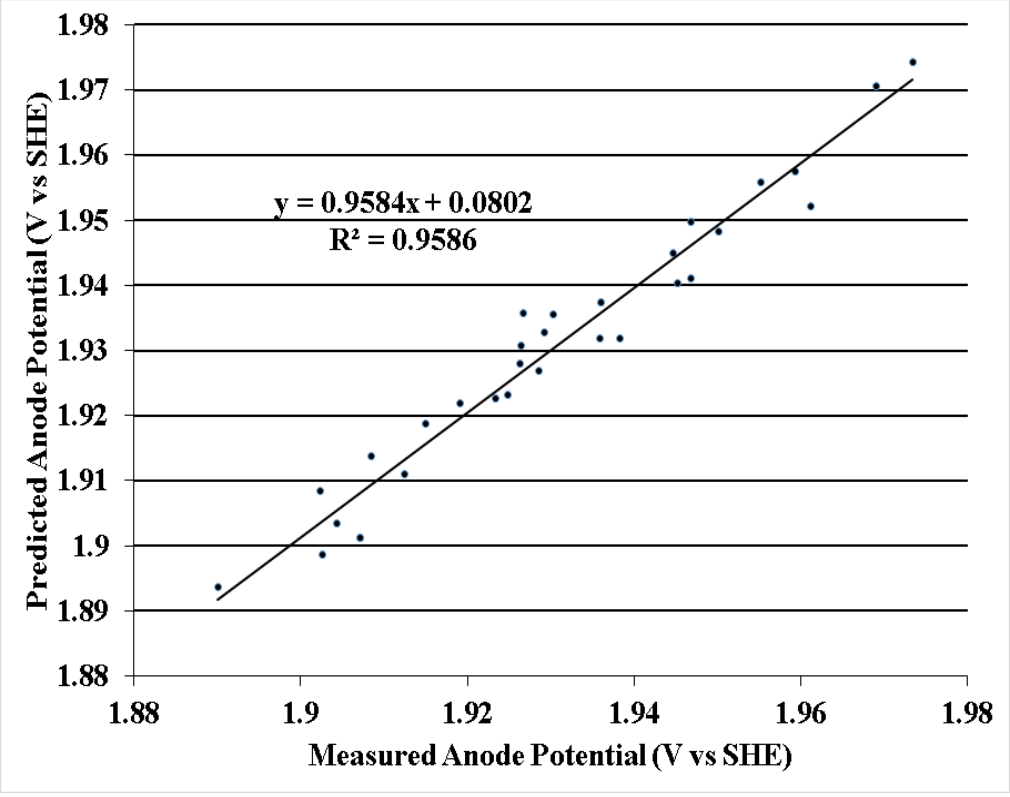

Figure 2. Predicted versus Measured Anode Potential Values of Independent Lab-Scale Experiments

3.3. LINEAR SWEEP VOLTAMMETRY

To further understand the empirical model, anodes were operated for 2 hours at 300 A/m^2. Following this treating linear sweep voltammetry was performed to interrogate the oxidized surface. Results from linear sweep voltammetry following constant current operation of the Pb-Ca-Sn working electrode are shown in Figures 3, 4 and 5 with different potential ranges to highlight the features or peaks.

Figure 3 shows the current generated when potential is sweep from 2.0 V to 1.8 V vs. SHE. This illustrates the current generated primarily by oxygen evolution reaction (OER) on the anode surface generated during the preceding constant current operation still in contact with the test electrolyte. The effect of acid and current density created an anode scale that appears to slightly polarized the OER. This is consistent with literature [30]. Increased [Co] and elevated temperature are shown to depolarize the OER as would be expected from Equation 4 and previous literature.

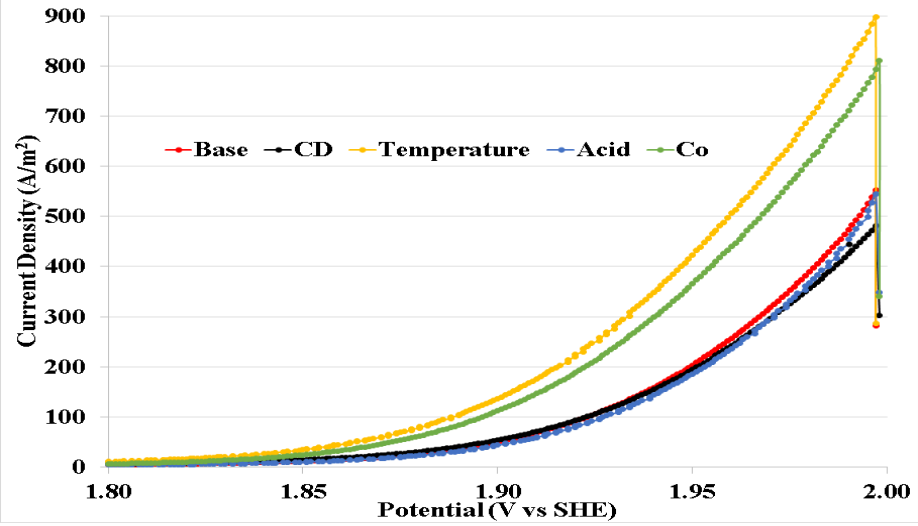

Figure 3. LSV Plots of Temperature, CD, Acid, Co and Base Conditions Showing Current Density Measured against Voltages from 1.8 V to 2.0 V

Figure 4 presents the voltammetry data as potential was sweep from 1.8 to 1.5 V vs. SHE. A series of convoluted oxidation peaks were observed that stretched having different forms depending on the conditions but indicative of two or three peak at various potentials. [26] observed similar peaks but did not offer an explanation to their identity. The lack of any net reduction currents between 1.6 and 1.5 V indicates that during the constant current operation minimal PbO_2 was formed leading to the absence of a PbO_2 to $PbSO_4$ reduction peak. This was also noted by not explained by [26].

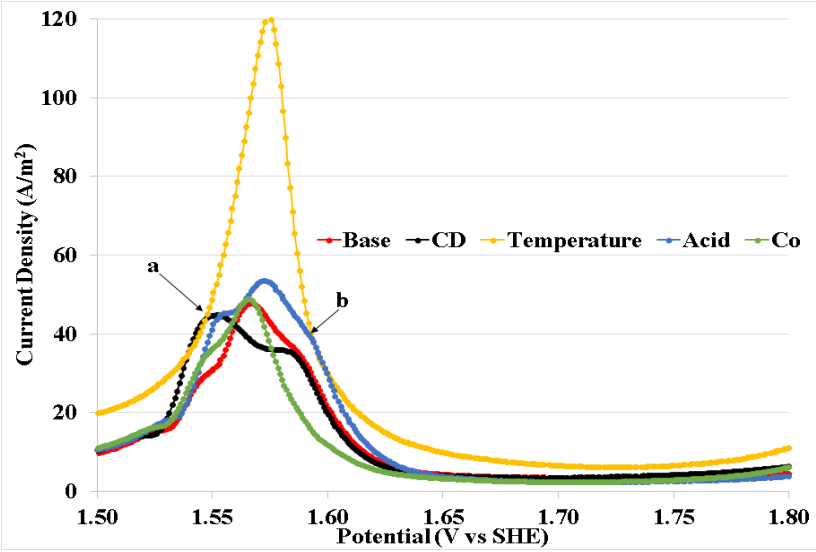

Figure 4. LSV Plots of Temperature, CD, Acid, Co and Base Conditions Showing Current Density Measured against Voltages from 1.5 V to 1.8 V

To understand these convoluted peaks separate experiments were conducted one element at a time to examine its response. These data are shown in Figure 5. Figure 5 shows that without Co in the electrolyte there is increased $PbSO_4$ oxidation to PbO_2 with a peak around 1.55 V vs. SHE. This is as a result of the instability of the PbO_2 layer formed. The layer corrodes into the electrolyte and more $PbSO_4$ is formed which oxidizes to PbO_2. This

results in increased anode corrosion. Without Mn presence a lower current density is recorded for $PbSO_4$ oxidation. This indicates that without Mn, the PbO_2 scale may be more stable. Both no Cl and no Fe plots show no shoulders b and a respectively. This also indicates that shoulder a and b are caused by Cl oxidation and Fe oxidation, respectively.

Using the knowledge gleaned from Figure 5, it appears that the convoluted peaks in Figure 4 are oxidation of lead exposed during the sweep as the middle peak with shoulder peaks (shoulders "a" and "b"), which is consistent with previous work [31]. Shoulder "a" is Fe^{2+} oxidation to Fe^{3+}. This was also observed in literature [31]. Shoulder "b" appears to be related to Cl^- oxidation. Since the maximum Co voltammetry shows no Cl shoulder it may indicate the inhibitive effect of Co on Cl oxidation at the anode. At increased temperature, more lead oxidation was observed, which may indicate that higher temperature produced a more porous or cracked scale surface. Increased acid showed a $PbSO_4$ peak with higher current density due to the excess sulfate ions readily forming $PbSO_4$ with any freshly exposed Pb surface.

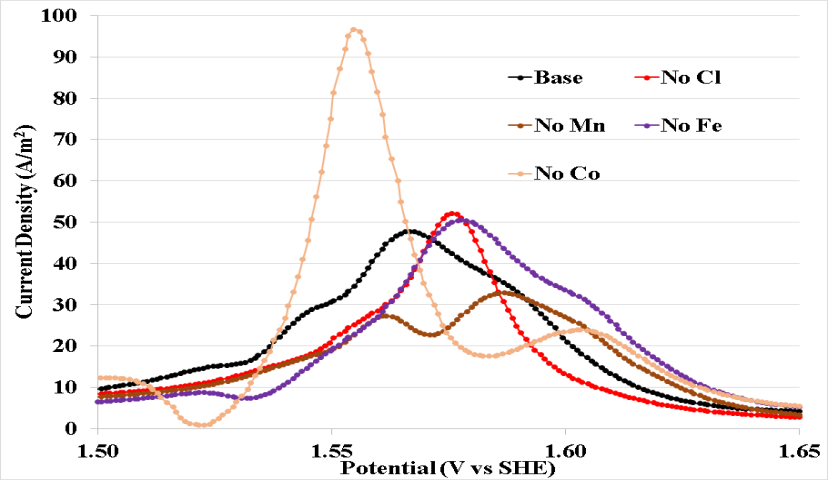

Figure 5. Linear Sweep Voltammetry from 1.5V to 1.65 V for Base Conditions without One Element at a Time to Interrogate the Effect of Each Element

3.4. ANODE POTENTIAL MODEL VALIDATION

While laboratory empirical models can be instructive for fundamental purposes. It was hoped that the model in Equation 4 could be used for industrial purposes. To validate the model, anode potentials were measured on every anode in multiple cells in two industrial electrowinning tankhouses. The number of cells measured, average measured anode potential and average predicted anode potential using Equation 4. The measured and predicted anode potential averages show reasonable correlation (as shown in Table 4). The positive values of the percent variations for each cell was calculated using Equation 5 from the industrial tankhouse measurements.

The average, maximum and minimum percent difference per circuit are provided in Table 4 and shown graphically in Figure 6 using a box and whisker plot.

Table 4. Anode Potential Average, Maximum and Minimum Percent Variations and Standard Deviations Calculated

Tankhouse	1		2	
Electrical Circuit	1	2	3	4
Number of Cells Measured	12	11	12	12
Average Measured Anode Potential (V)	1.92	1.93	1.90	1.94
Average Predicted Anode Potential (V)	2.02	2.01	1.91	1.91
Average Variation (%)	5.76%	4.97%	3.47%	1.62%
Maximum Variation (%)	8.87%	9.08%	7.80%	3.63%
Minimum Variation (%)	1.22%	1.91%	0.51%	0.49%

The percent difference between the measured and predicted anode potentials in all circuits were below 10% with the average percent difference ranging from 1.6% to 5.8%.

It is believed that Tankhouse 1 had a higher AP than predicted. It is possible that this was caused by current distribution issues related to tankhouse furniture and electrode alignments and/or anode age. Even so, it appears that the empirical anode potential model in Equation 4 provides a reasonable estimate of anode potentials in a commercial setting.

$$\%\ Difference = \left(\frac{Measured\ AP - Calculated\ AP}{Measured\ AP}\right) * 100\ \% \quad (5)$$

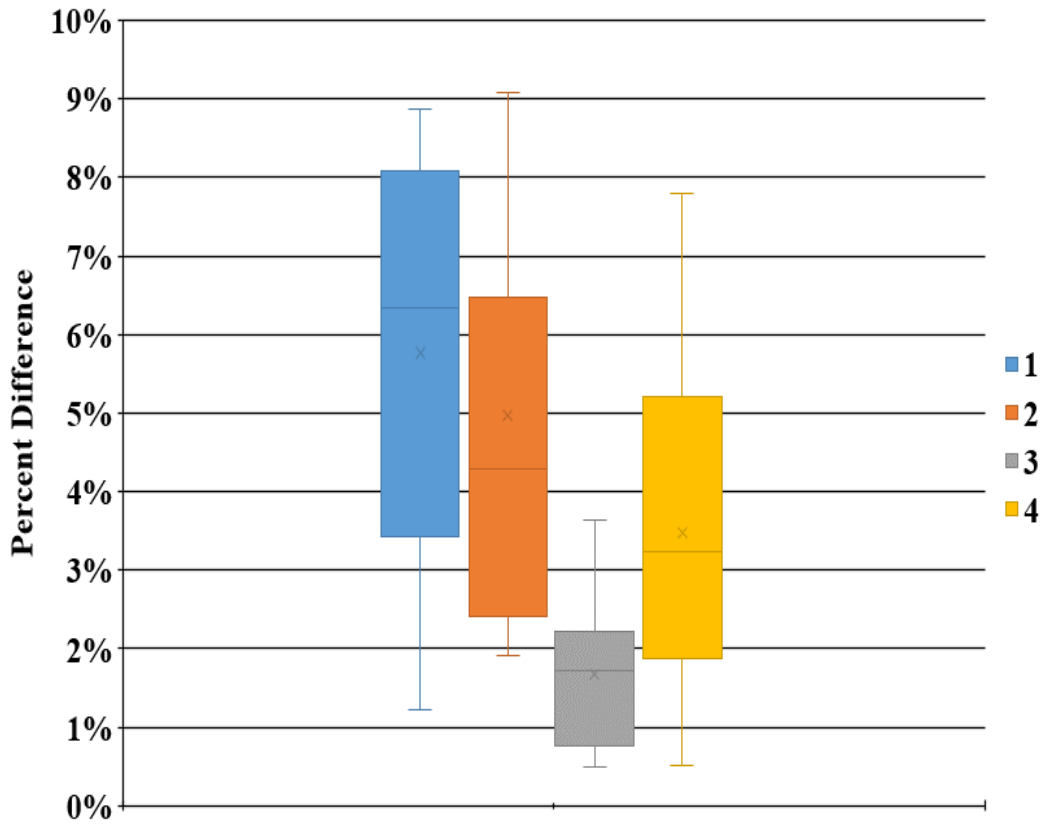

Figure 6. Box and Whisker Plot of Percent Difference Between Model and Measured Anode Potentials for Four Industrial Electrowinning Circuits

3.5. ENERGY OPTIMIZATION

The new anode potential model as shown in Equation 4 can be combined with other models to generate an energy consumption model for process analysis. Cell voltage can be calculated by combining the new anode potential model with fundamental and empirical equations for thermodynamic potentials, potential for current flow through the electrolyte, contact voltage and cathode potential [28]. Cell voltage can be estimated using Equation 6.

$$Cell\ Voltage\ (V) = (E_a + \eta_a) - (E_c - \eta_c) + IR_{solution} + IR_{contacts} \quad (6)$$

where E_c is the thermodynamic potential of the cathode, η_c is the cathodic overpotential, E_a is the thermodynamic potential of the anode, η_a is the anodic overpotential. $IR_{solution}$ and $IR_{contacts}$ are the solution voltage and contact voltage respectively.

$E_a + \eta_a$ is calculated by Equation 4 using industrially relevant parameter levels Co (0.18 g/L), temperature (40°C), current density (300 A/m^2) and sulfuric acid (180 g/L). The AP is therefore calculated to be 1.929 V.

$E_c - \eta_c$ is the cathode potential. E_c (0.275 V) was obtained from data published from cyclic voltammograms produced using 40 °C electrolyte with 40 g/L Cu, 180 g/L H_2SO_4, 20 mg/L Cl^- with various concentrations of HydroStar (a commercial smoothening agent) [32]. Cathode overpotential of plating copper on stainless steel was obtained by the voltage difference between the backward sweep and the standard potential at 300 A/m^2 in the cyclic voltammogram from the same publication [32]. The various concentrations of the organic additive did not affect polarization significantly. η_c was measured at 0.1 V.

The voltage drop caused by solution resistance can be calculated using current density and electrolyte conductivity. A suitable empirical equation for electrolyte conductivity was presented by Price and Davenport [33]. The conductivity of a 40 g/L Cu, 180 g/L sulfuric acid, 40°C electrolyte was calculated at 61.02 S/m. Using 300 A/m^2, electrode areas of 1m^2 (typical industrial electrode area) and a face-to-face anode to cathode separation of 0.0465 m (105 mm cathode-to-cathode centerline distance with 9 mm thick anodes and 3 mm cathodes) [8], $IR_{solution}$ was calculated to be 0.229 V.

The voltage component related to the contact resistance between electrode header bars and the cell busbars was also calculated to have a resistance of 50 μΩ for a triangular and dogbone contacts [34] which are the most commonly used [8]. Combining this with a 300 A/m^2 current density (2 m^2 per electrode) at two contact points per cell (one anode and one cathode) produces a potential drop of 0.030 V. Combining all the individual voltage components as shown in Table 5 produces a cell voltage of about 2.043 V which is similar to commonly reported values [18].

A predictive formula for current efficiency controlled by ferric reduction is presented in Equation 7 [35], where Fe(III) is the ferric concentration in g/l, Cu(II) is the copper concentration in g/l and C.D. is the current density in A/m^2. The current efficiency model is accurate at the tested ranges (1.27 g/L to 6.27 g/L). For consistency, values of 40 g/L Cu, 1.3 g/L ferric and 300 A/m^2 were used to calculate a current efficiency of 95.24 %.

To minimize electrical energy consumption, an industrial operation should attempt to minimize cell voltage and maximize current efficiency. For this example, electrical energy consumption was calculated by combining the calculated cell voltage and current efficiency to be ~1809 kWh/tonne. This value is lower than the average energy 2000 - 2160

kWh/tonne [15, 18] reported to produce eletrowon Cu. The calculated energy consumption assumes no short circuits and does not include electrical consumption due to rectification and resistances in the electrical bus system.

Table 5. Values of Voltage Contributors for Cell Voltage Including Anode Potential, Cathode Potential, Solution Voltage and Contact Voltage Calculated from Various

Cell Voltage Component	Value (V)
Anode Potential ($E_a + \eta_a$)	1.929
Cathode Potential ($E_c - \eta_c$)	0.175
$IR_{Solution}$	0.229
$IR_{Contacts}$	0.030
Total Cell Voltage	2.043

$$CE\ (\%) = 88.19 - 4.91 \times Fe(III)(g/l) + 0.52 \times Cu(II)(g/l) + 1.81 \times 10^{-3} \times CD(A/m^2) - 6.83 \times 10^{-3} \times Cu(II)^2(g/l) + 0.028 \times Fe(III)(g/l) \times Cu(II)(g/l) + 4.015 \times 10^3 \times Fe(III)(g/l) \times CD(A/m^2) \quad (7)$$

Within the ranges of all the parameters tested in this study the minimum energy consumption (1694 kWh/tonne) was calculated at 1.5 g/L Fe, 40 g/L Cu ions, 0.18 g/L Co, 200 g/L H_2SO_4, 200 A/m^2 current density and 50 °C. The minimized energy consumption does not consider corrosion, production rate and other tankhouse considerations. There are always tradeoffs that has to be made. For instance, operating at higher current density produces more copper cathodes per time but results in higher lead anode corrosion rates, increased energy consumption, increased risk of nodulation and short circuiting. All factors

have to be considered to generate a synergistic effort towards venture profitability. The essence of this forecast is to assist in budgeting for existing operations or project economic viability for new projects. Combining all of these components is important. For example, even though increasing sulfuric acid concentration increases the anode potential, its overall effect on the cell voltage is the opposite since increased acid concentration reduces the electrolyte voltage which overwhelms the effect of increased acid concentration on the anode potential.

Furthermore, increasing current density increases the anode potential but also increases the current efficiency. The current density effect on the cell voltage is much higher than the current efficiency effect. Figure 7 shows how the temperature affects energy consumption for various current densities.

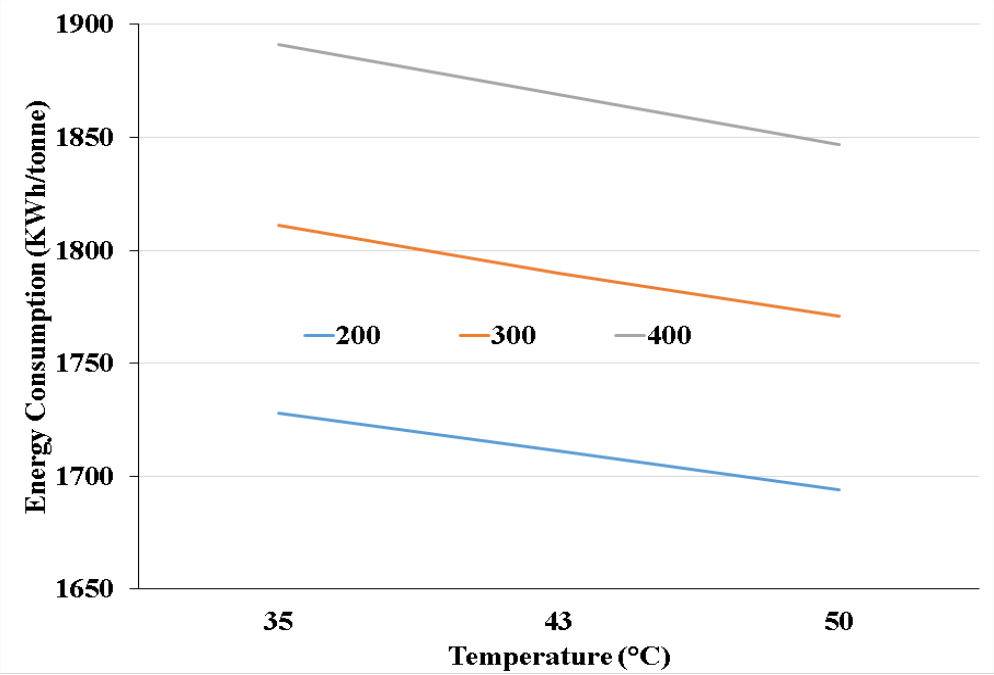

Figure 7. Energy Consumption Plots vs Temperatures for Three Different Current Densities in A/m^2

At any current density, higher temperatures results in lower energy consumption, but excessively high temperatures of the electrolyte will degrade solvent extraction organic reagents and accelerate anode corrosion. A critical balance of all determinant considerations including cathode production rates, anode corrosion rates, costs, etc. would yield an optimum energy consumption.

4. CONCLUSIONS

A new model for estimating the anode potential of rolled Pb-Ca-Sn anodes within industrially relevant levels of electrolyte chemistries has been developed. The significant parameters were established to be temperature, current density, Co concentration, and acid concentration. There is a Co*temperature two way interaction that is also significant at the levels tested. The highest effect on anode potential was determined to be by temperature, followed by current density, acid concentration, and Co concentration. Model validation established average percent differences between measured and predicted to be between 2 and 6% for industrial operations. Therefore, it is believe that Equation 4 can be used to design and/or optimize copper electrowinning facilities.

ACKNOWLEDGEMENT

The authors would like to acknowledge Freeport McMoRan for their support towards the completion of this research especially Paddy Craig for his ideas and fabrication of the anode potential measuring probe.

REFERENCES

1. Marsden, J.O., *Energy efficiency and copper hydrometallurgy*. Hydrometallurgy, 2008: p. 29-42.

2. Moats, M.S., *Energy efficiency of electrowinning*, in *Energy Efficiency in the Minerals Industry*. 2018, Springer. p. 213-232.

3. Robinson, T.G., et al., *Copper Electrowinning: 2013 World Tankhouse Operating Data.* Copper 2013 Proceedings, 2013. V, Santiago, Chile, IIMCh.

4. Aqueveque, P.E., et al. *Measurable variables in copper Electrowinning and their relevance to predict process performance*. in *Industry Applications Society Annual Meeting, 2013 IEEE*. 2013. IEEE.

5. Beukes, N. and J. Badenhorst, *Copper electrowinning: theoretical and practical design.* Journal of the Southern African Institute of Mining and Metallurgy, 2009. 109(6): p. 343-356.

6. Free, M.L., *The fundamentals of electrometallurgy in aqueous media.* JOM Journal of the Minerals, Metals and Materials Society, 2007. 59(5): p. 28-33.

7. Bautista, R. and R. Wesely, *Energy reduction techniques in metal electrochemical processes*. 1985, The Metallurgical Society, Inc., Warrendale, PA.

8. Barmi, M.J. and A.N. Nikoloski, *Electrodeposition of lead–cobalt composite coatings electrocatalytic for oxygen evolution and the properties of composite coated anodes for copper electrowinning.* Hydrometallurgy, 2012. 129: p. 59-66.

9. Clancy, M., et al., *The influence of alloying elements on the electrochemistry of lead anodes for electrowinning of metals: a review*. Hydrometallurgy, 2013. 131: p. 144-157.

10. Brown, A., R. Loutfy, and G.M. Cook, *Electrorefining of copper from a cuprous ion complexing electrolyte. II. Experimental comparison of possible alternative electrolytes and preliminary cost engineering analysis*. 1980, Argonne National Lab., IL (USA).

11. Cooper, W.C., *Advances and future prospects in copper electrowinning.* Journal of applied Electrochemistry, 1985. 15(6): p. 789-805.

12. Moats, M.S., *Will lead-based anodes ever be replaced in aqueous electrowinning?* JOM Journal of the Minerals, Metals and Materials Society, 2008. 60(10): p. 46-49.

13. Morimitsu, M., *Performance and Commercialization of the Smart Anode, MSA™, for Environmentally Friendly Electrometallurgical Process.* Electrometallurgy 2012, 2012: p. 49-54.

14. Morimitsu, M., et al. *Energy-efficient Electrowinning Process with smart anode comprising nanooxide catalyst*. in *Proceedings of European Metallurgical Conference*. 2011.

15. Free, M., et al., *Electrometallurgy-Now and in the Future.* Electrometallurgy 2012, 2012: p. 3-28.

16. Sandoval, S.P., et al., *System and method for producing copper powder by electrowinning using the ferrous/ferric anode reaction*. 2010, Google Patents.

17. Robinson, D.J., *SO 2 electrowinning in copper hydrometallurgy for energy conservation.* JOM, 1984. 36(1): p. 43-47.

18. Schlesinger, M.E., et al., *Extractive metallurgy of copper*. 2011: Elsevier.

19. Miller, G., *Methods of managing manganese effects on copper solvent extraction plant operations.* Solvent Extraction and Ion Exchange, 2011. 29(5-6): p. 837-853.

20. Nguyen, T., et al., *Influence of cobalt ions on the anodic oxidation of a lead alloy under conditions typical of copper electrowinning.* Journal of Applied Electrochemistry, 2008. 38(2): p. 215-224.

21. Nikoloski, A. and M. Nicol, *Effect of cobalt ions on the performance of lead anodes used for the electrowinning of copper—A literature review.* Mineral Processing and Extractive Metallurgy Review, 2007. 29(2): p. 143-172.

22. Nikoloski, A. and M. Nicol, *Addition of cobalt to lead anodes used for oxygen evolution—a literature review.* Mineral Processing and Extractive Metallurgy Review, 2009. 31(1): p. 30-57.

23. Yu, P. and T.J. O'Keefe, *Evaluation of lead anode reactions in acid sulfate electrolytes. I. Lead alloys with cobalt additives.* Journal of the Electrochemical Society, 1999. 146(4): p. 1361-1369.

24. Abbey, C. and M. Moats, *Effect of Cobalt and Iron Concentration on the Potential for Oxygen Evolution from Pb–Ca–Sn Anodes in Synthetic Copper Electrowinning Electrolytes*, in *Applications of Process Engineering Principles in Materials Processing, Energy and Environmental Technologies*. 2017, Springer. p. 89-95.

25. Miller, G., *Recent Experience with Manganese and its Effects on Copper SX-EW Operations.* 2011.

26. Tjandrawan, V., *The role of manganese in the electrowinning of copper and zinc*. 2010, Murdoch University.

27. Montgomery, D.C., *Design and analysis of experiments*. 2017: John Wiley & Sons.

28. Abbey, C. and M. Moats, *Pb–Ca–Sn Anode Potential as a Function of Cobalt, Iron and Manganese in Synthetic Sulfuric Acid Electrolytes*, in *Extraction 2018*. 2018, Springer. p. 1535-1546.

29. Panda, B. and S. Das, *Electrowinning of copper from sulfate electrolyte in presence of sulfurous acid.* Hydrometallurgy, 2001. 59(1): p. 55-67.

30. Subbaiah, T., et al., *Sulphurous acid as anodic depolarizer in copper electrowinning Part II.* Journal of applied electrochemistry, 2000. 30(2): p. 181-186.

31. Tjandrawan, V. and M.J. Nicol, *Electrochemical oxidation of iron (II) ions on lead alloy anodes.* Hydrometallurgy, 2013. 131: p. 81-88.

32. Cui, W., *Effect and interactions of commercial additives and chloride ion in copper electrowinning*. 2014: Missouri University of Science and Technology.

33. Price, D.C. and W.G. Davenport, *Densities, electrical conductivities and viscosities of CuSO4/H2SO4 solutions in the range of modern electrorefining and electrowinning electrolytes.* Metallurgical Transactions B, 1980. 11(1): p. 159-163.

34. Boon, C., et al., *Comparison of intercell contact bars for electrowinning plants*, in *Ni-Co 2013*. 2013, Springer. p. 177-189.

35. Khouraibchia, Y. and M.S. Moats, *Evaluation of the effect of copper electrowinning parameters on current efficiency and energy consumption using surface response methodology.* ECS Transactions, 2010. 28(6): p. 295-306.

SECTION

3. CONCLUSIONS, KNOWLEDGE CONTRIBUTIONS AND FUTURE WORK

There are vast prospects for research into base metal electrowinning. A better understanding of the anode processes, anode corrosion and energy utilization offers the biggest prospects for improvement of this vital industrial process. Chemical species reactions and interactions are still not well understood due to several challenges with the ability to accurately characterize scale species. This dissertation examined electrolytes species interactions, anode corrosion rates and energy utilization and optimization in Zn EW and Cu EW.

In Zn EW, it was concluded that [Mn^{3+}] is approximately 4-5% of the total [Mn] in the zinc electrowinning electrolyte. Mn/Cl ratio affects anode corrosion rate. The anode corrosion rate decreases with increasing Mn/Cl ratio to about 10 and then plateaus. Mn and Cl^- losses from the electrolyte were correlated but not correlated to the Mn/Cl ratio. Chloride loss was found to be higher than manganese loss.

Additionally, the anode scale appearance, phases, and tenacity were not correlated to the Mn/Cl ratio. Scale tenacity did correlate to presence of permanganate ion in the electrolyte that drained from the anode scale layer. Scales that were less tenacious had a purple solution drain from the anode layer when the electrodes were removed from the cell. These experiments indicate that scale appearance and structure were affected by an uncontrolled variable, but it is not clear what that variable was.

Four runs of 28 day testing was completed in an anode corrosion testing system to evaluate the effects of power outage, temperature and [Mn] and [Co] on corrosion rates

and current efficiency. The corrosion rates after 28 days did not show any significant trends. It is believed that the presence of at least 150 mg/L Co in all of the experiments minimized corrosion. Maintaining a 150 mg/L minimum [Co] seems to have overwhelmed any effect of power outages, temperature or [Mn] on anode corrosion. Temperature, power outages, [Mn] and [Co] at the levels tested did not significantly affect the current efficiency. The losses of Mn and Cl from the electrolytes were correlated (R^2 = 93 %).

Larger losses occurred at the higher [Mn] concentration. The low temperature high Mn run showed the most MnO_2 formation and Cl_2 evolution. The low temperature high Mn run also showed differences in cell mud formation and revealed the power outages and [Co] affected the amount and type of mud formed.

Results of experiments examining the effect of cobalt concentration on Pb-Ca-Sn anode potential under typical copper electrowinning conditions show that the anode potential increases with decreasing cobalt concentration with or without the presence of 0.6 g/L Fe for [Co] up to 0.6 g/L. Empirical equations were developed to allow the prediction of anode potentials as a function of [Co] between 0-0.6 g/L when there is Fe in the electrolyte or not. The two equations are given as Equations 3.1 and 3.2.

$$AP\ (V)\ \ w/\ Fe = 1.928\text{-}0.135\ Co^{0.32}\ (g/L) \qquad (3.1)$$

$$AP\ (V)\ \ w/o\ Fe = 1.951\text{-}0.0958\ Co^{0.43}\ (g/L) \qquad (3.2)$$

Since iron was shown to possibly affect anode potential, a CCD experimental design was used to evaluate the response of anode potential of rolled Pb-Ca-Sn samples versus surface active species - [Fe], [Mn] and [Co] - in synthetic electrolytes. ANOVA

analyses show that there is no significant interaction among Co, Fe and Mn within the ranges tested and the significant effects were caused by Co, Mn and Fe*Fe. AP was found to be lowest at high [Co], low [Mn] and either low or high [Fe]. Response surface methodology was used to analyze the data and an empirical equation was developed to estimate the anode potential (AP) at various concentrations of Co, Fe and Mn. The data was again used to obtain a second model for estimating the anode potential by using a Co function constraint. The two models are comparable with the Co function model being more accurate at higher anode potentials. The Co function equation is given as Equation 3.3.

$$AP\ (V\ vs.\ SHE) = 1.961 - 0.0962\ [Co]^{0.32} + 0.0114\ [Fe]^{0.25} + 0.0524\ [Mn] \qquad (3.3)$$

Combining the cobalt function anode potential equation with other equations and estimations in literature yielded a method to estimate cell voltage, current efficiency and energy consumption within industrially relevant concentration ranges for Co, Mn and Fe. Process engineers may find the ability to estimate energy consumption useful while optimizing their copper electrowinning operation.

Finally a new model for estimating the anode potential of rolled Pb-Ca-Sn anodes within industrially relevant levels of electrolyte chemistries, temperature and current density has been developed for copper tankhouses that add cobalt to their electroltyes. The significant parameters were established to be temperature, current density, Co concentration, and acid concentration. There is a Co*temperature two way interaction that is also significant at the levels tested. The highest effect on anode potential was determined

to be by temperature, followed by current density, acid concentration, and Co concentration. The model is given as Equation 3.4. Model validation established average percent differences between measured and predicted to be between 2 and 6% for industrial operations.

$$AP\ (V) = 1.9884 - 0.393\ Co\ (g/L) + 0.000189\ Acid\ (g/L) - 0.002736\ T\ (°C) + 0.000147\ CD\ (A/m^2) + 0.00591\ Co\ (g/L) * T\ (°C) \quad (3.4)$$

3.1. CONTRIBUTIONS TO KNOWLEDGE

In zinc cellhouse operations, this report has generated data showing that manganic concentration is 2-6% in electrolyte under conditions similar to Zn industrial cellhouse operations. Manganic disproportionates to Mn^{4+} and Mn^{2+}. Manganous is a precursor to the formation of manganese dioxide. Manganese and chloride losses are correlated across various Mn/Cl ratios even though either Mn and/or Cl losses are not correlated with Mn/Cl ratios. Initial hypothesis postulated on the causes of anode short circuits are that Mn/Cl ratios less than 10 or 11 result in accelerated corrosion possibly due to the presence of chlorine gas near the metal/scale interface. Additionally, lower Mn/Cl ratio appear to form flaky scales that exfoliate over time. These flakes could make contact with cathodes while still attached to anodes or could bridge the cathode and anode when they fall to cause short circuits.

This work contributes critical components that provide a more accurate estimation of copper tankhouse electrical energy consumption and power consumption. All the various models generated can be used in their specific ranges where they are applicable for

predicting anode potentials of a new EW project to establish economic viability and also assess sensitivity analysis. It can also be used by operating tankhouses to assess the effect of one or several parameter changes on energy and power consumption. An instance is the ability to calculate the effect of extracting or reducing Co concentration on energy consumption as shown in Paper I. The various models also provides a quantifiable effect of all the significant parameters on energy consumption. The models also provide important knowledge of what parameter can be increased or decreased to provide a desired effect on the energy consumption. For example increasing temperature decreases energy consumption. The Co*temperature interaction that was also evident from the data analysis in Paper V has not been previously reported.

An anode potential probe (Rolla Anode Potential Probe) prototype was designed, fabricated and tested. This new probe provides egonomic advantages and speed of anode potential measurements and electrical safety. The probe accuracy and sensitivity is dependent on the accuracy and sensitivity of the multimeter being used. This probe can be commercialized for tankhouses to measure anode potentials fast, easily, accurately and safely.

3.2. FUTURE WORK

While working on this research new ideas, concepts and directions were apparent and future research efforts could be worthwhile in pursuing. This provides opportunity for sustained research and industrial activity in these areas.

In both Zn and Cu EW, better anode scale characterization would help in understanding the mechanisms behind the phenomenon, interactions and observations in

their respective systems. Characterization could include physical (SEM, XRD etc.) and electrochemical methods (linear sweep voltammetry, cyclic voltammetry etc.). The electrochemical quartz crystal microbalance could be used to study the rate of formation of the anode scales and possibly the corrosion rates if the balance can be modified with the particular anode alloys for either Zn or Cu EW.

There also exists the possibility of using the rotating disk and or the rotating ring disk electrodes for further electrode kinetics studies. The rotating ring disk electrode might be used to understand the catalyzing role of Co in Cu EW.

More detailed corrosion studies can be conducted to quantify the effects of various EW operating parameters on the corrosion rates of anodes typically used in both Zn and Cu EW. This could also culminate in the formulation of a model like the anode potential model to estimate corrosion rates at various levels of operating parameters. This would be a critical addition to knowledge and help to better estimate optimum anode replacement forecasts.

In the Zn EW benchscale tests, control of the system was a challenge just like any industrial cellhouse. In future work it may provide more advantagous to run lab size tests to study effects of electrolyte concentrations on electrolyte composition, anode corrosion and scale formation. To test the hypothesis that lower Mn/Cl ratios form flaky scales, it would be necessary to characterize the scales and cell sludge in terms of morphology, particle sizes, porosity and surface appearance and possibly relate these parameters to the Mn/Cl ratios. Additionally, if manganic disproportionation reactions were better studied it would help to find a means of suppressing higher oxidation states of manganese (permanganate and manganese dioxide) from forming and generating excessive manganese

dioxide. This would decrease the need for frequent cell cleaning and increase cell availability.

In Cu EW, the Co*temperature interaction can be studied further. The low temperature, high Mn effect on MnO_2 formation can be studied further to understand the defining mechanisms. In the cell voltage estimation, to calculate the energy and power consumption in Cu EW, a cathode overpotential model would also be beneficial to have a better estimation. This model will provide a relation between significant parameters and the cathode potential.

BIBLIOGRAPHY

1. Bard, A.J. and L.R. Faulkner, *Electrochemical methods: fundamentals and applications*. Vol. 2. 1980: wiley New York.

2. Moats, M.S., *Will lead-based anodes ever be replaced in aqueous electrowinning?* JOM Journal of the Minerals, Metals and Materials Society, 2008. 60(10): p. 46-49.

3. Schlesinger, M.E., et al., *Extractive metallurgy of copper*. 2011: Elsevier.

4. Group, I.L.a.Z.S. *Lead and Zinc Statistics*. 2018 [cited 2018 2/26/2018]; Available from: http://www.ilzsg.org/static/statistics.aspx?from=1.

5. Jha, M.K., V. Kumar, and R. Singh, *Review of hydrometallurgical recovery of zinc from industrial wastes.* Resources, conservation and recycling, 2001. 33(1): p. 1-22.

6. Cachet, C., C. Le Pape-Rérolle, and R. Wiart, *Influence of Co2+ and Mn2+ ions on the kinetics of lead anodes for zinc electrowinning.* Journal of Applied Electrochemistry, 1999. 29(7): p. 811-818.

7. Cachet, C., C. Rerolle, and R. Wiart, *Kinetics of Pb and Pb-Ag anodes for zinc electrowinning—II. Oxygen evolution at high polarization.* Electrochimica Acta, 1996. 41(1): p. 83-90.

8. Chen, T. and J. Dutrizac. *Characterization of the Manganese Oxide Scales Formed on a Grooved Cast Pb-Ag Anode from a Zinc Electrowinning Operation*. in *EPD Congress 2011*. 2011. Wiley Online Library.

9. Clancy, M., et al., *The influence of alloying elements on the electrochemistry of lead anodes for electrowinning of metals: a review.* Hydrometallurgy, 2013. 131: p. 144-157.

10. Asselin, E., *Zn ELectrowinning Powerpoint Presentation.* 2016.

11. Biegler, T. and E. Frazer, *The coulombic efficiency of zinc electrowinning in high-purity synthetic electrolytes.* Journal of applied electrochemistry, 1986. 16(5): p. 654-662.

12. Gonzalez-Dominguez, J. and R. Lew, *Evaluating additives and impurities in zinc electrowinning.* JOM Journal of the Minerals, Metals and Materials Society, 1995. 47(1): p. 34-37.

13. Krause, B. and R. Sandenbergh, *Optimization of cobalt removal from an aqueous sulfate zinc leach solution for zinc electrowinning.* Hydrometallurgy, 2015. 155: p. 132-140.

14. Mackinnon, D., R. Morrison, and J. Brannen, *The effects of nickel and cobalt and their interaction with antimony on zinc electrowinning from industrial acid sulphate electrolyte.* Journal of applied electrochemistry, 1986. 16(1): p. 53-61.

15. Tjandrawan, V., *The role of manganese in the electrowinning of copper and zinc*. 2010, Murdoch University.

16. Kelsall, G., et al. *Effects of manganese (II) and chloride ions in zinc electrowinning reactors*. in *Proceedings—Electrochemical Society*. 2000.

17. Lagerstedt, A., *The effect of Manganese on Lead Anodes in Zinc Electrowinning*, in *Materials Science and Engineering Department*. 2005, Helsinki University of Technology: Helsinki, Finland. p. 82.

18. Mahon, M. and A. Alfantazi, *Manganese consumption during zinc electrowinning using a dynamic process simulation.* Hydrometallurgy, 2014. 150: p. 184-191.

19. Nicol, M., et al., *The effects of halides in the electrowinning of zinc. I. Oxidation of chloride on lead-silver anodes.* Hydrometallurgy, 2017. 173: p. 125-133.

20. Nicol, M., et al., *Effect of halides in the electrowinning of zinc. II. Corrosion of lead-silver anodes.* Hydrometallurgy, 2017. 173: p. 178-191.

21. Sorour, N., et al., *Effect of ionic liquid additives on oxygen evolution reaction and corrosion behavior of Pb-Ag anode in zinc electrowinning.* Electrochimica Acta, 2017.

22. Rodrigues, J. and E. Meyer. *Improving the performance of anodes for zinc electrowinning*. in *EPD Congress 1996*. 1996.

23. Pakhomova, G. and L. Marenkova, *Some Reactions on the Insoluble Lead Anode During Electrodeposition of Zinc.* TSVETNYE MET, 1966(8): p. 38-41.

24. Rerolle, C. and R. Wiart, *Kinetics of Pb and Pb□ Ag anodes for zinc electrowinning—I. Formation of PbSO4 layers at low polarization.* Electrochimica acta, 1995. 40(8): p. 939-948.

25. Zhang, W., et al., *Electrochemical impedance spectroscopy evaluation of behaviour of Pb–Ag anodes for zinc electrowinning.* Corrosion Engineering, Science and Technology, 2013. 48(6): p. 452-460.

26. Zhang, W., Y. Chen, and G. Houlachi, *Influence of silver content and MnSO4 addition on performance of different lead–silver alloys during polarisation and decay periods.* Canadian Metallurgical Quarterly, 2013. 52(1): p. 60-68.

27. Zhang, W. and G. Houlachi, *Electrochemical studies of the performance of different Pb–Ag anodes during and after zinc electrowinning.* Hydrometallurgy, 2010. 104(2): p. 129-135.

28. Yang, H.T., et al., *Electrochemical behavior of rolled Pb–0.8%Ag anodes.* Hydrometallurgy, 2013. 140: p. 144-150.

29. Prengaman, R.D. and C.E. Morgan, *Electrowinning anodes which rapidly produce a protective oxide coating*. 2001, Google Patents.

30. Ivanov, I., et al., *Insoluble anodes used in hydrometallurgy: Part I. Corrosion resistance of lead and lead alloy anodes.* Hydrometallurgy, 2000. 57(2): p. 109-124.

31. Ivanov, I., et al., *Insoluble anodes used in hydrometallurgy: Part II. Anodic behaviour of lead and lead-alloy anodes.* Hydrometallurgy, 2000. 57(2): p. 125-139.

32. Ramachandran, P., et al., *Effect of pretreatment on the anodic behaviour of lead alloys for use in electrowinning operations. I.* Journal of applied Electrochemistry, 1980. 10(5): p. 623-626.

33. Gonzalez, J., *Zinc electrowinning: Anode conditioning and current distribution studies.* 2001.

34. Jin, S., et al., *Effect of sandblasting and shot-peening on the corrosion behavior of Pb-Ag alloy anodes in acid zinc sulfate electrolyte at 38 o C,* in *Environmental degradation of materials and corrosion control in metals*. 2003.

35. Newnham, R., *Corrosion rates of lead based anodes for zinc electrowinning at high current densities.* Journal of applied electrochemistry, 1992. 22(2): p. 116-124.

36. Rodrigues, J., D. Garbers, and E. Meyer, *Recent developments in the Zincor cell house.* Canadian metallurgical quarterly, 2001. 40(4): p. 441-449.

37. Tjandrawan, V. and M.J. Nicol, *Electrochemical oxidation of iron (II) ions on lead alloy anodes.* Hydrometallurgy, 2013. 131: p. 81-88.

38. Burbank, J., *Anodization of lead in sulfuric acid.* Journal of the Electrochemical Society, 1956. 103(2): p. 87-91.

39. Pavlov, D. and N. Iordanov, *Growth processes of the anodic crystalline layer on potentiostatic oxidation of lead in sulfuric acid.* Journal of the Electrochemical Society, 1970. 117(9): p. 1103-1109.

40. Rüetschi, P., *Ion selectivity and diffusion potentials in corrosion layers.* J. Electrochem. Soc, 1973. 120: p. 226-331.

41. Ruetschi, P. and R. Angstadt, *Anodic oxidation of lead at constant potential.* Journal of the Electrochemical Society, 1964. 111(12): p. 1323-1330.

42. Kao, W.-H. and V. Weibel, *Electrochemical oxidation of manganese (II) at a platinum electrode.* Journal of applied electrochemistry, 1992. 22(1): p. 21-27.

43. McGinnity, J. and M. Nicol, *The effects of periodic open-circuit on the corrosion of lead alloy anodes in sulfuric acid electrolytes containing manganese.* 2008.

44. Pajunen, L., J. Aromaa, and O. Forsén, *The effect of dissolved manganese on anode activity in electrowinning.* Electrometallurgy and Environmental Hydrometallurgy, 2003. 2: p. 1255-1265.

45. Rodrigues, S., A. Shukla, and N. Munichandraiah, *A cyclic voltammetric study of the kinetics andmechanism of electrodeposition of manganese dioxide.* Journal of applied electrochemistry, 1998. 28(11): p. 1235-1241.

46. Yu, P. and T.J. O'Keefe, *Evaluation of lead anode reactions in acid sulfate electrolytes II. Manganese reactions.* Journal of the Electrochemical Society, 2002. 149(5): p. A558-A569.

47. Pajunen, L., J. Aromaa, and O. Forsén, *The effect of dissolved manganese on anode activity in electrowinning.* Electrometallurgy and Environmental Hydrometallurgy, Volume 2: p. 1255-1265.

48. Skaftun, S.M., et al., *An Electrochemical Quartz Crystal Microbalance Investigation of Manganese Oxide Deposition and Dissolution in Sulfuric Acid Relevant for Zinc Electrowinning.* ECS Transactions, 2018. 85(4): p. 103-119.

49. Ault, A.R. and G.C. Bratt. *Control of Mn Level in an Electrolytic Zn Plant Circuit by Anodic Deposition of Oxide*. in *Proc. Aust. Inst. Min. Metall.* 1975.

50. Mohammadi, M. and A. Alfantazi, *Evaluation of manganese dioxide deposition on lead-based electrowinning anodes.* Hydrometallurgy, 2016. 159: p. 28-39.

51. Robinson, T., et al. *Developments in base metal electrowinning cellhouse design*. in *TMS Annual Meeting*. 2012.

52. Wiechmann, E.P., et al. *Measurement of cathodic currents in equipotential inter-cell bars for copper electrowinning and electrorefining plants*. in *Conference Record - IAS Annual Meeting (IEEE Industry Applications Society)*. 2007.

53. Miller, G., *The Problem of Manganese and Its Effects on Copper SX-EW Operations, Paper from COPPER 95, Volume III, Electrorefining and Hydrometallurgy of Copper, International Conference held in Santiago, Chile, November 26-29, 1995.* Papers, 1995: p. 649-663.

54. Miller, G., *Recent Experience with Manganese and its Effects on Copper SX-EW Operations.* 2011.

55. Miller, G., *Methods of managing manganese effects on copper solvent extraction plant operations.* Solvent Extraction and Ion Exchange, 2011. 29(5-6): p. 837-853.

56. Miller, G., D. Readett, and P. Hutchinson, *Experience in operating the Girilambone copper SX-EW plant in changing chemical environments.* Minerals Engineering, 1997. 10(5): p. 467-481.

57. Shaw, D. *Iron, chloride and permanganate control in copper electrowinning tankhouses*. in *Proc. COPPER 99 Int. Conf.* 1999.

58. Al Shakarji, R., Y. He, and S. Gregory, *Performance evaluation of acid mist reduction techniques in copper electrowinning.* Hydrometallurgy, 2013. 131: p. 76-80.

59. Boon, C., et al., *Comparison of intercell contact bars for electrowinning plants*, in *Ni-Co 2013*. 2013, Springer. p. 177-189.

60. Wiechmann, E.P., et al., *Contact system design to improve energy efficiency in copper electrowinning processes.* IEEE Transactions on Industry Applications, 2013. 49(6): p. 2461-2465.

61. Robinson, T.G., et al., *Copper Electrowinning: 2013 World Tankhouse Operating Data.* Copper 2013 Proceedings, 2013. V, Santiago, Chile, IIMCh.

62. Hrussanova, A., L. Mirkova, and T. Dobrev, *Electrochemical properties of Pb–Sb, Pb–Ca–Sn and Pb–Co3O4 anodes in copper electrowinning.* Journal of applied electrochemistry, 2002. 32(5): p. 505-512.

63. Ettel, V., B. Tilak, and A. Gendron, *Measurement of cathode mass transfer coefficients in electrowinning cells.* Journal of the Electrochemical Society, 1974. 121(7): p. 867-872.

64. Zhong, S., et al., *Influence of silver on electrochemical and corrosion behaviours of Pb–Ca–Sn–Al grid alloys Part I: Potentiodynamic and potentiostatic studies.* Journal of applied electrochemistry, 1999. 29(1): p. 1-6.

65. Prengaman, R.D., *The metallurgy of lead alloys for electrowinning anodes.* Anodes for Electrowinning, 1984: p. 49-57.

66. Stelter, M., H. Bombach, and P. Saltykov. *Corrosion behavior of lead-alloy anodes in metal winning*. in *Sohn International Symposium Advanced Processing of Metals and Materials*. 2006.

67. Yang, J., et al., *Effect of rolling technologies on the properties of Pb-0.06 wt% Ca-1.2 wt% Sn alloy anodes during copper electrowinning.* International Journal of Minerals, Metallurgy, and Materials, 2015. 22(11): p. 1205-1211.

68. Camurri, C., et al., *Lead-Based Anodes for Copper Electrowinning: Effect of Grain Size on Mechanical and Anticorrosion Properties.* MATERIALS TRANSACTIONS, 2018. 59(4): p. 620-624.

69. Zhang, Y. and Z. Guo, *Anodic behavior and microstructure of Pb-Ca-0.6% Sn, Pb-Co3O4 and Pb-WC composite anodes during Cu electrowinning.* Journal of Alloys and Compounds, 2017. 724: p. 103-111.

70. Petersson, I., E. Ahlberg, and B. Berghult, *Parameters influencing the ratio between electrochemically formed α-and β-PbO 2.* Journal of Power Sources, 1998. 76(1): p. 98-105.

71. Barmi, M.J. and A.N. Nikoloski, *Electrodeposition of lead–cobalt composite coatings electrocatalytic for oxygen evolution and the properties of composite coated anodes for copper electrowinning.* Hydrometallurgy, 2012. 129: p. 59-66.

72. Huang, H., J.-Y. Zhou, and Z.-C. Guo, *Effect of added cobalt ion on copper electrowinning from sulfate bath using doped polyaniline and Pb-Ag anodes.* Transactions of Nonferrous Metals Society of China, 2010. 20: p. s55-s59.

73. Nikoloski, A. and M. Nicol, *Effect of cobalt ions on the performance of lead anodes used for the electrowinning of copper—A literature review.* Mineral Processing and Extractive Metallurgy Review, 2007. 29(2): p. 143-172.

74. Nikoloski, A. and M. Nicol, *Addition of cobalt to lead anodes used for oxygen evolution—a literature review.* Mineral Processing and Extractive Metallurgy Review, 2009. 31(1): p. 30-57.

75. Nguyen, T. and A. Atrens, *Composition and morphology of the film formed on a lead alloy under conditions typical of the electro-winning of copper.* Hydrometallurgy, 2009. 96(1-2): p. 14-26.

76. Bôas, R.C.V., *Synergetic phenomena in zinc electrowinning*. 1977: Universidade Federal do Rio de Janeiro, Programa de Engenharia Metalúrgia e de Materiais.

77. Koch, D., *The effect of cobalt on the kinetics of oxygen evolution at a lead dioxide anode in sulphuric acid.* Australian Journal of Chemistry, 1959. 12(2): p. 127-137.

78. Gendron, A.S., V.A. Enel, and S. Abe, *Effect of cobalt added to electrolyte on corrosion rate of Pb-Sb anodes in copper electrowinning.* Canadian Metallurgical Quarterly, 1975. 14(1): p. 59-61.

79. Yu, P. and T.J. O'Keefe, *Evaluation of lead anode reactions in acid sulfate electrolytes. I. Lead alloys with cobalt additives.* Journal of the Electrochemical Society, 1999. 146(4): p. 1361-1369.

80. Nguyen, T. and A. Atrens, *Influence of lead dioxide surface films on anodic oxidation of a lead alloy under conditions typical of copper electrowinning.* Journal of Applied Electrochemistry, 2008. 38(4): p. 569-577.

81. Nguyen, T., et al., *Influence of cobalt ions on the anodic oxidation of a lead alloy under conditions typical of copper electrowinning.* Journal of Applied Electrochemistry, 2008. 38(2): p. 215-224.

82. Subbaiah, T., et al., *Sulphurous acid as anodic depolarizer in copper electrowinning Part II.* Journal of applied electrochemistry, 2000. 30(2): p. 181-186.

83. Subbaiah, T., et al., *Electrowinning of copper in the presence of anodic depolarisers-a review*. Mineral Processing and Extractive Metullargy Review, 2000. 21(6): p. 479-496.

84. Ravindran, K., L. Heerman, and L. Van Simaeys, *The anodic behaviour of lead in acid sulphate solutions. Influence of manganese ions and electrochemical oxidation of manganese ions at lead anodes.* Bulletin des Sociétés Chimiques Belges, 1975. 84(1-2): p. 83-90.

85. Price, D.C. and W.G. Davenport, *Densities, electrical conductivities and viscosities of CuSO4/H2SO4 solutions in the range of modern electrorefining and electrowinning electrolytes.* Metallurgical Transactions B, 1980. 11(1): p. 159-163.

86. Price, D.C. and W.G. Davenport, *Physico-chemical properties of copper electrorefining and electrowinning electrolytes.* Metallurgical Transactions B, 1981. 12(4): p. 639-643.

87. Joy, S., et al., *Understanding and improvement of electrowinning current efficiency at Freeport-McMoRan Bagdad.* Copper 2010 proceedings, 2010. 4: p. 1379-1392.

88. Harvey, W., *Material balance and current efficiency in electrowinning.* Hydrometallurgy, 1976. 2(1): p. 35-50.

89. Khouraibchia, Y. and M.S. Moats, *Evaluation of the effect of copper electrowinning parameters on current efficiency and energy consumption using surface response methodology.* ECS Transactions, 2010. 28(6): p. 295-306.

90. Moats, M. and Y. Khouraibchia. *Effective diffusivity of ferric ions and current efficiency in stagnant synthetic copper electrowinning solutions*. in *SME Annual Meeting and Exhibit and CMA's 111th National Western Mining Conference 2009*. 2009.

91. Moats, M.S., *How to evaluate current efficiency in copper electrowinning.* Separation Technologies for Minerals, Coal, and Earth Resources, 2012: p. 333.

92. Moats, M.S., *Energy efficiency of electrowinning*, in *Energy Efficiency in the Minerals Industry*. 2018, Springer. p. 213-232.

93. Kawaguchi, K., G.M. Haarberg, and M. Morimitsu, *Suppression of PbO2 Deposition on Nano-Structured IrO2-Ta2O5/Ti Anodes in Acidic Solutions.* ECS Transactions, 2013. 50(19): p. 75-85.

94. Kawaguchi, K. and M. Morimitsu, *Effects of Oxide Composition on Structure, Surface Morphology, and Oxygen Evolution Behaviors of IrO 2-Ta 2 O 5/Ti Anodes Prepared at a High Temperature.* Electrochemistry, 2015. 83(4): p. 256-261.

95. Moats, M., K. Hardee, and C. Brown Jr, *Mesh-on-lead anodes for copper electrowinning.* JOM, 2003. 55(7): p. 46.

96. Morimitsu, M., *Performance and Commercialization of the Smart Anode, MSA™, for Environmentally Friendly Electrometallurgical Process.* Electrometallurgy 2012, 2012: p. 49-54.

97. Morimitsu, M., et al. *Energy-efficient Electrowinning Process with smart anode comprising nanooxide catalyst*. in *Proceedings of European Metallurgical Conference*. 2011.

98. Sandoval, S.P., et al., *System and method for producing copper powder by electrowinning using the ferrous/ferric anode reaction*. 2010, Google Patents.

99. Cui, W., *Effect and interactions of commercial additives and chloride ion in copper electrowinning*. 2014: Missouri University of Science and Technology.

100. Moats, M.S. and A. Derrick, *Investigation of nucleation and plating overpotentials during copper electrowinning using the galvanostatic staircase method.* Electrometallurgy 2012, 2012: p. 125-137.

101. Winand, R., *Electrodeposition of metals and alloys—new results and perspectives.* Electrochimica Acta, 1994. 39(8-9): p. 1091-1105.

102. Luyima, A., et al., *Examination of copper electrowinning smoothing agents. Part II: Fundamental electrochemical examination of DXG-F7.* Minerals and Metallurgical Processing, 2016. 33(1): p. 14-22.

103. Cifuentes, G., et al. *The corrosion of lead anodes in copper electrowinning*. in *Proceedings of the COPPER'99 International Conference*. 1999.

104. Cifuentes, L., A. Montes, and G. Crisóstomo, *Corrosion behaviour and catalytic effectiveness of Pb–Ca–Sn, RuO2–IrO2/Ti and IrO2–Ta2O5/Ti anodes for copper electrowinning.* Corrosion Engineering, Science and Technology, 2011. 46(6): p. 737-744.

105. Cifuentes, L. and D. Pino, *Effect of solution components on stability of protective PbO2 layers on Pb–Ca–Sn anodes for copper electrowinning.* Corrosion Engineering, Science and Technology, 2009. 44(6): p. 474-476.

106. Addison, J., et al., *Implementing technology: Conversion of Phelps Dodge Morenci, Inc. Central EW tankhouse from copper starter sheets to stainless steel technology.* Copper 99- Cobre 99, 1999: p. 609-618.

VITA

Charles Ebenezer Abbey was born in La, Accra, Ghana and received a BSc Minerals Engineering degree in May 2006 and MPhil Minerals Engineering degree in February 2010 from the University of Mines and Technology in Tarkwa Ghana.

Prior to his PhD, Charles was a lecturer (2010-2015) at the University of Mines and Technology. During this time, Charles taught seven different courses and supervised 17 undergraduate theses.

He earned a PhD degree in Materials Science and Engineering from the Missouri University of Science and Technology in May 2019 under Associate Professor Michael Scott Moats.